universität wien

# MASTERARBEIT | MASTER'S THESIS

Titel | Title

Modelling the effect of microscale spatial structure on soil extracellular enzyme kinetics

verfasst von | submitted by

Paul Prinz BSc

angestrebter akademischer Grad | in partial fulfilment of the requirements for the degree of

Master of Science (MSc)

Wien | Vienna, 2025

| | |
|---|---|
| Studienkennzahl lt. Studienblatt \| Degree programme code as it appears on the student record sheet: | UA 066 833 |
| Studienrichtung lt. Studienblatt \| Degree programme as it appears on the student record sheet: | Masterstudium Ecology and Ecosystems |
| Betreut von \| Supervisor: | Assoz. Prof. Mag. Dr. Christina Kaiser |

# Acknowledgements

First, I would like to thank my parents for their support, love, and nurturing they have given me over my lifetime which provided opportunities to develop and learn free from constraints and threats that are sadly a reality for many others.

Next, I would like to thank my colleagues at TER. I especially want to thank Ksenia for her support and guidance. Her valuable input of ideas was crucial to my work. I also want to thank Eva, Thayer, Erika, Dave, Anne-Sophie, Kian, Dennis, Lauren, Sean, Moritz, Stefan and Julia for introducing me to the exciting life of scientific practice I was able to witness in many brilliant presentations and engaging group discussions.

Finally special thanks go to Tina. She was able to ignite in me the fascination for science I hold today.

# Contents

# 1 General introduction

Soil organic carbon (SOC) constitutes the majority of actively-cycling carbon in the terrestrial realm. Looking ahead, climate and land-use change will alter its biogeochemical cycling dynamics in unexpected, non-linear ways due to possibly substantial feedbacks, making predictions — of large societal and ecological relevance — difficult (Friedlingstein et al., 2014; Georgiou et al., 2021; Todd-Brown et al., 2014; Wieder et al., 2018). Central players that have a non-trivial impact on these non-linear processes are microbes, which decompose SOC. The decomposed organic carbon is then taken up by the microbes and partly turned into $CO_2$.

To better understand how global change might alter microbially mediated carbon circulation, here we investigate mechanisms that, in part, regulate the protection of SOC that prevents the decomposition process (Schimel, 2023).

The carbon cycle–climate feedback refers to the interplay between the Earth's carbon cycle and climate system, where changes in one can amplify or mitigate changes in the other. As global temperatures rise due to increased greenhouse gas emissions, several feedback mechanisms are triggered, potentially leading to non-linear dynamics (so-called 'tipping points') in global carbon circulation. For example, in terrestrial ecosystems, warming could lead to a rise in soil microbial respiration. This might cause soils to release more $CO_2$. On the other hand, nutrient limitations and an increased frequency of drought events could alter soil environmental factors, such as soil architecture and water content, which might lead to greater sequestration of carbon (Schimel and Carroll, 2024). As they can significantly influence the trajectory of climate change, understanding these complex relationships is crucial.

Terrestrial ecosystems are the third-largest reservoir of carbon on Earth containing approximately 3000 PgC, with its largest fraction 75% (2300 PgC) stored in soils and the remaining 25% in terrestrial vegetation. In terms of size, it is surpassed only by the oceanic carbon pool, which contains 38,000 PgC, and fossil fuel reservoirs, which hold nearly 10,000 PgC (Shukla et al., 2019). Global land-atmosphere carbon fluxes have been estimated to be net 3.3 ± 0.8 PgC/y during the 2013–2022 decade whereby the entirety of all terrestrial ecosystems act as sinks (Friedlingstein et al., 2023). Given the

vast size of the soil carbon pool and the net land-atmosphere carbon flux, soil systems play a significant role in global carbon dynamics and are therefore fundamental to our understanding of the impacts of climate change. For this reason, they are incorporated as a central component of Earth system models (ESMs). ESMs represent flows between compartments (carbon or other element pools) through equations. These flows attempt to model processes that affect carbon circulation, which are often coupled, creating feedback loops. There are still significant unknowns about these feedbacks, which certainly affect our predictive capacity (Houghton, 2007; Azar and Johansson, 2022). Incorporating carbon cycle feedbacks in land-to-atmosphere carbon fluxes into ESMs generally results in higher temperature projections compared to when these fluxes are static (Asaadi et al., 2024). Additionally, when carbon cycle feedbacks are included, ESMs still exhibit large uncertainty in $CO_2$ projections, primarily due to uncertainties in the land carbon cycle projections (Arora et al., 2020).

At every scale there are processes that need to be better understood to reduce the uncertainty in carbon cycle models. Numerous individual events are aggregated and summarised into flows that attempt to represent the dynamics of the entire Earth system. One of the mesoscale processes involved is plant growth. Plants fix carbon from atmospheric $CO_2$ through photosynthesis and store it as metabolic products in their cells. A part of the plant ends up as litter making its way into the soil. Additionally, root exudation from plants releases carbon compounds into the soil system. These long-chained carbon polymers are then broken down by microbial extracellular enzymes into smaller molecules. A process that occurs entirely outside the microbial cell (Xiao et al., 2018). The microbes are then able to take up these smaller molecules, synthesise metabolic products with them, or use them for energy, oxidising the carbon back into $CO_2$ that gases out of the soil into the atmosphere (Wieder et al., 2015).

The decomposition step is currently modelled using enzyme kinetics, which ignore spatial relationships by assuming that reaction partners are well-mixed and move randomly without constraints. However, SOC decomposition occurs within spatially heterogeneous soil and is influenced by environmental factors such as temperature, moisture, and soil architecture. How these factors may influence the microbial degradation dynamics is still an open question and investigated here by means of computational spatially explicit micro-scale models.

As an example of the interdependence of the carbon cycle involving the atmosphere, vegetation, and the soil system, consider that higher atmospheric $CO_2$ concentrations will increase plant growth leading to the production of more plant detritus. When more carbon is eventually brought into the soil system, extracellular enzymes break down that carbon

into dissolved organic carbon (DOC) that can readily be taken up by microorganisms. After this initial extracellular digestion, there is more DOC available to be taken up by microbes. This fuels microbial growth, which in turn generates more microbial biomass carbon. This then will increase — as microbes are the main producers of extracellular degradative enzymes — the carbon pool of enzymes decomposing even more SOC into DOC (Allison et al., 2010). Because of this dynamic, some models predict that higher SOC inputs — driven by increased root exudation and plant litter deposition due to the atmospheric-carbon-concentration-fertilization-feedback — will not necessarily lead to greater carbon sequestration. Rather, microorganisms may respire the additional carbon into the atmosphere as $CO_2$ or potentially degrade even more than before, which would make the soil carbon pool paradoxically shrink (Fontaine et al., 2004). Therefore, carbon output from soils might not depend on SOC input, but rather it may depend partly on the effect of environmental soil conditions — for instance temperature, moisture, and soil architecture — on the functioning of extracellular enzymes (García-Palacios et al., 2021).

In macro-scale models and measurements there are three enzyme kinetics equations that are used to represent the digestion of SOC into DOC: the Michaelis-Menten equation MM (Briggs and Haldane, 1925; Johnson and Goody, 2011), the reverse Michaelis-Menten equation rMM (Wang and Post, 2013) and the equilibrium chemistry approximation ECA (Tang and Riley, 2013; Tang, 2015). MM, rMM and ECA kinetics have not been specifically derived for large-scale carbon flux models. Rather they are general mathematical models of enzymatic reaction rate. While they all are trying to capture the fundamental process of enzyme kinetics, MM, rMM, and ECA differ in their underlying assumptions: whether substrate (MM) or enzymes (rMM) are the components that are limiting the reaction $R$. Conversely, the ECA equation has been developed to deal with a situation where enzymes or substrate both could be the rate-limiting factor for SOC degradation. How these equations are used in biogeochemical models is still a matter of active debate.

To address this issue, we develop individual-based models that explicitly simulate enzyme kinetics by representing enzyme and substrate particles and their interactions. We adjust the parameter settings of these particles to capture the influence of environmental factors on extracellular enzyme degradation dynamics. To account for spatial heterogeneity in soil, we employ an idealized soil architecture by placing spatial barriers particles reflect from into the models. In one model, the idealized soil architecture is based on the Hilbert space-filling curve — a bidimensional fractal-like structure previously used in micro-scale models (Arellano-Caicedo et al., 2023). In the other model, a single simplified pore setup is used. Crucially, the kinetics of extracellular enzymes might be different when heterogeneity is considered as opposed to the assumption of well-mixed conditions that

underlie current kinetics equations.

Relating the substrate or enzyme concentration to the reaction rate, all three equations (MM, rMM and ECA) describe how the turnover rate per enzymes changes depending on the concentration of substrate (MM), enzymes (rMM) or both (ECA). There are two catalytic constants in those functions: (1) the maximum rate of reaction $V_{max}$, which is the reaction velocity when the catalysis is governed by zero-order kinetics — i.e. substrate or enzyme independence is reached — and (2) the half-saturation or Michaelis constant $K_m$, which corresponds to the substrate (MM) or enzyme (rMM) or both concentrations (ECA) at $\frac{1}{2}V_{max}$. Generally, the smaller $K_m$, the higher is the binding affinity of the enzyme for a substrate (Marangoni, 2003).

At the macro- and meso-scale, the three soil factors temperature, moisture and architecture are effected by climate and land-use change. By the end of this century, atmospheric temperatures will likely increase globally by 1.5 to 4.8°C compared to preindustrial levels (Rogelj et al., 2012; O'neill et al., 2017; Masson-Delmotte et al., 2021) because of the increase in greenhouse gases due to burning fossil fuels that trap long wave length radiation. To understand how the soil system behaves several warming field-experiments have been carried out. With these long-term multi-factor field experiments in relevant biomes, direct and indirect impacts of climate change on the soil system can be investigated (Bardgett et al., 2008). Furthermore, land-use significantly impacts soil architecture and therefore soil function in part by altering soil biota composition that act as ecosystem engineers (Spurgeon et al., 2013). Soil moisture is influenced by climate-change through altered precipitation patterns and by land-use change by a change in soil water retention capacity (Acín-Carrera et al., 2013).

A complex interplay of biochemical and physical factors effect the micro-scale dynamics of SOC decomposition. Soil factors such as soil architecture, temperature, and moisture play a pivotal role in determining the encounter rates between enzymes and their substrates. Characterized by soil porosity and aggregate structure, soil architecture determines the spatial distribution and accessibility of enzymes and substrates, thereby influencing their interaction probabilities. By confining molecules within closer proximity smaller pore spaces might enhance enzyme-substrate encounters. However, enzyme mobility and substrate accessibility may be restricted (Burns et al., 2013a). Changes in soil architecture — affected by vegetation where more diverse plant communities have been associated with higher soil porosity and greater presence of 60–150 µm pores — surprisingly led to higher SOC protection and more overall carbon sequestration. Also, 30–150 µm pores in soils with more homogeneous plant communities were associated with greater extracellular enzyme activities and therefore a greater zone of influence (or spatial

footprint) of microbial decomposers (Kravchenko et al., 2019). Moreover, a modelling study showed (Pérez-Reche et al., 2012) that size, shape and interconnection of pores can differ in ploughed versus soil with no tillage and this affects the expansion of microbial colonies. Soil pore size distribution controls water potential, gas diffusivity and microbial accessibility and therefore affects SOC persistence (Lugato et al., 2009). This could be a way forward to mitigate climate change by land-use change. Furthermore, quantifying how soil architecture affects SOC protection could be used in agricultural transformation plans. Moreover, as another critical factor soil temperature not only affects the kinetic energy of molecules and therefore increasing their diffusion rates, but also influences activity rates and enzyme stability (Stotzky, 1965). Additionally, by mediating the aqueous pathways necessary for enzyme-substrate interactions soil moisture content significantly impacts enzyme dynamics. Water acts as a medium that dissolves and transports enzymes and substrates, enhancing their mobility and the likelihood of interactions. Optimal moisture levels facilitate these interactions, while either drought or waterlogging can severely impair them (Wallenstein and Hall, 2012). Drought conditions can severely inhibit enzyme activity in soil, leading to decreased rates of soil nutrient cycling (Manzoni et al., 2014). On the other hand, waterlogging can lead to adverse effects on enzyme degradation processes by creating anaerobic conditions (Chen et al., 2011), reducing enzyme stability and altering pH as well as ionic strength. Because water has a high specific heat capacity, meaning it can absorb a lot of heat before it changes temperature, under wet conditions soils can have cooler temperatures further reducing the rate of enzymatic reactions. These micro-scale environmental factors (soil moisture, temperature and architecture) are important for extracellular enzyme mediated decomposition of SOC by changing the encounter rate of enzymes and substrates as well as the efficiency of the enzymatic reaction process. Determining broader biogeochemical and ecological cycles, these soil factors are in turn influenced by land-use and climate change creating significant feedback loops.

The main producers of extracellular enzymes in soil are microbes. From the perspective of a microbe, the synthesis and secretion of extracellular enzymes requires nitrogen as well as other elements and is costly for the cell. Also, extracellular enzymes are lost to the cell due to a lack of protein import systems and thus are not recycled like intracellular proteins. Therefore, a matching return on this metabolic investment in the form of products is vital, which is managed by the adaptation of extracellular enzyme synthesis and secretion to substrate availability (Dekel and Alon, 2005). Cells also employ cost-minimisation strategies such as reducing the number of costly amino acids used for extracellular enzymes (Smith and Chapman, 2010), and enzymes involved in the decomposition of

carbon and mineralisation of sulphur are known to be depleted in exactly those elements (Baudouin-Cornu et al., 2001).

Looking at the micro-scale dynamics of extracellular digestion, the activity of an individual enzyme can be described in the following manner: an extracellular enzyme $E$ meets a substrate $S$ (here, an SOC compound) outside the cell and forms a complex $ES$ or $C$ in a reversible process. After some time, an irreversible reaction $R$ may occur that generates one or several products $P$ (here DOC). After $R$, we have free products and free enzymes once again (Marangoni, 2003). This process is fundamental to all enzymes and assumes that the individual particles involved are homogeneously distributed in space and well-mixed. Crucially, this model is used in soil science to measure extracellular enzyme activity — i.e., the kinetics of the whole decomposition process formed by combining all catalysed reactions mediated by an extracellular enzyme system (Roberts, 1977; Wang and Post, 2013).

In 1913, Leonor Michaelis and Maud Leonora Menten developed a quantitative theory of enzyme kinetics, famously known as the Michaelis-Menten (MM) equation. This model is based on the assumption that substrate concentration far exceeds enzyme concentration, allowing the substrate concentration to be considered constant. This assumption simplifies the analysis by focusing on the rapid attainment of equilibrium, where the rate of complex formation and its reversal are balanced, leading to the so-called equilibrium approximation. However, this approach is not always sufficient, especially in cases where the assumption of constant substrate concentration does not hold. To account for these situations, an alternative approximation was introduced by G. E. Briggs and J. B. S. Haldane in 1925, known as the quasi-steady-state approximation. This method assumes that the concentration of the enzyme-substrate complex remains constant during the reaction, particularly after the initial transient phase. This is particularly useful when the final step in catalysis, in which the complex dissociates into product and free enzyme, occurs much faster than the earlier steps.

These approximations are critical in enzyme kinetics because they simplify the complex differential equations governing reaction rates, making it easier to derive meaningful insights into the catalytic process. Despite their utility, it is important to note that these assumptions may not always reflect actual biological conditions, where enzyme concentration can exceed substrate concentration and reaction rates can be difficult to measure directly.

The chemical properties of many extracellular enzymes are well known. Most of those that break down organic matter in soil are hydrolytic or oxidative. While oxidative enzymes — using (among many others) hydrogen peroxide (peroxidases) or oxygen

(oxygenases) as electron acceptors — have a broad range of target bonds, hydrolytic enzymes cleave only certain chemical bonds. Extracellular enzymes can be classified into groups according to the biogeochemical cycle they are involved in, e.g., the sulphur, phosphorus, nitrogen, and carbon cycles (Dick, 2020).

Soil temperature, moisture, and architecture affect the degradation dynamics of extracellular enzymes by influencing their movement through the soil matrix and thus their rate of encounters. As dissolved molecules, extracellular enzymes are assumed to move randomly in solution — a process termed Brownian motion. It is documented that Brownian motion was first noticed by Dutch physician Jan Ingenhousz in 1785 and later properly described by Robert Brown in 1828. But the reason for this random movement of fine particles — including dust, pollen, and soot on liquid surfaces — was revealed much later by Albert Einstein (Einstein, 1905) as being the result of fluid molecules in random thermal motion striking these small particles and causing them to undergo a random walk (RW). RW models have been used in biology (Codling et al., 2008), for example, in population genetics (Ewens, 2004), in neuroscience and cognition (Tuckwell, 1988; Usher and McClelland, 2001; Gold and Shadlen, 2007; Gabbiani and Cox, 2010) and, of course, in ecology to represent animal movement (Viswanathan et al., 1999; Okubo et al., 2001; Humphries et al., 2010). RW models are a good approximation for the motion of molecules in solution such as extracellular enzymes. However, in soil, extracellular enzymes encounter other phases besides liquid (solid and gaseous) which act as barriers constraining their random movement.

The micro-scale spatial organisation of extracellular enzymes is difficult to generalise. Most extracellular enzymes diffuse away from their producer cell after secretion. However, some remain attached as cell-bound extracellular enzymes. The advantages of being bound to the cytoplasmic membrane include reduced diffusional losses of the product and decreased competition from other microbes. Additionally, such enzymes are partly shielded by the membrane from proteases of other microorganisms. Whereas the disadvantage compared to freely diffusible enzymes is that substrate must be in the immediate vicinity of the cell in order to react with the enzyme (Burns et al., 2013b). Indeed, it has been shown in a model (Traving et al., 2015) that freely diffusible extracellular enzymes tend to generate more product — due to more frequent substrate–enzyme collisions — than membrane-attached extracellular enzymes. In situations where the environment is oligotrophic — as soil generally is — and organic molecules are only present in the nanomolar range (Leitner et al., 2017), cell bound extracellular enzymes might be the strategy of choice because there are too few microbes that secrete extracellular enzymes meaning that a sufficient enzyme pool would never build up. To increase their scavenging

abilities microbes that have a lot of cell-bound extracellular enzymes may have evolved chemotaxis, i.e., the ability to move towards increased substrate concentration, as can be seen in computational soil models (Centler et al., 2011). Another strategy is to produce extracellular polymeric substances (EPS) (Or et al., 2007; Nunan et al., 2020) which serve partly to even out fluctuations in environmental conditions (Roberson and Firestone, 1992), partly to reduce the diffusivity of extracellular enzymes and products. This helps retain enzymes, as well as nutrients and substrate, closer to the cell (Romaní et al., 2008; Costa et al., 2018).

Some of the freely-diffusible extracellular enzymes have disulphide bonds and are glycosylated, making them more resilient than intracellular enzymes in terms of a broader pH range for activity, thermostability, and resistance to proteases. Moreover, enzyme diffusivity might be optimised and should increase with the distance of the producer cell from the target substrate, however, the further the substrate is away from the cell the higher the probability that the products are taken up by a competitor or lost in another way, which would create selection pressure towards extracellular enzymes with lower diffusivity (Allison et al., 2011).

While diffusing in soil pore space, extracellular enzymes can adsorb to clay minerals or become entrapped inside humic acids and particulate organic matter. This stabilisation reduces enzymatic activity due to occlusion of active sites, conformational changes in the enzyme and restricted access to the substrate (Dick and Tabatabai, 1987). Nevertheless, being protected against pH and thermal denaturation as well as proteolysis by proteases, these soil-bound enzymes make up a significant fraction of the active extracellular enzyme pool (Burns et al., 2013b; Nannipieri et al., 2002).

One aspect of the spatial heterogeneity of soil is so-called hot-spots. Microorganisms can only grow in favourable microhabitats, the so-called biological space (Pietramellara et al., 2002), which is only a small fraction of the total soil space — less than $10^{-6}$% of the total soil surface area (Or et al., 2007). These hot-spots of microbial activity can be found in soil, on organic debris, within and at the surface of porous soil aggregates and at root surfaces. In soil, we see a wide range of habitats with distinct microbial communities varying in population density, composition, and activity (Sokol et al., 2022). Zones of elevated biological activity — such as the hyphosphere, rhizosphere, and detritusphere — differ from the surrounding bulk soil in several environmental factors, such as nutrient, carbon, and water availability, as well as ionic composition, growth factors, pressure, temperature, pH, air composition, oxidation–reduction potential, spatial relationships, microbial interactions, and the genetic composition of the microbial community (Nannipieri et al., 2003).

Therefore, soil is heterogeneous at multiple scales (Nunan, 2017; Nunan et al., 2020). Although most biogeochemical models generalise micro-scale processes to the macro-scale, this type of upscaling ignores this spatiotemporal variability. Moreover, the heterogeneity of the soil matrix causes a decrease in microbial activity by making the substrate less accessible to microbes (Shi et al., 2021) and should thus be included in predictive models of soil carbon dynamics. For spatially implicit models, we would need to include the heterogeneity of space in their ordinary differential equations as a hard-coded, a priori feature. For instance, the uptake or decomposition rate equations could be modified to account for spatial heterogeneity.

The intricate arrangement of solids, which typically comprise more than half of the soil's volume, forms the soil matrix. The spaces between these solids, known as pore space, create a complex and tortuous network filled with liquid and gaseous phases. This geometry of pore space, which is better described using fractal geometry rather than traditional Euclidean methods (Dathe and Thullner, 2005), reflects the random assembly of soil components as a result of weathering and erosion from various sources, such as biological (Meysman et al., 2006; Aleklett et al., 2018), chemical, and physical processes, across different scales. These processes contribute to a self-similar structure that can be observed in the classification of pores by size, ranging from macropores (75–100 µm) to cryptopores (0.007–0.1 µm) (Cameron and Buchan, 2006). This self-similarity is a characteristic of fractals, objects that maintain a consistent shape across different scales of observation (Feder, 2013). However, in nature, this recursion has limits and is represented by non-integer dimensions. The fractal dimension, which varies depending on the complexity of the structure, underscores the diverse processes that generate natural fractals (Mandelbrot, 1983). The interplay between inheritance and multi-scaled randomness, both of which may contribute to the assembly of fractal-like structures, is crucial in shaping the soil's porous architecture, influencing its function, formation, and adaptation (Halley, 1996; Halley and Kunin, 1999).

To better understand the role of the spatial component of soil, micro-scale models have been leveraged, which can be characterized by the modelling strategy employed: the nature of the grid node/cell attributes and the degree of representativeness of soil architecture (Pot et al., 2022). For example, in a fairly simple model, connected, spherical spots of organic matter and of microorganisms are distributed in a three-dimensional volume. The size of the spots is the only variable accounting for spatial heterogeneity (Nunan et al., 2020). This approach ignores soil architecture while still considering heterogeneity by having the grid nodes vary in only one aspect. On the other side of the spectrum regarding architecture are models leveraging three-dimensional CT images of

undisturbed soil samples (Vogel et al., 2015, 2018; Portell et al., 2018) that need a lot of computational resources to run both in terms of floating point operations per second and random access memory. To have more manageable models, information from CT scans have been simplified. These simplifications range from so called morphological models where voxels are averaged into spheres and actual soil morphology is retained albeit coarse-grained (Vogel et al., 2005), to irregular pore-network models where CT information is used to build networks with varied node links (Xiong et al., 2016), to models where soil architecture is described using a regular grid of nodes/cells having either solid or pore phases according to statistical estimates inferred from multiple soil CT scans (Resat et al., 2012). As opposed to modelling soil pore space from CT images, another technique to model spatial relationships in soil is idealised soil architecture models to which the models in this study belong. These models such as two-dimensional regular pore-network models have been used to investigate for example emergence in bacterial colonies (Wang and Or, 2014) or their expansion by modelling motility of bacteria in soil (Wang and Or, 2010). Other idealised soil architecture models simulate soil pore space by assigning cells or nodes solid to pore phases along a continuous scale according to random distributions — e.g. to model interactions in soil fungi (Falconer et al., 2008). Clusters of nodes representing barriers to fungal hyphae and diffusion of solutes have also been used (de Ulzurrun et al., 2017). In ecosystem-scale models, soil architecture is also currently overlooked in soil hydraulic information used in pedotransfer functions that characterise the flow of water in soils. When soil structural features are included hydrologic and climatic responses are affected. Nevertheless, it remains to be seen whether their inclusion in ESMs has implications for global-scale climate predictions (Fatichi et al., 2020). Despite the unquestionable importance of spatial organisation, models that explicitly incorporate space remain the exception (Schimel, 2023).

In the following manuscript, we use computational models to explore how the micro-scale architecture of soil may influence SOC degradation dynamics by applying the same model to different spatial arrangements simulating pore space. We explore enzyme kinetics across a pore while varying its size. Furthermore, the Hilbert space-filling curve (a fractal) will be used to simulate pore space at different degrees of complexity. We also vary attributes of the individual particles to represent the effects of soil temperature and moisture. Our aim is to test whether spatial heterogeneity and structure, inherent properties of soil at the microscale, are consistent with traditional MM kinetics, which are based on the assumptions that the system is well-mixed and are used in larger-scale carbon circulation models — or whether we need to account for SOC decomposition differently.

# 2 Manuscript

## 2.1 Introduction

Soil constitutes a major reservoir of carbon on Earth, with about 2300 PgC stored in the top three metres, making soil organic carbon (SOC) the majority of actively cycling carbon in the terrestrial realm (Shukla et al., 2019). Earth system models (ESMs) have been constructed to predict the response of the Earth system to climate change. However, there remains considerable uncertainty in those models, especially regarding the land carbon cycle (Houghton, 2007; Azar and Johansson, 2022).

Microbes play a central role in soil carbon dynamics by transforming SOC into carbon dioxide through decomposition and respiration. The former process is mediated by extracellular enzymes that break down long-chain organic carbon compounds into much smaller molecules that can be taken up by microbial cells (Schimel and Schaeffer, 2012).

Environmental factors influence extracellular enzymes in soil through various mechanisms. As global temperatures are expected to rise by 1.5 to 4.8°C above pre-industrial levels by the end of this century (Rogelj et al., 2012; O'neill et al., 2017; Masson-Delmotte et al., 2021), extracellular enzyme activity could change as well in response. Since extracellular enzymes mediate numerous reactions in soil and contribute to several ecosystem functions such as nutrient cycling, decomposition, plant-microbe interactions and ultimately productivity and net carbon balance of the ecosystem, changing temperatures and precipitation patterns as well as elevated SOC input due to the fertilisation effect of higher carbon dioxide concentrations could trigger unexpected feedbacks that might amplify the initial warming (Arora et al., 2020). Understanding how extracellular enzyme kinetics are influenced by soil environmental factors such as moisture, temperature and soil architecture can provide insights into these feedbacks and improve predictions in biogeochemical models.

Another environmental factor that influences extracellular enzyme kinetics is soil moisture. Water availability affects the decomposition process mechanically by altering the ratio of liquid and gaseous phases in soil as well as the viscosity of the liquid, and therefore changes the accessibility of the substrate. Furthermore, as a key factor in

extracellular enzyme activity and community composition, soil moisture determines the diffusion rate of substrates, enzymes, and reaction products (Song et al., 2012) and therefore influences the activity of extracellular enzymes in soil (Burns et al., 2013a).

One assumption that current enzyme kinetics models have is that particles are purported to move freely and randomly in a well-mixed solution. In real soil, enzyme kinetics occurs in a tortuous network of tunnels called the pore space (Brady and Weil, 1999). Because weathering and erosion from multiple sources (biological, chemical, physical) and at multiple scales have created soil, the geometry of the pore space exhibits some level of self-similar scaling properties, resembling a fractal. Due to these multi-scale random processes that can generate self-similar structures, the geometry of pore space is more effectively described in models with the tools of fractal geometry than with traditional Euclidean geometry (Dathe and Thullner, 2005). Therefore, fractal geometry could become a powerful tool in order to understand soil processes that play out in soil pore space. Fractals are mathematical objects that have non-integer dimensions and show a degree of self-similarity (Halley, 1996; Halley and Kunin, 1999). Objects in the real world, such as soil, do not have to be true fractals, however, they must exhibit a certain degree of self-similarity over multiple scales.

Soil clearly has structures — such as pore openings — that can be found in a multitude of sizes. Pores can range in diameter from 0.007 $\mu m$ to 100 $\mu m$ (Cameron and Buchan, 2006). Soil therefore exhibits an incredible diversity of scales. This immense spatial heterogeneity, which extends down to the molecular scale, is overlooked by current mean-field descriptions of enzyme kinetics used in modern biogeochemical models, such as the Millennial V2 model (Abramoff et al., 2022), to represent microbial decomposition.

The assumption that soil extracellular enzymes move freely and exist in a well-mixed state is also challenged by the long-established fact that they can adsorb to clay minerals or become entrapped within humic acids and particulate organic matter. This stabilisation reduces enzymatic activity due to occlusion of active sites, conformational changes in the enzyme and restricting access to the substrate (Dick and Tabatabai, 1987). Additionally, some extracellular enzymes remain attached to the cell wall (Burns et al., 2013b; Traving et al., 2015).

In general, the activity of enzymes can be represented by a standard model of enzyme kinetics. Consider the following reaction:

$$\mathrm{E} + \mathrm{S} \underset{\mathrm{k_{-1}}}{\overset{\mathrm{k_1}}{\rightleftharpoons}} \mathrm{C} \xrightarrow{\mathrm{k_{cat}}} \mathrm{E} + \mathrm{P}, \tag{2.1}$$

where E, S, C, P are enzyme, substrate, enzyme-substrate complex and product,

respectively and the phenomenological rate constants for the reaction steps are $k_1$ and $k_{-1}$ for the reversible complex formation and $k_{cat}$ for the catalysis step (Marangoni, 2003). From the consideration of this fundamental process several mean-field descriptions of the relationship between the reaction rate and the substrate or enzyme concentration have been developed — for example, the Michaelis-Menten equation MM (Briggs and Haldane, 1925; Johnson and Goody, 2011), the reverse Michaelis-Menten equation rMM (Wang and Post, 2013) and the equilibrium chemistry approximation ECA (Tang and Riley, 2013; Tang, 2015) that describe the saturation of the reaction rate as substrate or enzymes are added to the system.

A quantitative theory of enzyme kinetics was first proposed in 1913 by Leonor Michaelis and Maud Menten. This first model (the MM equation) assumes that the substrate concentration has reached a stable equilibrium very early due to the rapid formation of the enzyme-substrate complex, governed by the very fast rate constants $k_1$ and $k_{-1}$. Termed the equilibrium approximation, it allows for the derivation of macro-parameters $V_{max}$ — the maximum reaction rate — and $K_m$ — the half-saturation or Michaelis constant — from the phenomenological rate constants ($k_1$, $k_{-1}$ and $k_{cat}$) and the total enzyme concentration. $V_{max}$ and $K_m$ determine the shape of the saturation curve that emerges when the reaction rate is plotted against the substrate concentration, where the curve converges to the reaction rate $V_{max}$ and $K_m$ is the substrate concentration at $\frac{1}{2}V_{max}$.

In 1925, G. E. Briggs and J. B. S. Haldane developed another model, termed the quasi-steady-state approximation. It assumes that $k_{cat}$ is much faster than $k_1$ and $k_{-1}$ leading to a near-constant concentration of the enzyme-substrate complex (Olkiewicz et al., 2020).

Soil architecture, temperature, and moisture influence the encounter rate of extracellular enzymes with their substrate, thereby affecting the rate constants ($k_1$, $k_{-1}$, and $k_{cat}$). Consequently, these factors can alter the conditions under which the fundamental assumptions of enzyme kinetic models remain valid (Marangoni, 2003).

Despite the fact that soils being spatially structured at the microscale, most soil models approximate enzyme reactions using MM kinetics which were developed for well-mixed systems (Chakrawal et al., 2020). It remains unknown whether these approximations correctly reflect enzyme dynamics in the diverse spatially structured environments of soil microbes, or how they may be affected by variations in spatial structure at the soil microscale.

As a bottom-up approach, individual-based models try to investigate patterns and processes from first principles, i.e., by deriving them from underlying assumptions on features of individuals, their behaviour, and their interactions within an explicitly modelled

space. These interactions gradually generate larger patterns and processes over time as emergent phenomena (Kaiser et al., 2014, 2015). Individual-based models, also known as agent-based models, endow each individual (in this study, particles) with certain attributes — also called state variables — and behaviours.

In order to better understand the effect of microscale spatial environments on extracellular enzyme kinetics, we developed an individual-based model that simulates enzyme reactions at the molecular level in spatially structured microenvironments. This model allows us to infer the effect of spatial structures that are typical of soil on enzyme kinetics and to evaluate how environmental factors that directly affect the first principles of molecular interaction ultimately govern enzyme kinetics in a spatial setting.

In this study, we leverage three individual-based models (also called scenarios) to address the question of how the heterogeneity of space might affect enzyme kinetics. The agents of our individual-based models are substrate, enzyme, substrate-enzyme complex, and product particles that undergo a random walk and interact with one another. By changing the attributes of these particles, we simulate soil environmental factors such as moisture and temperature. Our first scenario reproduces enzyme kinetics under well-mixed conditions. It functions as a null model without spatial structures. The second and third scenarios have spatial structures incorporated into their grids to simulate soil architecture. One investigates enzyme kinetics across a pore, while the other examines enzyme kinetics within a maze composed of self-similar fractal structures.

Recently, increasingly complex models involving soil microbes have been developed to reduce uncertainty in terrestrial carbon cycle predictions. Furthermore, soil architecture is currently overlooked by modellers, who assume enzyme kinetics occurs in well-mixed systems without spatial heterogeneity. We aim to shed light on how microscale heterogeneity of soil pore space affects microbial SOC degradation dynamics.

In our study, the individual-based model approach allows us to directly investigate the phenomenological rate constants $k_1$, $k_{-1}$ and $k_{cat}$, something that would be impossible to achieve in the laboratory. Four micro-parameters controlling the enzyme kinetics have been implemented as attributes of the particles in our model. By relating these micro-parameters, as well as spatial arrangements of barriers representing soil architecture to the macro-parameters of the Michaelis-Menten curve, we can directly test the underlying assumptions of current enzyme kinetics models.

The intricate dynamics of extracellular enzymes at the molecular scale are relevant to larger biogeochemical models because the selection of enzyme kinetics representing the microbial decomposition step in soil influences the large-scale dynamics of carbon cycling in these models (Schwarz et al., 2024; Chakrawal et al., 2020).

## 2.2 Methods

### 2.2.1 Micro-parameters and Behaviour of Models

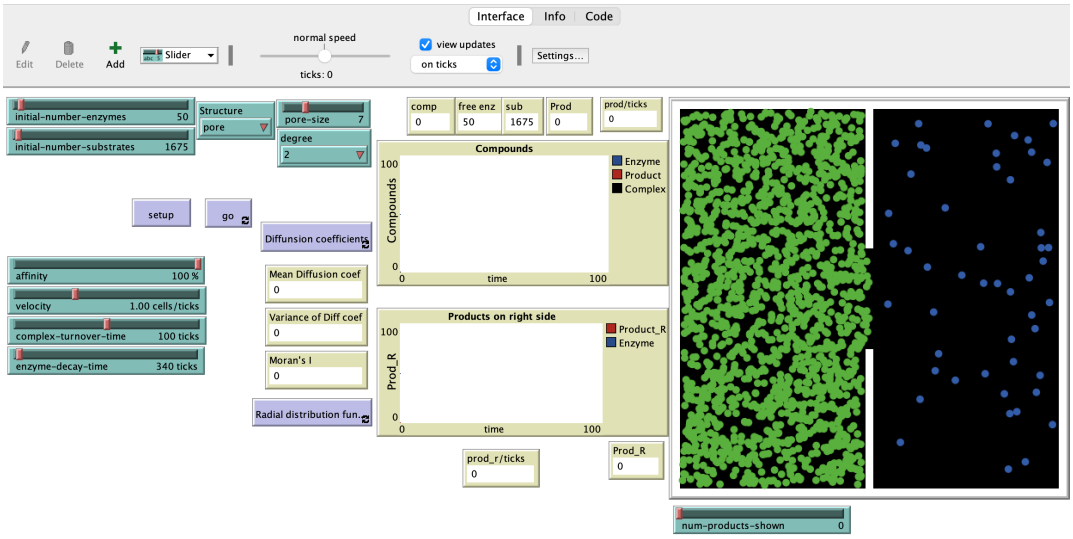


Figure 2.1: Layout of the Netlogo simulation

Individual-based models are leveraged in Netlogo version 6.3 (Fig. 2.1) to investigate how extracellular enzyme kinetics respond to environmental factors under different degrees of spatial heterogeneity. The agents or individuals in this model are substrate, enzyme, complex, and product particles. These individuals move on a two-dimensional grid and interact with one another. At the molecular scale, the enzyme reacts with the substrate forming a complex and after some time the complex turns into product and enzyme. However, this enzymatic process is calculated in biogeochemical models at the aggregated scale using Michaelis-Menten kinetics. While the macro-scale derived parameters $V_{max}$ and $K_m$ are needed to describe the enzyme reactions in aggregated models, the parameters which are necessary to describe the process at the molecular scale are directly related to the molecular properties of the particles, which are 1) particle velocity, 2) substrate-enzyme complex turnover rate, 3) affinity between enzymes and substrate and 4) enzyme decay time. We used these particle properties as micro-parameters in our individual-based model. In this model, velocity represents the distance particles travel per time step, substrate-enzyme complex turnover rate is the inverse of the time required for the complex to form the product, affinity is the probability that an enzyme forms a complex upon encountering a substrate, and enzyme decay time refers to the duration an enzyme remains

active. As soon as the enzyme has decayed a new enzyme enters the model keeping the enzyme concentration always constant throughout the run.

As time passes, a production rate emerges that is constant for a certain enzyme and substrate concentration. By adding more and more substrate the production rate increases until a saturation is achieved. This saturation curve, that is the Michaelis-Menten curve, changes when we vary the micro-parameters. We therefore can relate the micro-parameters (particle properties) to the macro-parameters ($V_{max}$ and $K_m$) of the Michaelis-Menten curve. This happens in varied spatial contexts that are meant to represent soil pore space.

There are three model variants that vary in their spatial structure: the well-mixed scenario, the pore scenario, and the maze scenario. All three models share that the point particles (enzymes, substrates, complexes and products) undergo a random walk with a certain speed determined by the velocity micro-parameter simulating Brownian motion. Dynamics of all three models play out on a grid. The central process of catalysis is also shared by all scenarios.

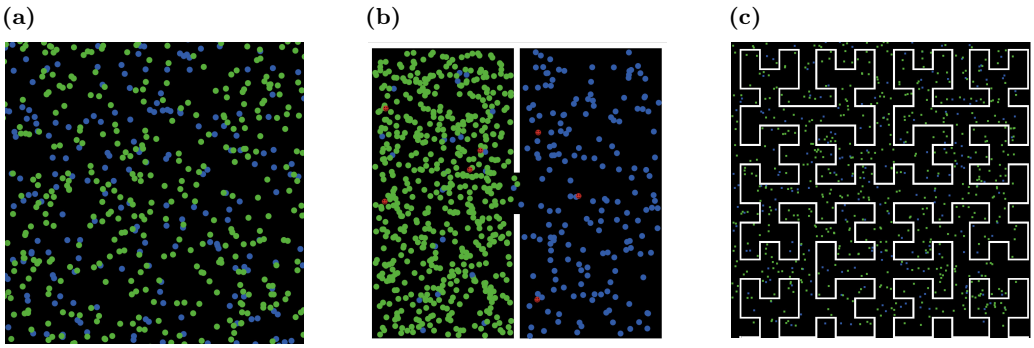


Figure 2.2: Systems of Netlogo models, substrate (green), enzyme (blue) and product particles (red), spatial barriers (white), (a) Well-mixed model; (b) Pore model; (c) Maze model (degree 4)

The well-mixed scenario (see Fig. 2.2a) has no spatial structure. Enzyme and substrate particles diffuse freely. This model serves as a null model in regards to the effects of spatial heterogeneity on enzyme kinetics and also with it the effect of the micro-parameters (velocity, complex turnover rate, affinity, decay time) on the macro-parameters ($K_m$, $V_{max}$) was investigated.

The pore scenario (see Fig. 2.2b) represents a pore that is filled with substrate. On the other side of the pore, the enzymes are secreted by a microbe. However, we only simulated the enzymes not the whole microbe. The model is a closed square that is split in the middle. Particles can diffuse from one side to the other across an opening representing a

pore. This model simulates the situation that substrate in a pore is inaccessible directly to the microbe because the pore is too small for the microbe to enter. Rather, it has to secrete enzymes that diffuse inside the pore, react with the substrate and generate product that has to diffuse outside again, for the microbe to take up the product. Therefore, the pore opening has to be crossed twice, the first time by the enzyme to get to the substrate and the second time by the product to reach the microbe. This process is quite different from traditional enzyme kinetics models.

With the maze scenario (see Fig. 2.2c) we investigated the effects of spatial heterogeneity on enzyme kinetics by placing progressively more complex arrangements of barriers into the grid using the Hilbert space-filling curve. One property of the Hilbert curve is that it is self-similar meaning we find similar shapes at different scales. We used it to try to mimic soil pore space assuming pore space to have fractal properties because of the way it is made, i.e., by biological, chemical and physical weathering and erosion across different scales.

Velocity, complex turnover rate and affinity are the three central micro-parameters of all three model variants controlling the kinetics of the system. The other micro-parameter that is only really relevant for the pore and maze scenarios is the decay parameter. The decay micro-parameter determines how long an enzyme exists in the world. When time is up, the enzyme stops existing and at the same time step a new enzyme is either randomly placed in the whole grid in the well-mixed and maze model variants or, in the pore model, randomly placed only on the right side of the grid representing the space outside the pore. The enzyme cannot decay while bound to the substrate in the complex.

### 2.2.2 Implementation of Particle Behaviours

There are four behaviours the particles can exhibit. Random movement (1) to simulate Brownian motion is implemented the following way: At every time step the heading of particles is changed by a random floating point number between 0° and 360°. After the heading is determined particles jump ahead by a certain number of grid cells specified by the velocity micro-parameter. Collision (2) of substrate and enzyme works as follows: at every time step all enzyme particles check if a substrate particle is present on the same grid cell. If at least one substrate particle is present, the enzyme particle and one randomly chosen substrate particle on the same cell disappear and on the same grid cell a complex particle is created which moves around in the same random manner as described above. After the complex has produced the product, the substrate particle reappears at some random position on the grid in the maze and the well-mixed models.

In the pore model the substrate particle is placed only on the left side of the grid, which represents the interior of a pore. Thus, the total number of substrate particles stays always the same which is a condition of the equilibrium approximation (see Methods: Derivation of macro-parameters). The assumption is that the substrate that is degraded by the enzyme is replaced by substrate from the outside, i.e the SOC pool. We therefore assume that at the time scales we measure enzyme kinetics this SOC pool is shrunk by the decomposition only in a marginal way that does not affect the replacement rate of the substrate. Production (3) of the product by the complex particle happens after a certain number of time steps determined by the complex turnover rate micro-parameter. The complex ceases to exist and on the same grid cell a product and an enzyme particle are created that have a certain random heading. The enzyme particle holds the same decay time as the enzyme that was involved in the creation of the complex. Reflection (4) — only relevant for the pore and maze models — is the interaction of the particles with the spatial barriers that were put into the grid. The particle checks if the grid cell ahead is a barrier. If it is, the particle calculates the angle between its current heading and the barrier's orientation. It then changes its heading by this angle away from the barrier, implementing elastic reflection, which assumes that the particle's momentum is conserved. This boundary handling technique is a necessary simplification to avoid particle build up at the barriers (Germano et al., 2023).

### 2.2.3 Conversion of Units

From the median of the range of the translational diffusion coefficients of enzymes in water at 20°C, which is 10 to 100 $\mu m^2/s$ (Zhang and Hess, 2019) and the maximum molecular size of a substrate (dissolved organic matter particle) which is 0.45 $\mu m$ (Xu and Guo, 2018), we estimated the time and length dimensions of the model, where one grid cell is estimated to be a square with 3.5 $\mu m$ lengths, due to the maximum density used being about 7.7 substrate/grid cell, and one time step being $10^{-5}$ seconds.

Our estimate is at the upper limit of a possible substrate molecule. Assuming smaller substrate particle sizes would reduce size of each grid cell and duration of a time step accordingly.

### 2.2.4 Derivation of Macro-parameters

Consider the following chemical reaction:

$$\mathrm{E} + \mathrm{S} \underset{\mathrm{k}_{-1}}{\overset{\mathrm{k}_1}{\rightleftharpoons}} \mathrm{C} \xrightarrow{\mathrm{k}_{\mathrm{cat}}} \mathrm{E} + \mathrm{P}, \tag{2.2}$$

where E, S, C, P, $k_1$, $k_{-1}$, $k_{cat}$ are enzyme, substrate, enzyme-substrate complex, product, and rate constants for the reaction steps, respectively. We can derive the following ordinary differential equations:

$$\frac{dS}{dt} = -k_1 \cdot E \cdot S + k_{-1} \cdot C, \tag{2.3}$$

$$\frac{dE}{dt} = -k_1 \cdot E \cdot S + (k_{-1} + k_{cat}) \cdot C, \tag{2.4}$$

$$\frac{dC}{dt} = k_1 \cdot E \cdot S - (k_{-1} + k_{cat}) \cdot C, \tag{2.5}$$

$$\frac{dP}{dt} = k_{cat} \cdot C. \tag{2.6}$$

The equilibrium approximation assumes that $k_1$ and $k_{-1}$ are very large so that a substrate equilibrium is reached very fast and $\frac{dS}{dt} = 0$. Then:

$$0 = -k_1 \cdot E \cdot S + k_{-1} \cdot C.$$

Let the total enzyme concentration be $E_T = E + C$, substituting this into the equation above:

$$0 = -k_1 \cdot (E_T - C) \cdot S + k_{-1} \cdot C.$$

Therefore:

$$C = \frac{E_T \cdot S}{S + \frac{k_{-1}}{k_1}}.$$

Substituting this into the production rate gives:

$$\frac{dP}{dt} = v = k_{cat} \cdot \frac{E_T \cdot S}{S + \frac{k_{-1}}{k_1}}. \tag{2.7}$$

When we define the macro-parameters $V_{max} = k_{cat} \cdot E_T$ and $K_m = \frac{k_{-1}}{k_1}$, we get the familiar Michaelis-Menten equation:

$$v = \frac{V_{max} \cdot S}{S + K_m}. \tag{2.8}$$

The quasi-steady-state approximation assumes that $k_{cat}$ is much larger than $k_1$ and $k_{-1}$ and that therefore the complex concentration is in equilibrium ($\frac{dC}{dt} = 0$). Then:

$$0 = k_1 \cdot E \cdot S - (k_{-1} + k_{cat}) \cdot C$$

.

Substituting $E_T = E + C$ gives us:

$$0 = k_1 \cdot (E_T - C) \cdot S - (k_{-1} + k_{cat}) \cdot C$$

.

Therefore:

$$C = \frac{E_T \cdot S}{S + \frac{k_{-1}+k_{cat}}{k_1}}.$$

Substituting this again into the production rate yields:

$$\frac{dP}{dt} = v = k_{cat} \cdot \frac{E_T \cdot S}{S + \frac{k_{-1}+k_{cat}}{k_1}}. \tag{2.9}$$

While $V_{max}$ stays the same no matter the assumptions chosen, $K_m = \frac{k_{-1}+k_{cat}}{k_1}$ has changed in comparison to the equilibrium approximation. (Olkiewicz et al., 2020)

### 2.2.5 Construction of the Hilbert Curve

To construct the Hilbert space-filling curve — that is used in the maze model to represent self-similar pore space — you start with the degree one curve as shown in Fig. 2.3a. For the next degree, the degree 1 curve is replicated in every quadrant. In the lower right quadrant, it is rotated anti-clockwise for 90° while in the lower left quadrant, it is rotated 90° clockwise. Also, the sense of curves in both lower quadrants is reversed. Both upper quadrants are replicated as is, without rotation or sense change. Connecting the quadrants gives us the Hilbert curve degree 2 (see Fig. 2.3b). For all higher degree curves (see Fig. 2.3c,d,e,f) this procedure is repeated with the curve one degree below them. (Jagadish, 1997)

### 2.2.6 Space Representation

In the well-mixed and maze scenarios, enzyme kinetics was carried out on squares with periodic boundary conditions. All dynamics happen at very small length and time scales. The size of the grid in the well-mixed model was 51 times 51 cells — which is estimated to be 31862.25 $\mu m^2$ or approximately 0.03 $mm^2$ —, whereas in the maze scenario, it

was 161 times 161 cells estimated to be 317532.25 $\mu m^2$ or approximately 0.3 $mm^2$. In the pore scenario, space is evenly split into right and left sides and has closed boundary conditions. In this model, the enzymes would start on the right and diffuse through a pore to the left side of the grid where the immobile substrate particles are located. After the product is generated, it also has to first diffuse through the pore. The grid of the pore scenario is like the well-mixed scenario approximately 0.03 $mm^2$ large.

### 2.2.7 Calculation of the Reaction Rate

The reaction rate was measured as the number of product particles generated by unit of time and was calculated for every model run in the following way:

$$v = \frac{P_2 - P_1}{t_2 - t_1}, \tag{2.10}$$

where $P_2$ is the number of product particles at the end of the simulation run and $P_1$ at half of the simulation run and $t_2$ are the number of time steps at the end of the simulation run and $t_1$ at half of the simulation run.

The first half of the time series was discarded to avoid incorrect calculation due to initial transient dynamics.

### 2.2.8 Non-linear Curve Fitting

Curve fitting using non-linear least squares regression was performed in R version 4.3.1 with the nls function. The Gauß-Newton algorithm was used to fit a Michaelis-Menten model (see Eq. 2.8) to simulation results by finding the optimal $K_m$ and $V_{max}$ values.

### 2.2.9 Relating Micro- to Macro-parameters

As a result of the non-linear least squares regression, the macro-parameters ($K_m$, $V_{max}$) determine the shape of the reaction curve where the substrate concentration is plotted against the reaction rate. Since the micro-parameters are known, a well-fitted curve can give us the relationship between micro- and macro-parameters.

Five values for complex turnover rate and affinity micro-parameters and six values for the velocity micro-parameter were varied (see Table 2.1) giving us $5 \times 5 \times 6 = 150$ parameter combinations. A Michaelis-Menten model was fitted to each of the combinations. Subsequently, a least squares linear regression model was performed in R using the lm function giving us an equation that relates the micro-parameters to the macro-parameters.

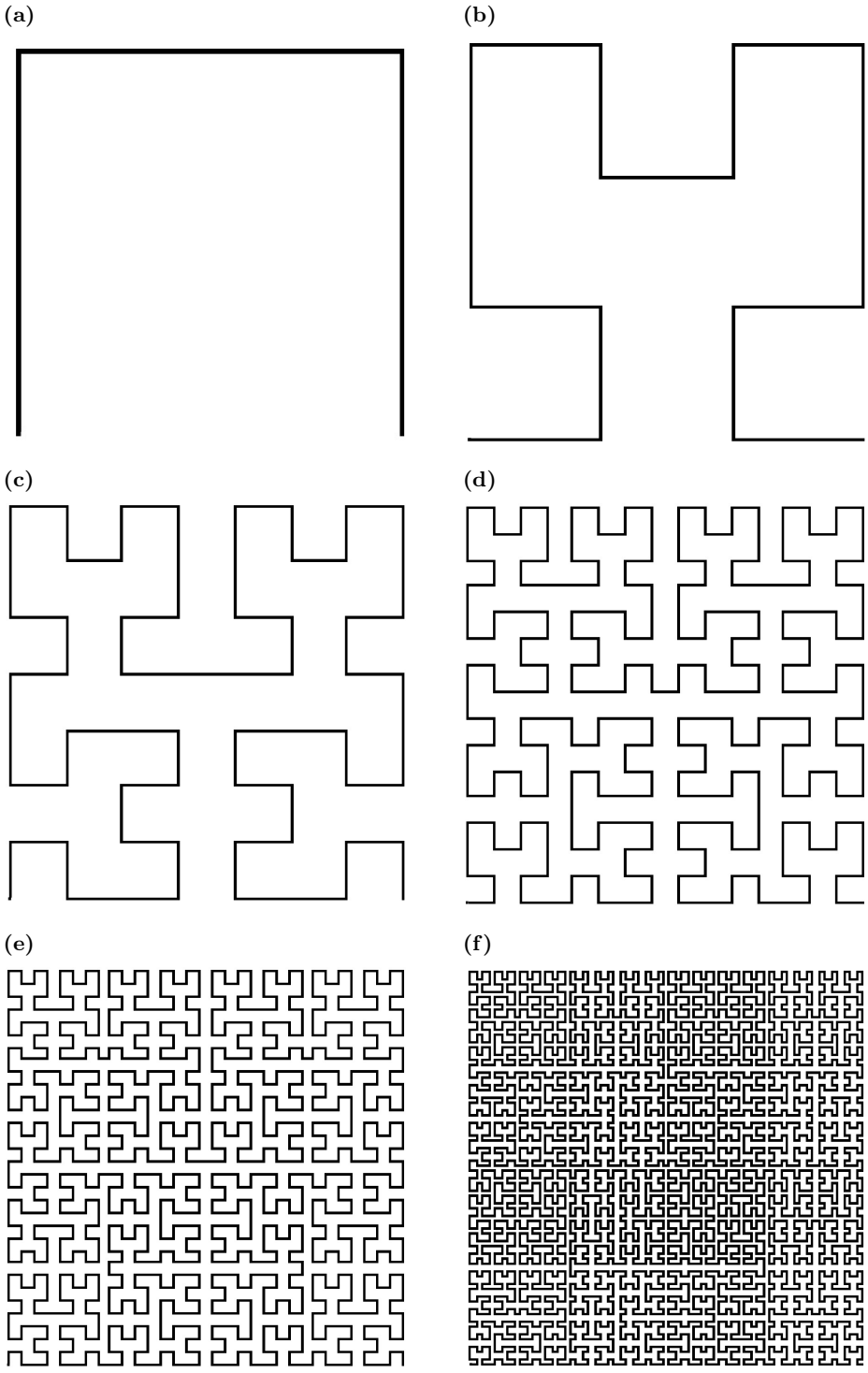


Figure 2.3: a-f Hilbert curves degrees 1-6, respectively

Table 2.1: Micro-parameter values

| velocity $[\mu m/ms]$ | complex turnover rate $[ms^{-1}]$ | Affinity[%] |
|---|---|---|
| 0.35 | 0.83 | 1 |
| 1.75 | 0.71 | 5 |
| 3.5 | 0.63 | 10 |
| 35 | 0.56 | 15 |
| 175 | 0.5 | 20 |
| 350 | — | — |

### 2.2.10 Local Diffusion Coefficient

In the maze models with spatial structure (models with degree 1 to 6), the location of the cell in relation to the barriers has an impact on its local diffusion coefficient.

The local diffusion coefficient D was calculated by sending out ten particles that undergo a random walk for ten time steps. After this time, the particles reported back their Euclidean distance to their origin cell. From these distances the mean squared displacement MSD = $\langle x^2 \rangle$ was calculated. D was calculated by dividing the MSD by the number of time steps. D was then averaged over all cells of a model variant.

In addition, Moran's I of the local diffusion coefficients — giving us a sense of the amount of spatial clustering due to structures that were placed in the maze models — was calculated the following way:

$$I = \frac{N}{W} \frac{\sum_{i=1}^{N} \sum_{j=1}^{N} w_{ij}(D_i - \bar{D})(D_j - \bar{D})}{\sum_{i=1}^{N}(D_i - \bar{D})^2},$$

where $N$ is the number of cells, $D$ is the local diffusion coefficient, $w_{ij}$ is the matrix of spatial weights and $W$ is the sum of all spatial weights. Moran's I is a measure of spatial autocorrelation, which tells us whether high or low values of a variable (in this case, the local diffusion coefficient D) are clustered, randomly distributed, or dispersed. A positive Moran's I suggests that similar diffusion values are spatially clustered, while I $\approx 0$ implies a random spatial distribution with no significant clustering. In contrast, a negative Moran's I indicates a dispersed pattern, where neighboring cells tend to have very different diffusion values. However, instead of a matrix of weights that defines how cells influence each other, we made a computational simplification only considering the 8 neighbouring cells of each cell (the $d = 1$ Moore neighbourhood).

### 2.2.11 Radial Distribution Function

The radial distribution function, $g(r)$, provides a measure of how the density of one type of particle (here, substrates) varies as a function of distance from another type of particle (here, complexes). It essentially tells us whether particles are randomly distributed, clustered, or evenly spaced. By calculating $g(r)$, we can determine how substrates are distributed around complexes and whether external factors influence this spatial organization.

The $g(r)$ was assessed from complexes to see whether a low velocity micro-parameter setting introduces heterogeneity in the distribution of substrates in the well-mixed model and to see whether spatial barriers bring about a seperation of enzymes from substrate in the maze model. $g(r)$ was calculated by counting the number of substrates a certain number of grid cells away from the complexes and dividing by the area. The local $g(r)$ of every complex was then averaged to give us a global $g(r)$.

## 2.3 Results

### 2.3.1 The Well-mixed Scenario

#### Model set-up and assumptions of the well-mixed scenario

Our model is set up in such a way that the substrate and enzyme concentrations are forced to be constant by replenishing those particles at key events — when the enzyme has decayed and when the substrate was turned into the product. The complex and product concentrations emerge from the interactions of enzymes with the substrate. To test the assumptions that the complex, substrate, enzyme, and product concentrations are in equilibrium, the time series of the particles were investigated (see Fig. 2.4).

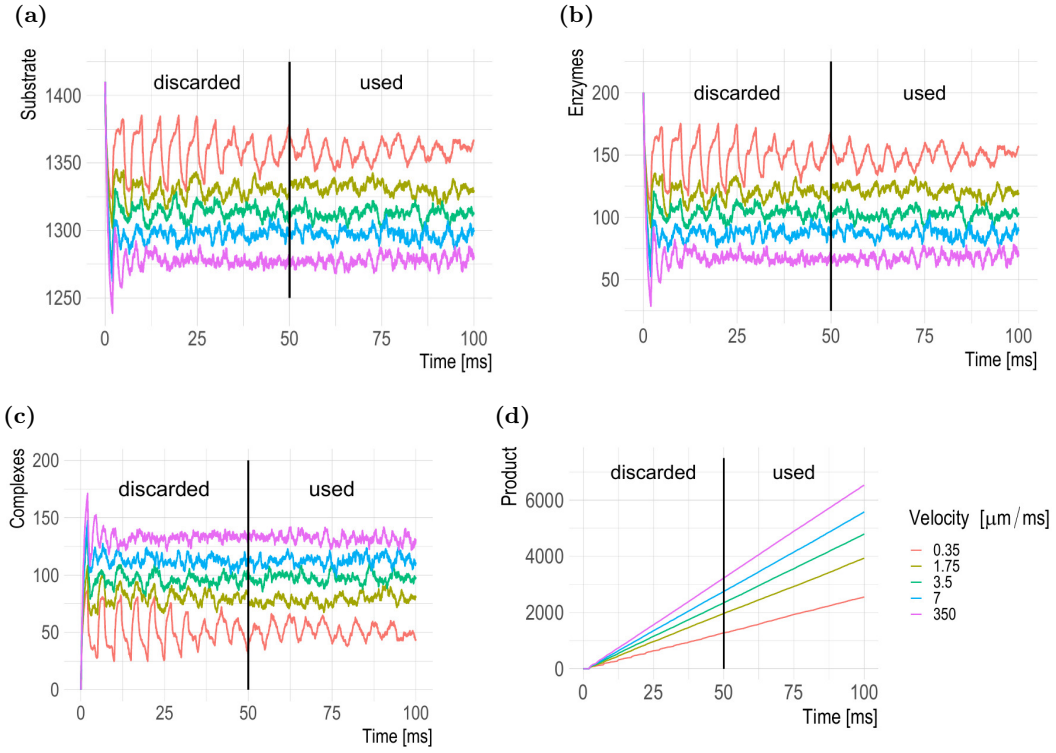


Figure 2.4: Time series of particles (substrate (a), enzymes (b), complexes (c), products (d)) in the well-mixed model under different velocity micro-parameter settings. The first half was discarded due to initial transients. Initial number of enzyme particles = 200. Initial number of substrate particles = 1410. Other micro-parameters: complex turnover rate = 0.5 $ms^{-1}$, affinity = 2%

The equilibrium approximation and the quasi-steady-state approximation from which

the Michaelis-Menten equation is developed have the assumption that the substrate or the complex concentration is in equilibrium, respectively. With velocity settings, the number of complex, enzyme, product and substrate particles change.

However, the average particle numbers of substrate, enzymes and complexes in one velocity class stay approximately the same with time when the system reaches dynamic equilibrium. The number of product particles increases linearly with time when the system has reached a steady state. For further analysis, the first half of the time series from 0 to 50 ms was discarded. It was especially critical to discard the product particle numbers at the very beginning of the time series in order to calculate the reaction rate accurately. For the well-mixed model, all average particle numbers behave as expected and the assumptions of the equilibrium approximation as well as the quasi-steady-state approximation hold. This is relevant because we test these models for the macro-parameters (that have been derived from the rate constants) by relating the micro- to the macro-parameters.

### Reaction curves in the well-mixed scenario

The well-mixed scenario serves as a null model without spatial structures. It allows us to examine how micro-parameters — such as complex turnover rate, velocity, and affinity — affect enzyme kinetics. Specifically, we study their influence on the Michaelis-Menten curve, which describes the relationship between substrate concentration and reaction rate. The Michaelis-Mente equation is characterized by two parameters: the half-saturation constant ($K_m$) and the maximum reaction rate ($V_{max}$). The constant $K_m$ represents the substrate concentration at which the reaction rate reaches half of $V_{max}$, while $V_{max}$ defines the upper limit of the reaction rate when the substrate concentration is sufficiently high.

To analyse this relationship, we generated reaction curves by varying the initial substrate concentration across multiple simulation runs while keeping the enzyme concentration fixed at 200 particles. In each run, we measure the reaction rate (see Eq. 2.10), which increases with substrate concentration until it approaches $V_{max}$. By plotting the reaction rate as a function of the initial substrate concentration, we obtain a set of data points that define the reaction curve. This curve is then fitted using the Michaelis-Menten equation.

To assess the impact of individual micro-parameters on the reaction curve, we systematically vary one micro-parameter at a time while keeping the others constant. This approach allows us to isolate their effects and better understand their role in shaping enzyme kinetics.

The decay micro-parameter shows no effect on reaction curves in the well-mixed scenario

(not shown). It is only really relevant for the pore and maze scenarios, because after the enzyme decayed a new enzyme is placed on the grid in a random location. Therefore, in the well-mixed scenario where there is no spatial structure, the location of enzymes did not matter.

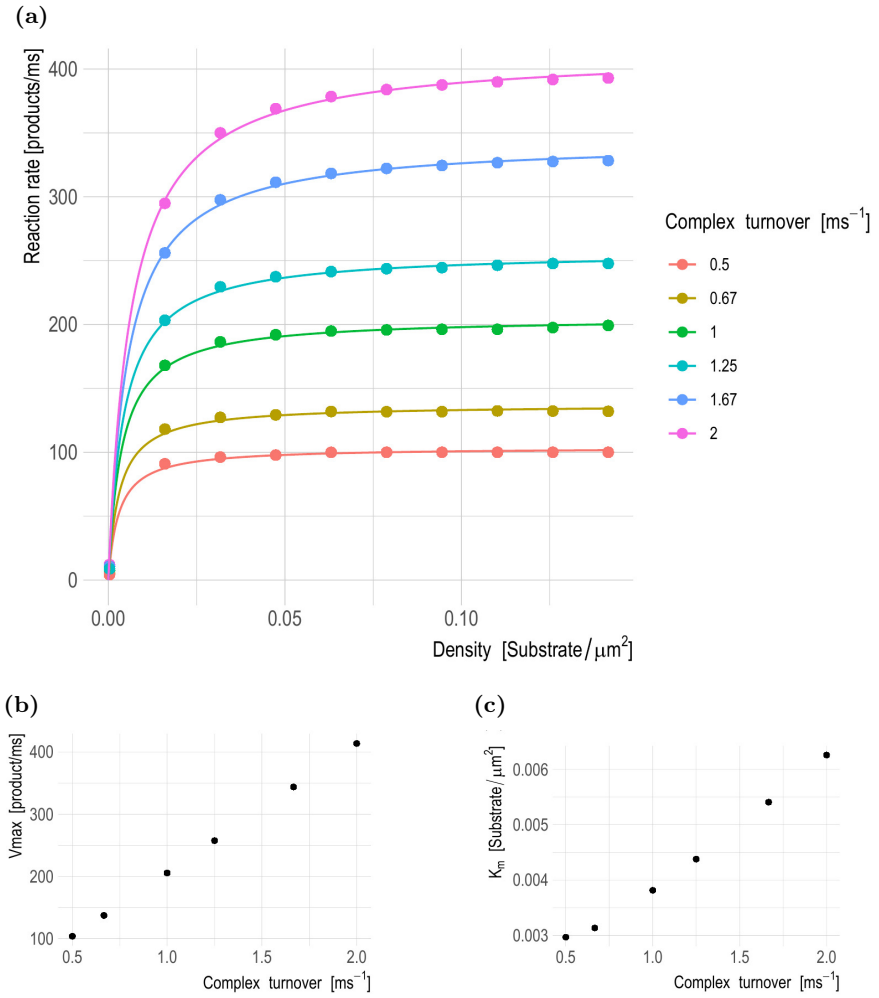


Figure 2.5: Reaction curves (a), the maximum rate of reaction $V_{max}$ (b) and the half-saturation constant $K_m$ (c) varying the complex turnover rate micro-parameter, i.e, the inverse of the lifetime of a complex in milliseconds (ms). Initial number of enzyme particles = 200. Other micro-parameters: affinity = 50%, velocity = 175 $\mu m/ms$

**Complex turnover rate.** The fully saturated reaction curves (see Fig. 2.5a) show a perfect fit for all simulated values of the complex turnover rate. We chose values between

0.5 $ms^{-1}$ and 2 $ms^{-1}$ for the complex turnover rate micro-parameter — which determines the time a complex exists from the initial binding of the enzyme to the substrate to the dissociation into product and free enzyme. For the other micro-parameters we chose an affinity of 50% resulting in half of the reactions, after an enzyme encountered a substrate particle, being successful, i.e., a complex was created, and a velocity of 175 $\mu m/ms$ which is a relatively high velocity avoiding effects that emerge under a low-velocity regime (see velocity section). Both $V_{max}$ and $K_m$ linearly increase with the complex turnover rate (see Fig. 2.5b and c, respectively). The reaction rate constant of the complex $k_{cat}$ (see Eq. 2.1) is in theoretical derivations proportional to $V_{max}$ in both the equilibrium approximation and the quasi-steady state approximation. However, for $K_m$, $k_{cat}$ is only present in the former. Since there is an effect of the complex turnover rate — which is a proxy for $k_{cat}$ — on $K_m$, our simulation results point towards the quasi-steady state approximation.

**Affinity.** Next, we test how the relation between the reaction rate and the initial number of substrate particles changes for different affinity settings. The reaction curves (see Fig. 2.6a) varying affinity show a good fit except at high affinities (affinity $> 40\%$). The difference in the height of the curves in Fig. 2.6a is because the simulation was only run to a substrate density of about 0.6 particles/$\mu m^2$. Only the curves with higher affinity are saturated at this substrate density. If we would run the model with high enough substrate concentrations we would see all curves converge to the same approximate maximum reaction rate (which is about 200 products/ms). This is shown in Fig. 2.6b, where $V_{max}$ does not change with affinity. On the other hand, $K_m$ increases linearly with the inverse of affinity (see Fig. 2.6c) which is the reason why we see in Fig. 2.6a the unsaturated reaction curves when affinity is lower than 10% where differences in $K_m$ become more pronounced. Affinity determines the efficiency of the binding process (how many enzyme-substrate-encounters are successful). When this process is less efficient the substrate density needs to be higher to reach the same reaction rate. We chose an affinity from 100% to 0.25%. For the other micro-parameters that were chosen to create the reaction curves we see in Fig. 2.6a, we picked a moderate complex turnover rate and a relatively high velocity to avoid the effects of the low-velocity regime. In theoretical models the rate constants $k_1$ and $k_{-1}$ describe the rate of the binding process and the reversal of the binding process, respectively. Affinity can be seen as a proxy for $k_1$ and $k_{-1}$, which play only a role for the $K_m$ macro-parameter in both the equilibrium approximation model and the quasi-steady state model. Thus, our simulation results are in agreement with both theoretical frameworks.

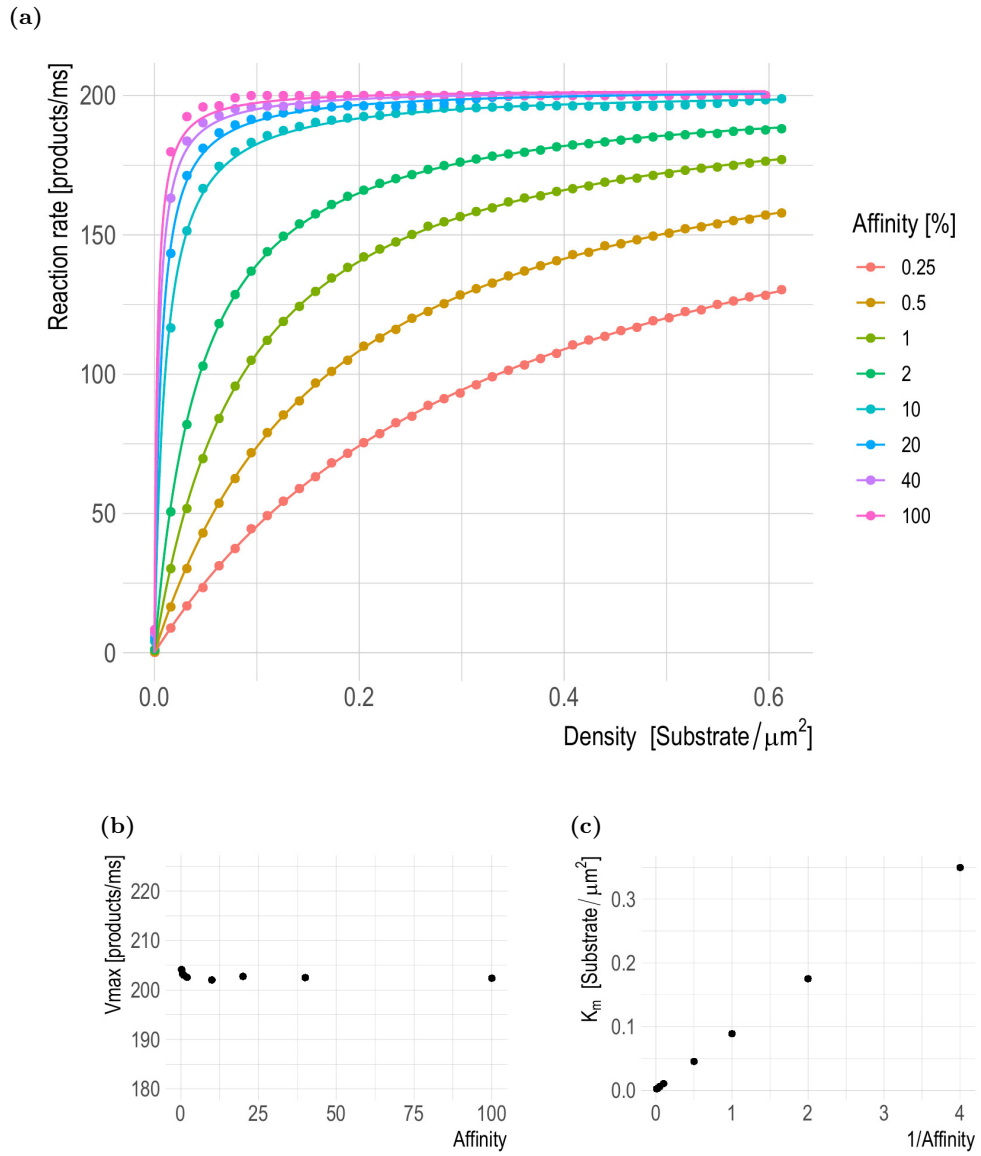


Figure 2.6: Reaction curves (a), the maximum rate of reaction $V_{max}$ (b) and the half-saturation constant $K_m$ (c) varying the affinity micro-parameter, i.e, the probability (measured in %) that a substrate-enzyme collision generates a complex particle. Initial number of enzyme particles = 200. Other micro-parameters: complex turnover rate = 1 $ms^{-1}$, velocity = 175 $\mu m/ms$

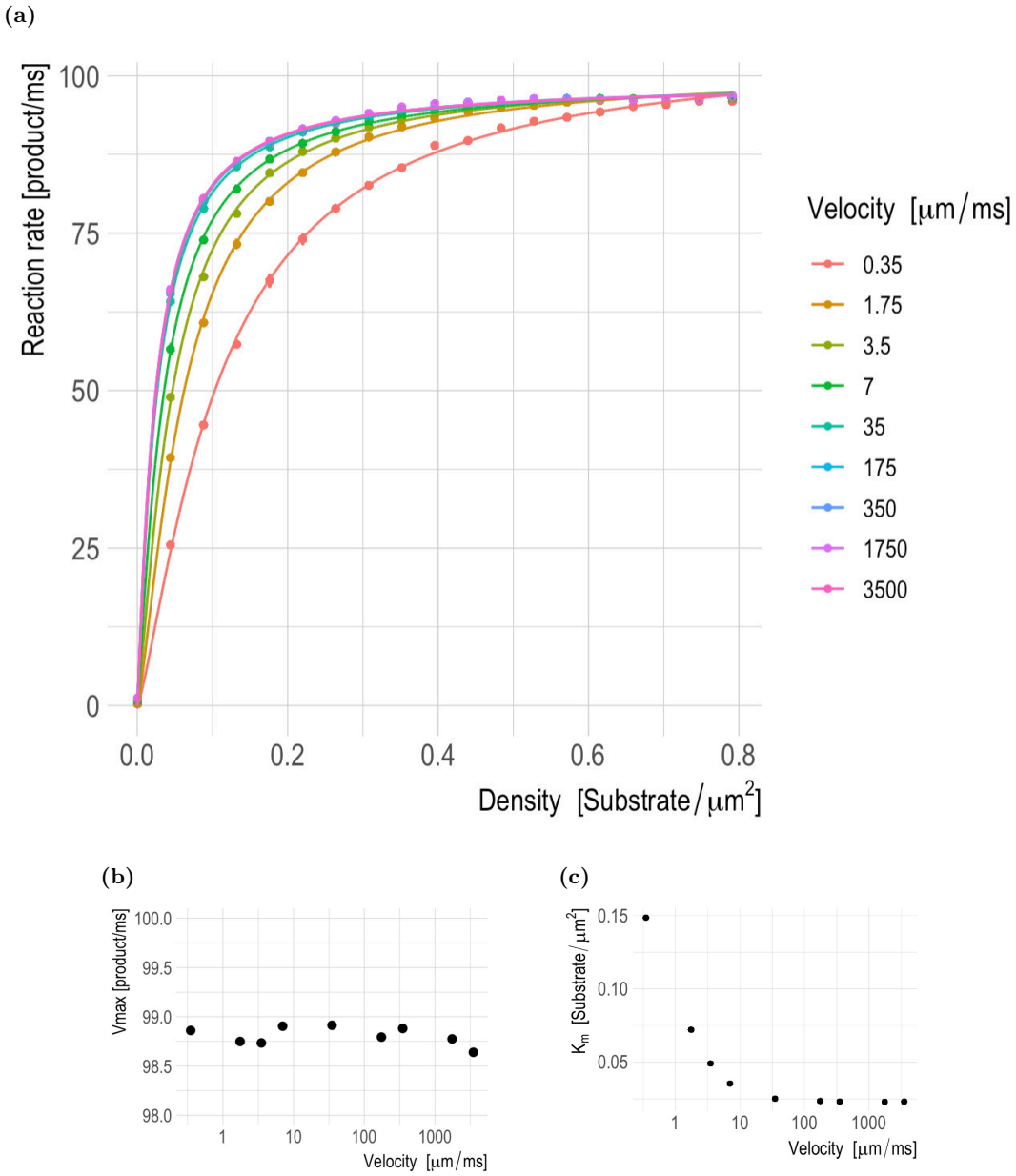


Figure 2.7: Reaction curves (a), the maximum rate of reaction $V_{max}$ (b) and the half-saturation constant $K_m$ (c) varying the velocity micro-parameter, i.e., the distance (in $\mu m$) that a particle travels in 1 $ms$. Initial number of enzyme particles = 200. Other micro-parameters: complex turnover rate = 0.5 products/ms, affinity = 2%; b, c: x-Axis has $log_{10}$ scale

**Velocity.** The reaction curves that emerge when varying the velocity micro-parameter while keeping the other micro-parameters constant (see Fig. 2.7a) show a good fit for all velocity values. Additionally, the reaction curves that emerged in the $> 7\ \mu m/ms$ regime do not differ from each other, while reaction curves where particles moved slower and equal to $7\ \mu m/ms$ do differ. We can see in Fig. 2.7b that $V_{max}$ is constant with velocity. On the other hand, $K_m$ (see Fig. 2.7c) decreases with velocity for velocity values under 35 $\mu m/ms$ and stays constant for higher velocity values. For the other micro-parameters, we chose a low affinity and complex turnover rate to improve the goodness of fit. As we will see below, there is a threshold that depends on velocity and affinity settings. Therefore, velocity has no effect on macro-parameters when a certain threshold is reached. Below that threshold — which lies somewhere between 7 $\mu m/ms$ and 35 $\mu m/ms$ — velocity seems to have an effect on $K_m$, while $V_{max}$ remains constant throughout.

**Velocity settings can introduce heterogeneity.** To test if the combination of affinity and velocity settings can introduce heterogeneity, the radial distribution function $g(r)$ was calculated. We see in Fig. 2.8 that at velocity micro-parameter settings of $\leq 3.5$ $\mu m/ms$ and affinity of 100% the substrate density g(r) points downwards at low r values and for a velocity of $> 3.5\ \mu m/ms$ g(r) is within one standard deviation a straight line. The affinity micro-parameter was fixed at 100%, at lower affinity the velocity threshold, when holes start to appear, would likely be lower. This suggests diffusion limitation at velocity micro-parameter settings of $\leq 3.5\ \mu m/ms$, where in the immediate vicinity (ca. $r < 30\ \mu m$) of complexes (and enzymes) the substrate density is lower introducing heterogeneity and violating the assumption that the system is well-mixed. Apparently, there is a threshold of velocity settings under which holes in the substrate around enzymes start to appear (see Fig. 2.9). This heterogeneity does not seem to have an effect on the goodness of fit, rather only the macro-parameter $K_m$ is effected.

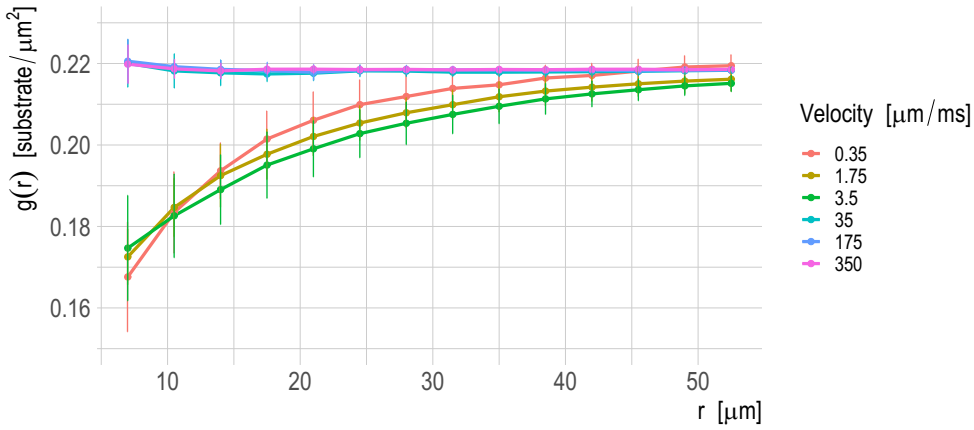


Figure 2.8: The radial distribution function of the number of substrates in the vicinity of complexes; r: radius [$\mu m$] from complexes; g(r): mean substrate density [substrate/$\mu m^2$], initial substrate density $\approx$ 0.31 substrate/$\mu m^2$ (= 10000 particles), initial number of enzymes = 50 particles, affinity = 100%, complex turnover rate = 1 $ms^{-1}$, snapshots of systems that were run for 75 ms

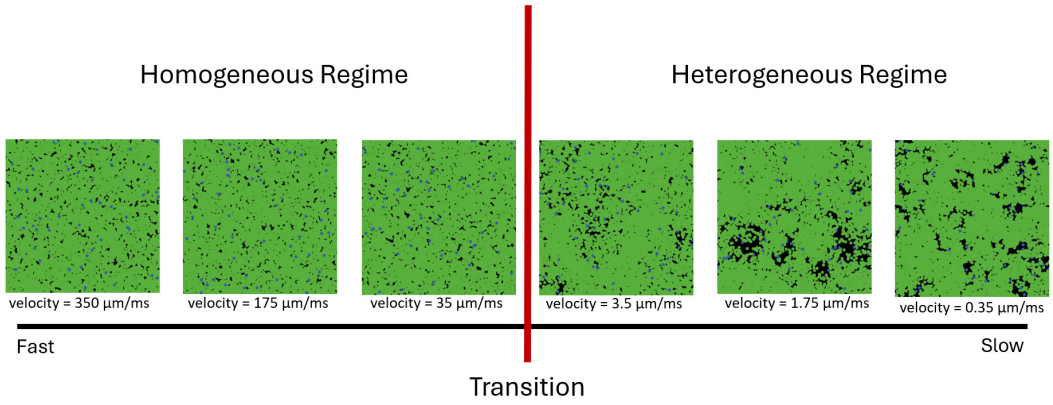


Figure 2.9: Transition where substrate particles (green) form holes around enzymes (blue), initial substrate density $\approx$ 0.31 Substrate/$\mu m^2$ (= 10000 particles), initial number of enzymes = 50 particles, affinity = 100%, complex turnover rate = 1 $ms^{-1}$, snapshots of systems that were run for 75 ms

**Testing the equilibrium approximation and the quasi-steady-state approximation.** To understand the relationship between micro- and macro-parameters 150 reaction curves were fitted (see table 2.1 for values). $V_{max}$ and $K_m$ (see Fig. 2.11a and b) increase with the complex turnover rate. However, complex turnover rate does not

affect $K_m$ at higher velocities. $K_m$ tends to decrease with affinity and velocity, especially at low velocity values. On the other hand, $V_{max}$ does not seem to be affected by either affinity or velocities, even at low velocities.

While keeping the complex turnover rate micro-parameter constant, the response of $V_{max}$ and $K_m$ to velocity and affinity settings was investigated (see Fig. 2.10). For $V_{max}$ there is no discernible pattern, meaning that values of the maximum reaction rate are constant with affinity and velocity. Conversely, $K_m$ increase only at and below a velocity of 3.5 $\mu m/ms$ as can also be seen in Fig. 2.7c. Moreover, affinity has less of an effect on $K_m$ except for the affinity class of 1%.

With the lm function in the R programming language different regression models were investigated to test the relationship between micro-parameters and rate constants in the equilibrium approximation and the quasi-steady-state approximation.

For regression models for $V_{max}$ (see Fig. 2.12) where all 150 curves were included in the analysis, the complex turnover rate micro-parameter is the best predictor for $V_{max}$ with over 70% of explained variation and a significant p-value. Affinity and velocity seem to have no effect on $V_{max}$. The data was then split into curves from micro-parameter combinations with velocity $\leq 3.5$ $\mu m/ms$ and curves from micro-parameter combinations with velocity $> 3.5$ $\mu m/ms$, because at velocity $\leq 3.5$ $\mu m/ms$ settings the system is no longer in a well-mixed state. For the 75 velocity $\leq 3.5$ $\mu m/ms$ curves, the situation is very similar to the analysis for $V_{max}$ done with all 150 curves except that adjusted $R^2$ value for the complex turnover rate is slightly higher compared to the $V_{max}$ regression models with all velocity classes included. For the regression models for $V_{max}$ in the well-mixed case (curves with velocity $> 3.5$ $\mu m/ms$), we see a clear relationship between $V_{max}$ and the complex turnover rate micro-parameter with almost 100% of variation explained and a significant p-value. The other micro-parameters explain no variation.

Regression models for $K_m$ for all velocity classes (see Fig. 2.13) show moderate associations with velocity alone (explaining ca. 22% of variation) and with the model $\frac{\text{affinity + complex turnover}}{\text{velocity}}$ (explaining ca. 41% of variation). Regression models for $K_m$ for velocity $\leq 3.5$ $\mu m/ms$ show low associations of about 9% explained variation for the complex turnover rate, the $\frac{\text{complex turnover}}{\text{affinity}}$ (10%) and the $\frac{\text{affinity + velocity}}{\text{complex turnover}}$ (7%) models and about 4% for affinity. Velocity is clearly the strongest predictor with about 66% explained variation followed by the model $\frac{\text{affinity + complex turnover}}{\text{velocity}}$, which has about 26% of explained variation. Finally, regression models for $K_m$ for velocity $> 3.5$ $\mu m/ms$ (see Fig. 2.13) with an adjusted $R^2$ of almost one the model $\frac{\text{complex turnover}}{\text{affinity}}$ is clearly the strongest predictor followed by models $\frac{\text{velocity}}{\text{affinity}}$, affinity alone, $\frac{\text{velocity + complex turnover}}{\text{affinity}}$ and $\frac{\text{affinity + velocity}}{\text{complex turnover}}$ that have all about 50% explained variation. With an adjusted $R^2$ of about

0.11 the $\frac{\text{affinity} + \text{complex turnover}}{\text{velocity}}$ model shows low association with $K_m$. All regression models described above that explain at least 10% of the variation have significant p-values. Exact results can be found in tables in the supplemental material section.

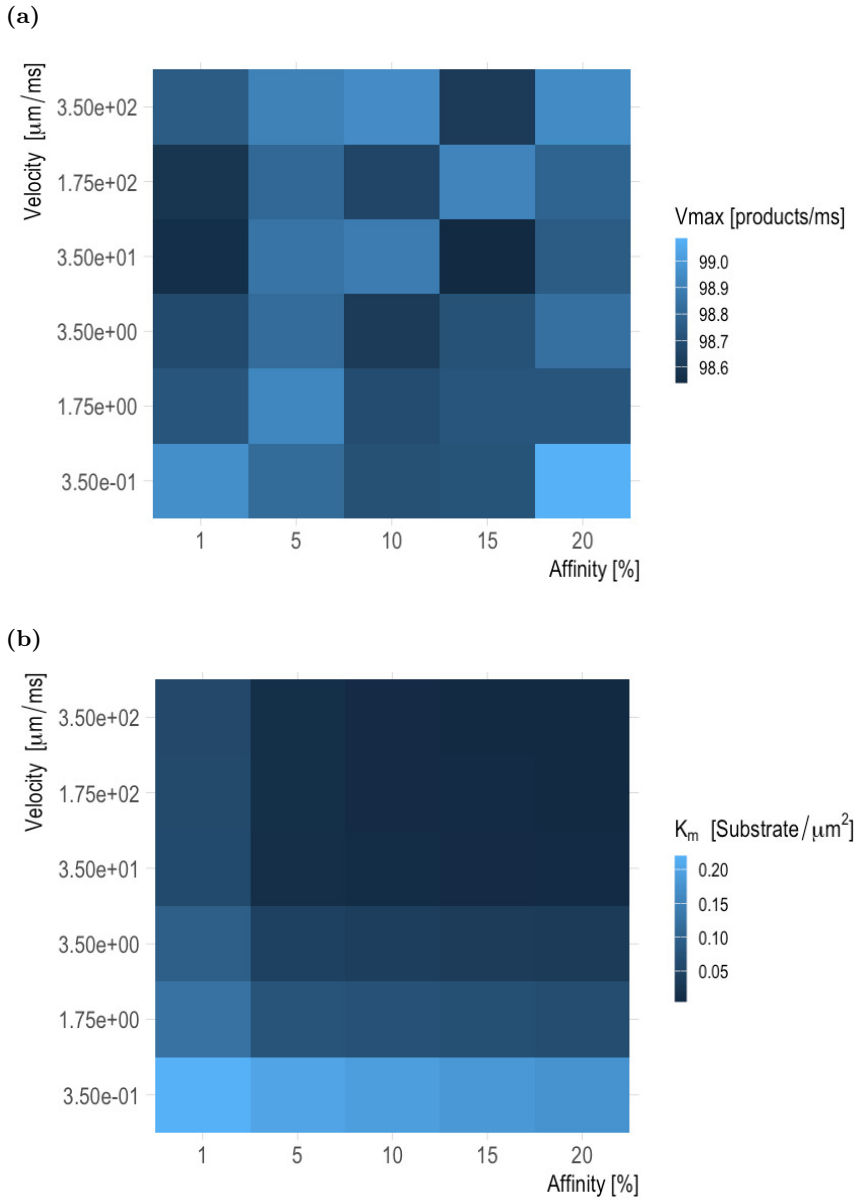


Figure 2.10: Varying the velocity and affinity micro-parameters for $V_{max}$ (a) and for $K_m$ (b), complex turnover rate = 0.625 $ms^{-1}$

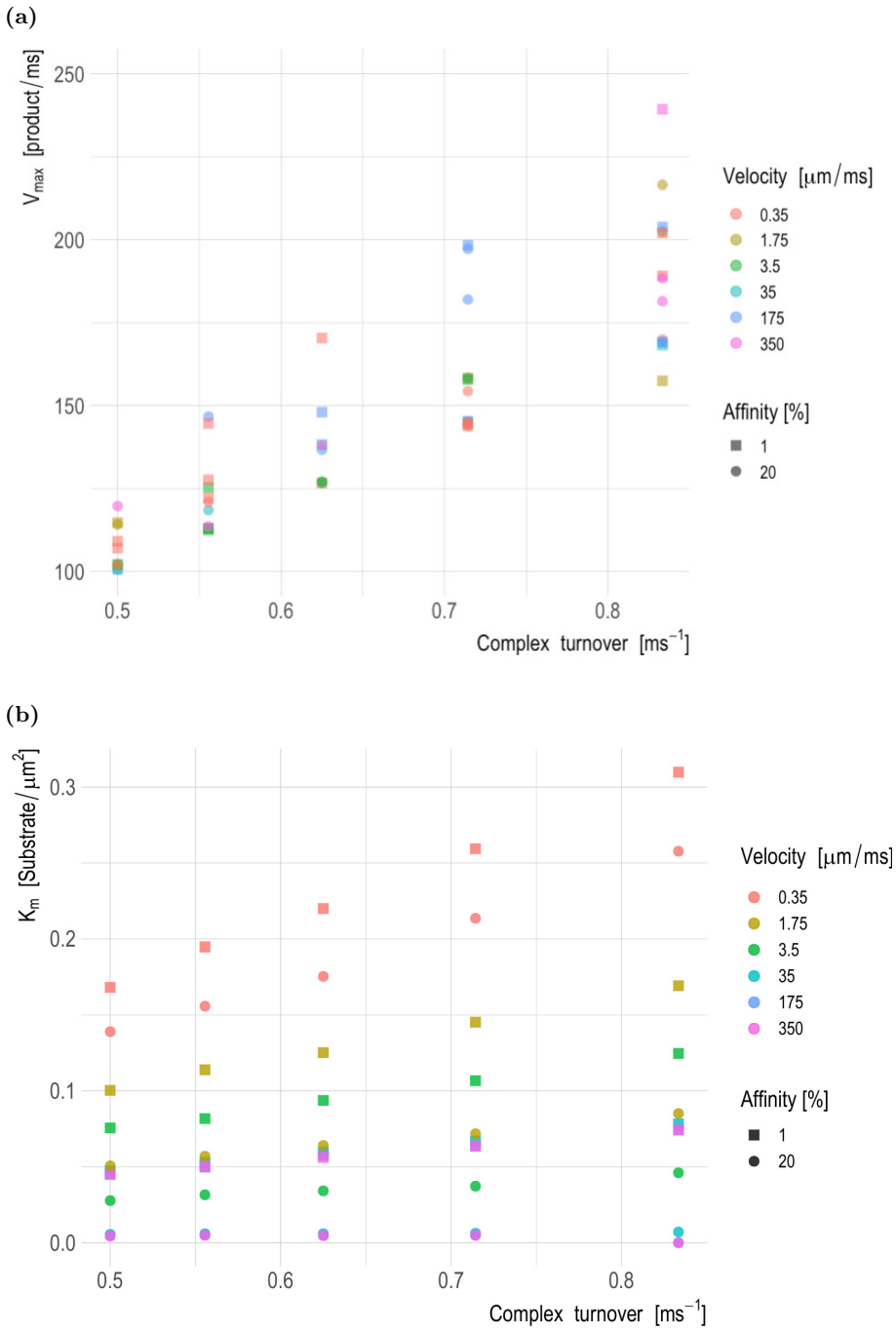


Figure 2.11: Varying the velocity, complex turnover rate and affinity micro-parameters for $V_{max}$ (a) and for $K_m$ (b)

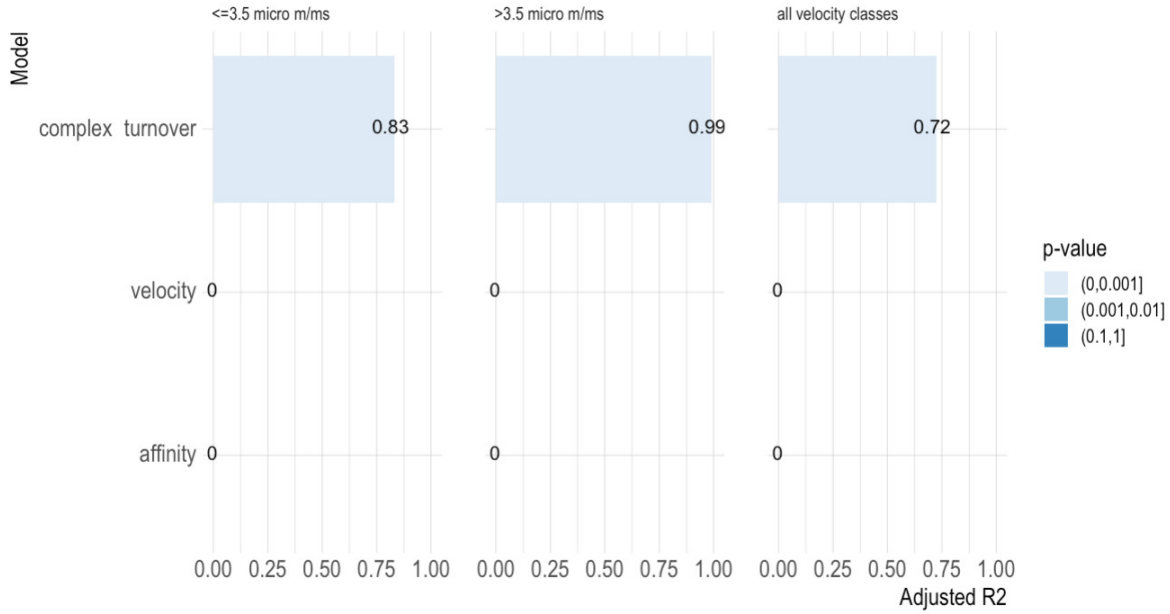


Figure 2.12: Regression models for $V_{max}$

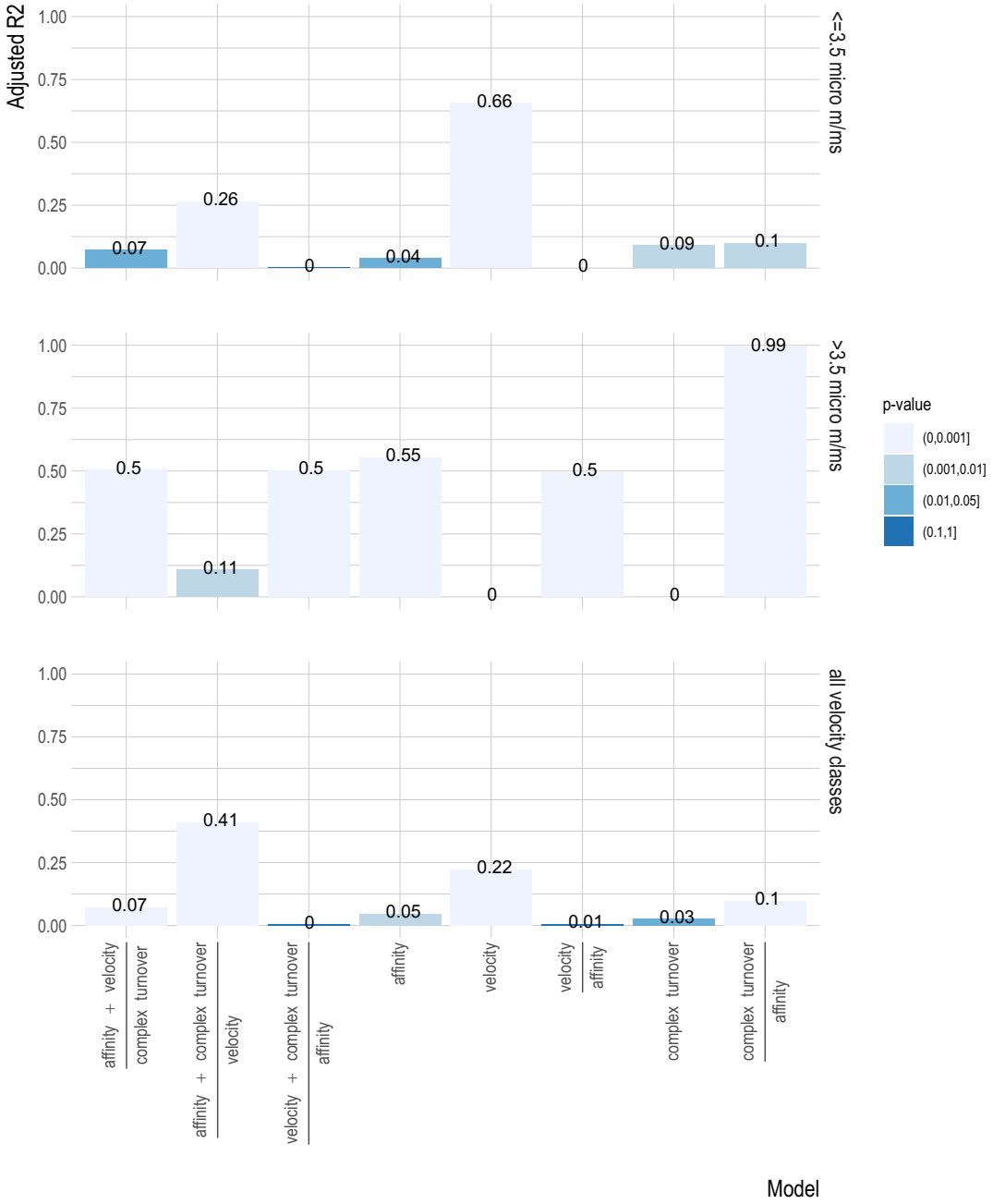


Figure 2.13: Regression models for $K_m$

### 2.3.2 The Pore Scenario

#### Model set-up and assumptions of the pore scenario

With the pore scenario we want to test whether the traditional MM equation, and also its parameters ($V_{max}$, $K_m$), that are usually obtained from well-mixed systems, would be suitable to describe the kinetics of enzyme reactions going on in pore systems. In this model, the randomly moving enzymes are produced on one side (on the right), but the immobile substrate is on the other side. We define the enzyme activity rate as only the products that arrive on the microbial-accessible side of the pore (on the right). Enzyme and product particles diffuse through the pore opening which can be varied in size.

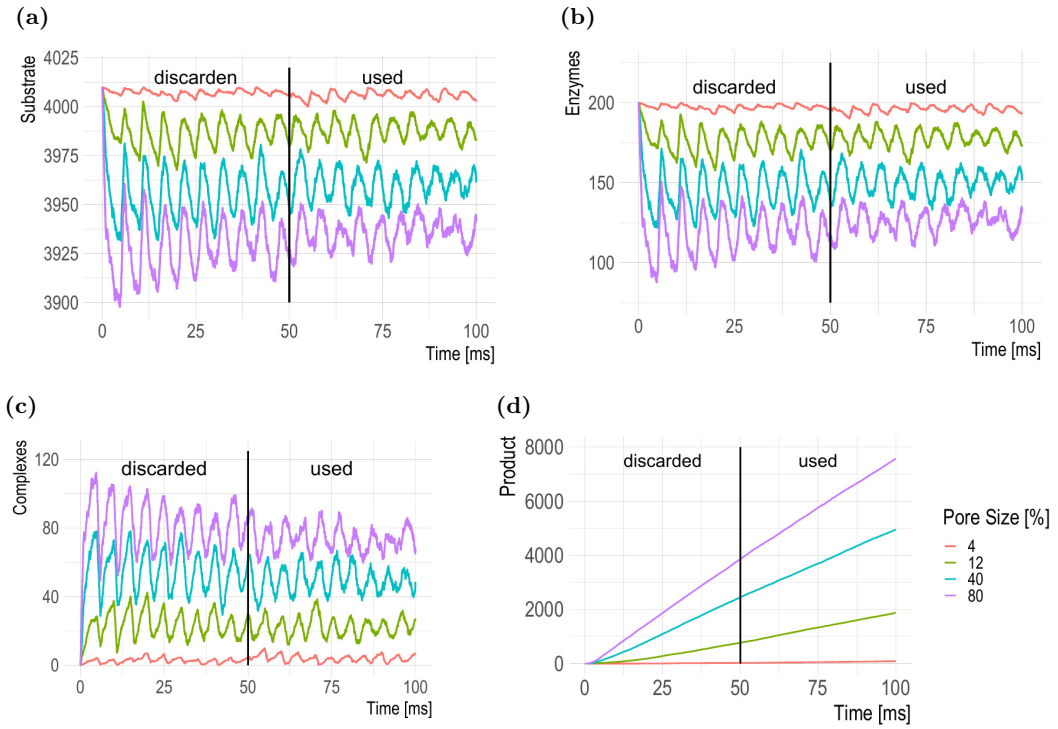


Figure 2.14: Time series of particles (substrate (a), enzymes (b), complexes (c), products (d)) in the pore model under different pore size (in % grid length) settings. For further analysis, the first half was discarded due to initial transients. Initial number of enzyme particles = 200. Initial number of substrate particles = 4010. Other micro-parameters: velocity = 175 $\mu m/ms$, complex turnover rate = 1 $ms^{-1}$, affinity = 50%, decay time = 5 ms

Therefore, the assumptions of MM kinetics are explicitly violated in the pore scenario

because the pore introduces spatial heterogeneity. Furthermore, the assumption of the equilibrium approximation that the equilibrium substrate concentration is constant and of the quasi-steady-state approximation that the equilibrium complex concentration is constant are important prerequisites because the MM model has been developed from them. Also, the product concentration increase (from which we calculate the reaction rate) should become linear when dynamic equilibrium is reached. To test the assumptions that the complex, substrate, enzyme, and product concentrations in the pore scenario are in equilibrium, time series of the particles were investigated (see Fig. 2.14). We see that with pore size settings in per cent of grid length, the number of complex, enzymes, product and substrate particles change. However, the average particle numbers of substrate, enzymes and complexes in one pore size class stayed approximately the same with time when the system reached dynamic equilibrium. The products increase linearly with time when the system has reached a steady state. All average particle numbers behave as expected in the pore scenario.

### Reaction curves in the pore scenario

As shown in the first part of the results, micro-parameters that influence enzyme kinetics in well-mixed systems are i) turnover rate of the enzyme-substrate complex, ii) affinity of enzymes and substrates, and iii) velocity of particles. The decay time of enzymes was not relevant for the well-mixed scenario. In the pore scenario, however, decay time of enzymes may become important, and also pore size could play a role for the overall rate of enzyme activity (defined as products arriving at the microbe-accessible side of the pore).

**Decay time.** In this scenario enzymes and substrate are not well mixed, and the enzymes have to travel through the pore so that the reaction can occur. Since this process takes some time, it is important to consider the decay time of the enzyme. If this time is too short, it is very unlikely that enzymes will reach the substrate at all. Despite, the obvious violation of MM main assumption — that the system is well-mixed —, we will try to fit the MM curve to simulation results of the reaction rate.

We start by considering a pore size of 4% of the grid length and changing the decay time of the enzymes, i.e., the time the enzyme exists in the system. When this time is up, the enzyme disappears and a new enzyme is added in a random position on the right side of the grid — which represents the outside of a substrate-filled pore where a soil microbe is located and produces extracellular enzymes. Despite systems heterogeneity, we are still able to fit the MM curve, i.e., a non-linear function that has a certain shape determined by $V_{max}$ and $K_m$ parameters that describes the increase of the reaction rate

with substrate concentration until it reaches a saturation point.

**(a)**

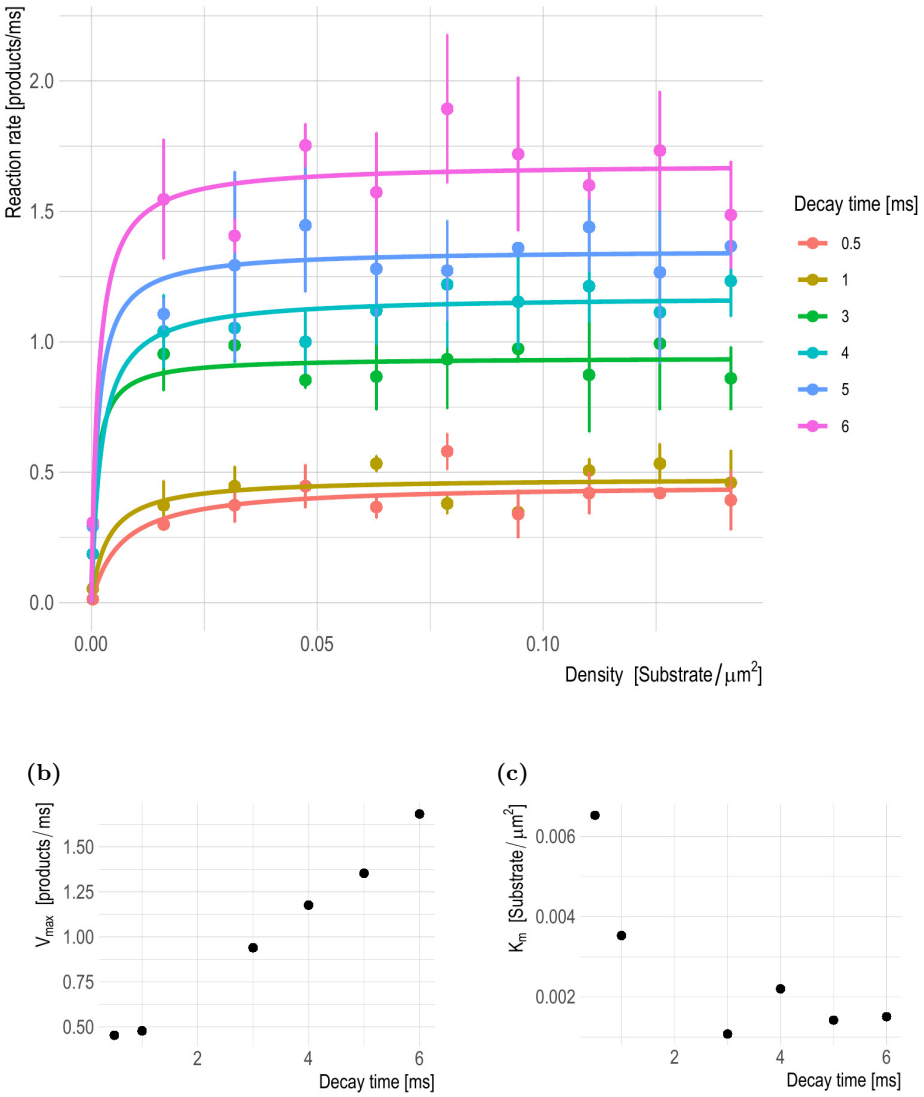


Figure 2.15: Reaction curves (a), the maximum rate of reaction $V_{max}$ (b) and the half-saturation constant $K_m$ (c) varying the decay rate micro-parameter. Initial number of enzyme particles = 200. Other micro-parameters: affinity = 50%, velocity = 175 $\mu m/ms$, complex turnover rate = 1 $ms^{-1}$, pore size = 4%

The MM curve occurs because at a certain point the number of enzymes inside the pore (at the left side of the grid) becomes constant and a dynamic equilibrium is reached. In addition, our simulations show that for shorter enzyme decay times the reaction rate is smaller, while for longer decay times the reaction rate is larger, as expected. The presence of the pore adds further stochasticity to the process since the probability of enzymes crossing the barrier/pore in their lifetime is an important step in the reaction.

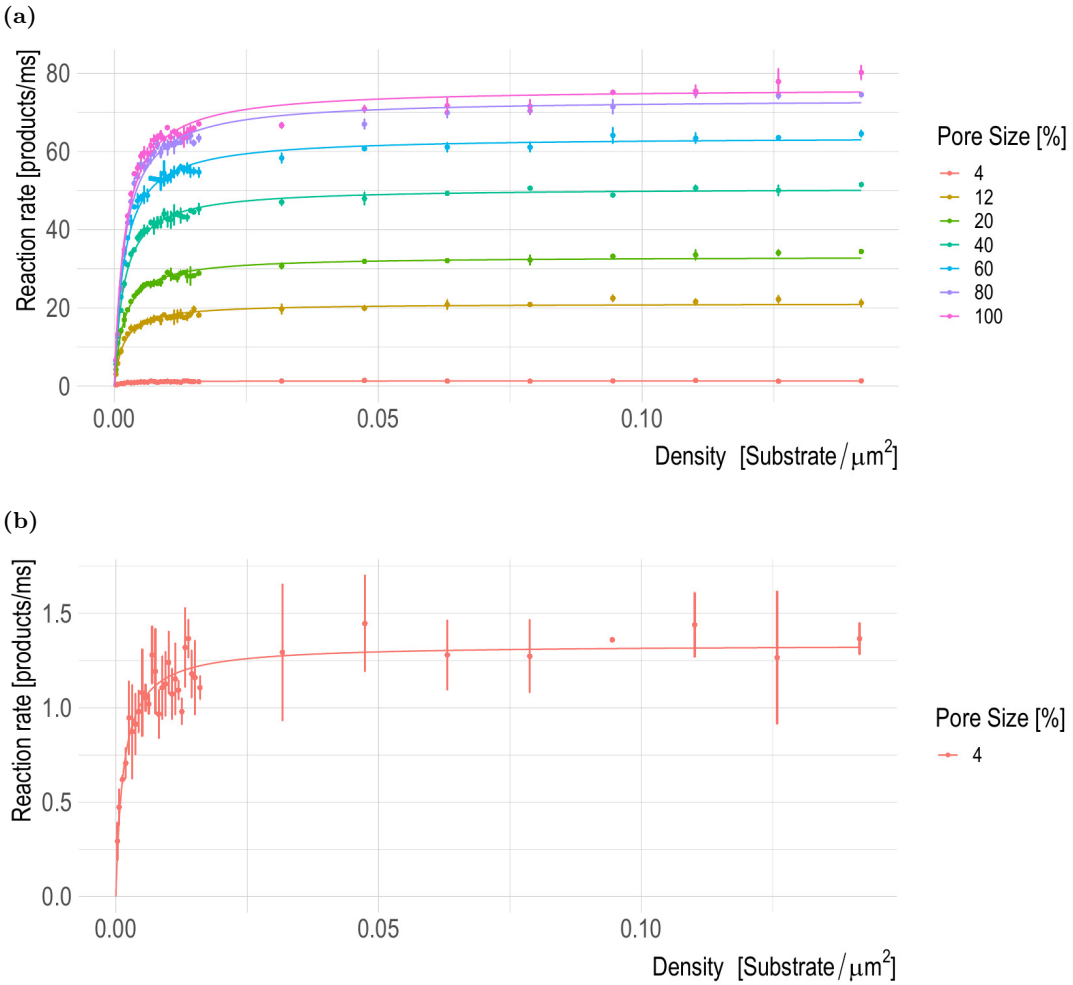


Figure 2.16: Reaction curves varying the pore size: (a) all curves (b) zoom of the reaction curve for the pore size 4%. Initial number of enzyme particles = 200. Micro-parameters: affinity = 50%, velocity = 175 $\mu m/ms$, complex turnover rate = 1 $ms^{-1}$, decay time = 5 ms

The stochasticity effect is stronger for longer decay times, see the top curves in Fig.

2.15a. We fit the MM curves for the data obtained and summarize our results in Fig. 2.15b and c. We observe that $V_{max}$ is linearly proportional to the decay time, while $K_m$ shows a decreasing trend. While the effect on $V_{max}$ was expected as described above, the changes in $K_m$ are less clear.

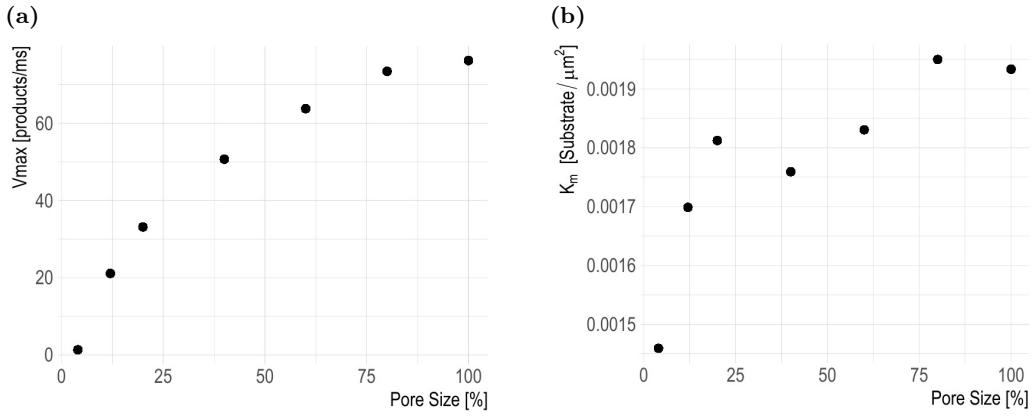


Figure 2.17: The maximum rate of reaction $V_{max}$ (a) and the half-saturation constant $K_m$ (b) varying the pore size (% of world length). 1 data point is the result of 102 (34 runs · 3 replicates) simulations, i.e., 1 curve. Initial number of enzyme particles = 200. Micro-parameters: affinity = 50%, velocity = 175 $\mu m/ms$, complex turnover rate = 1 $ms^{-1}$, decay time = 5 ms

**Pore size.** Next, we evaluate the effect of the pore size on the reaction rate. The pore scenario explores enzyme kinetics across a pore. The pore can change as a percentage of the total length of the grid, which is 178.5 $\mu m$ large, making it possible to relate the pore size to the macro-parameters. For this analysis, we assume a medium enzyme decay time. Like the decay time micro-parameter, we observe that the pore size also strongly affects the maximum reaction rate obtained as well as at which substrate density curves saturate (see Fig. 2.16). Note that for the same micro-parameters, the $V_{max}$ reached in a well-mixed scenario is more than two times higher (200 product/ms) than the top curve in the pore model (see Fig. 2.5). This is partly because only products that diffused onto the right side are counted, partly because the substrate is immobile and enzymes are on the other side of the grid making encounters less frequent. Additionally, the reaction curves varying the pore size show a bad fit for the largest pore sizes of 100% or 178.5 $\mu m$ and 80% or 142.8 $\mu m$, a moderately good fit for pore sizes 60% or 107.1 $\mu m$ to 20% or 35.7 $\mu m$ and a good fit for pore sizes 12% or 21.42 $\mu m$ and 4% or 7.14 $\mu m$. This bad fit means that the MM model might not describe the data accurately for larger pore size

settings and we would need to develop another model for enzyme kinetics across such pores. Larger pore sizes increase the flux of particles (enzymes and products) between the inside and the outside of the pore. Since the system is still not well-mixed (substrate is still immobile and only on one side of the grid), the increased flux could cause the bad fit by making the heterogeneity of the spatial organization of the substrate matter more.

Furthermore, the standard deviation is much higher compared to the well-mixed scenario. Thus the stochasticity of the pore scenario is larger. $V_{max}$ and $K_m$ increase with pore size, see Fig. 2.17(a, b), in a manner that resembles a saturation curve. The trend of $K_m$ is less clear than the trend of $V_{max}$ due to irregularities seen in Fig. 2.17(b).

This asymptotic relationship means that at small pore sizes, the increase in $V_{max}$ and $K_m$ is much larger than at large pore sizes, where other factors such as decay time play a more dominant role. A larger pore size means more particle collisions and there for a higher reaction rate (higher $V_{max}$), but also the effectiveness of one enzyme is less (higher $K_m$), probably because the probability that enzymes can diffuse back to the right side is larger (enzymes do not become trapped inside the pore until they decay).

### Combined effects

Finally, it is important to note the interplay between the effect of the pore size and the decay time as well as the effect of the pore size and the complex turnover rate.

**Pore size and decay time.** Varying the decay time and the pore size parameters for $V_{max}$ and for $K_m$ (see Fig. 2.18(a, b)) while keeping the complex turnover rate, the velocity and the affinity micro-parameters constant, reveals the combined effects of both parameters.

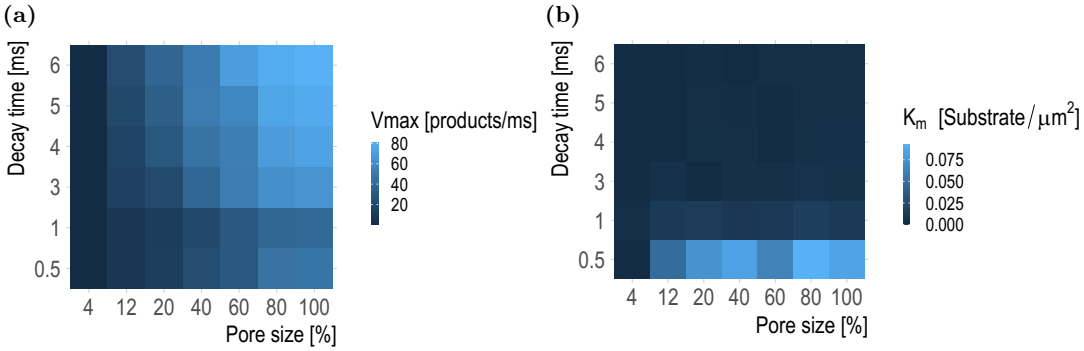


Figure 2.18: Varying the decay time and the pore size parameters for $V_{max}$ (a) and for $K_m$ (b), complex turnover rate = 1 $ms^{-1}$, velocity = 175 $\mu m$/ms, affinity = 50%

At long decay times of the enzyme and large pore openings the maximum rate is high and decreases gradually with decreasing pore size and decay time. For the combined effect for the half-saturation constant (see Fig. 2.18(b)) the effect of decay time is less when pore sizes are very small and the effect of decay time is larger when pore sizes are medium to large. The half-saturation constant is almost constant for longer decay times (above a decay time of 1 ms) and higher for shorter decay times, but only for pore sizes above 4% or 7.14 $\mu m$. This means that the reaction curve is flatter (i.e., increases at higher substrate densities) when the decay time is shorter.

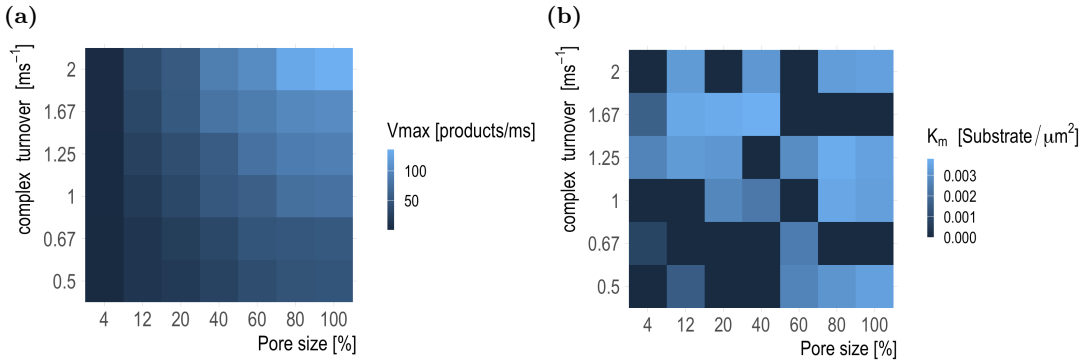


Figure 2.19: Varying the complex turnover rate and the pore size parameters for $V_{max}$ (a) and for $K_m$ (b), dacay time = 5 ms, velocity = 175 $\mu m$/ms, affinity = 50%

**Pore size and complex turnover rate.** To reaveal the combined effects of the complex turnover rate — a physiolgical variable of the enzyme — and the pore size — an environmental variable of the soil — we varied both parameters for $V_{max}$ and for $K_m$ (see Fig. 2.19(a, b)) while keeping the decay time, the velocity and the affinity micro-parameters constant. $V_{max}$ increases gradually with the complex turnover rate and the pore size. Pore size seems to have a stronger effect on $V_{max}$ than complex turnover rate. To varify this, we performed an analysis of variance using complex turnover rate, pore size and their interaction as predictor and $V_{max}$ as response variables, which confirmed that pore size explains the most of the variation with about 65%. Complex turnover rate explains about 28% and the interaction about 7% of the variance in $V_{max}$. All predictors have significant p-values. Therefore, since pore size has a stronger effect on $V_{max}$ than complex turnover rate, physiological properties of the enzyme system might be less relavent on enzyme kinetics in pore-structured systems than previously thought, because enzyme kinetics was only measured in the lab under well-mixed conditions and not directly in the soil. For $K_m$, there is not a clear pattern visible.

### 2.3.3 The Maze Scenario

#### Model set-up and assumptions of the maze scenario

To investigate the effect of spatial heterogeneity on enzyme kinetics further we leveraged the maze scenario where we placed progressively more complex arrangements of barriers into the grid using the Hilbert space-filling curve. The Hilbert curve is a fractal object meaning we find similar shapes at different scales (self-similarity). Assuming pore space to have fractal properties, we used the Hilbert curve to try to mimic it.

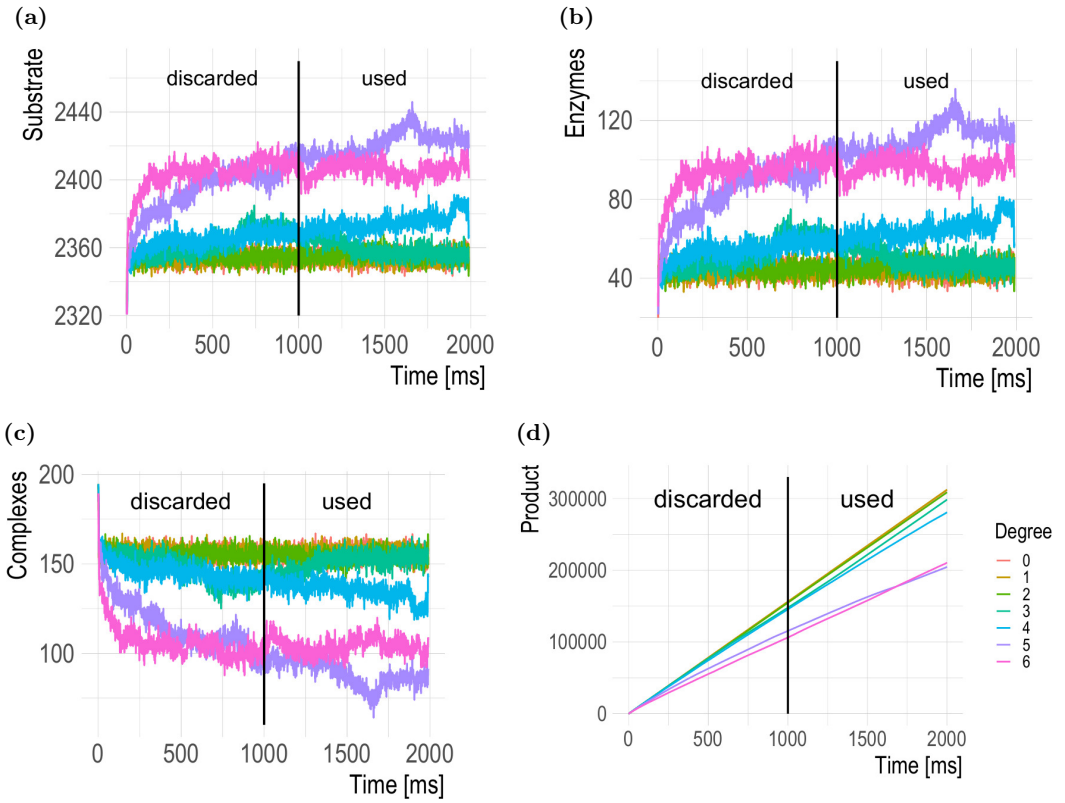


Figure 2.20: Time series of particles (substrate (a), enzymes (b), complexes (c), products (d)) in the maze scenario under different degree settings. Initial number of enzyme particles = 200. Initial number of substrate particles = 4310; complex turnover rate = 1 $ms^{-1}$, affinity = 50%, velocity = 175 $\mu m/ms$, decay time = 2000.1 ms

To test the assumptions that the complex, substrate, enzyme, and product concentrations in the maze scenario are in equilibrium, time series of the particles were investigated

(see figure 2.20). We see that with different levels of maze complexity (i.e., degree of the Hilbert curve), the number of complex, enzymes, product and substrate particles, as well as their ratio to each other, change. For degree settings four and above, substrate, enzyme and complex particle numbers change gradually until they reach constant levels. Substrate and enzyme particle numbers increase with time for degrees four and above and complex particles decrease with time.

Only the data where particle numbers are approximately constant were considered which is the second half of the simulation run. The assumption that product numbers — from which the reaction rate is calculated — increase linearly with time holds for all degree classes.

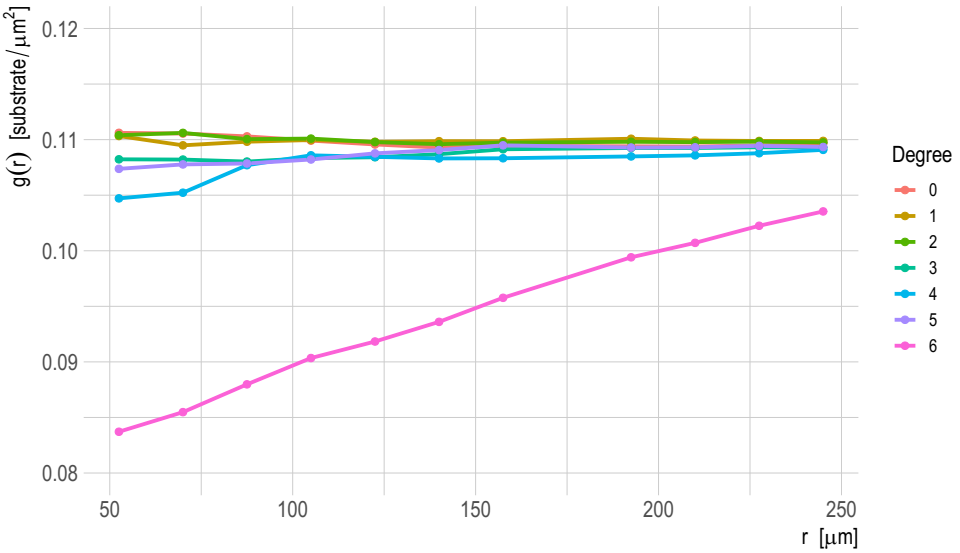


Figure 2.21: The radial distribution function of the number of substrates in the vicinity of complexes; r: radius [$\mu m$] from complexes; g(r): mean substrate density [substrate/$\mu m^2$], initial number of substrate = 10000, initial number of enzymes = 50, affinity = 100%, complex turnover rate = 1 $ms^{-1}$, velocity = 175 $\mu m/ms$, decay time = 2000.1 ms, snapshots of systems that were run for 1500 ms

### Spatial structures separate enzymes from substrate

The maze model tries to investigate the effect of spatial structure on enzyme kinetics. The radial distribution was calculated, giving the substrate density at certain distance from the enzymes after 1500 ms (see Fig. 2.21). Only in the maze scenario with degree 6 setting an unmixing effect is visible, where the substrate and enzymes that started out well-mixed (because they were placed randomly into the grid), are now more separated due to the interaction within the maze structures.

### Maze degree

We can see in figure 2.22a that for higher degrees (degrees 4 to 6) the reaction curves differ. There is a change in $V_{max}$ (see figure 2.22b) for curves from models with degrees 5 and 6. This is because the curves do not fit the data points accurately, since we would expect the opposite effect — higher degree means more spatial heterogeneity and therefore less accessible substrate which would lower the maximum rate.

Therefore, $V_{max}$ may be considered constant. On the other hand, $K_m$ is increasing with degree with a sharp rise from degree 3 to degree 6 (see Fig. 2.22c). Similar to the low-velocity regime in the well-mixed scenario, higher spatial complexity causes the effectiveness of one enzyme (the inverse of $K_m$) to be less because of an apparent change in spatial organization of particles (see Fig. 2.23).

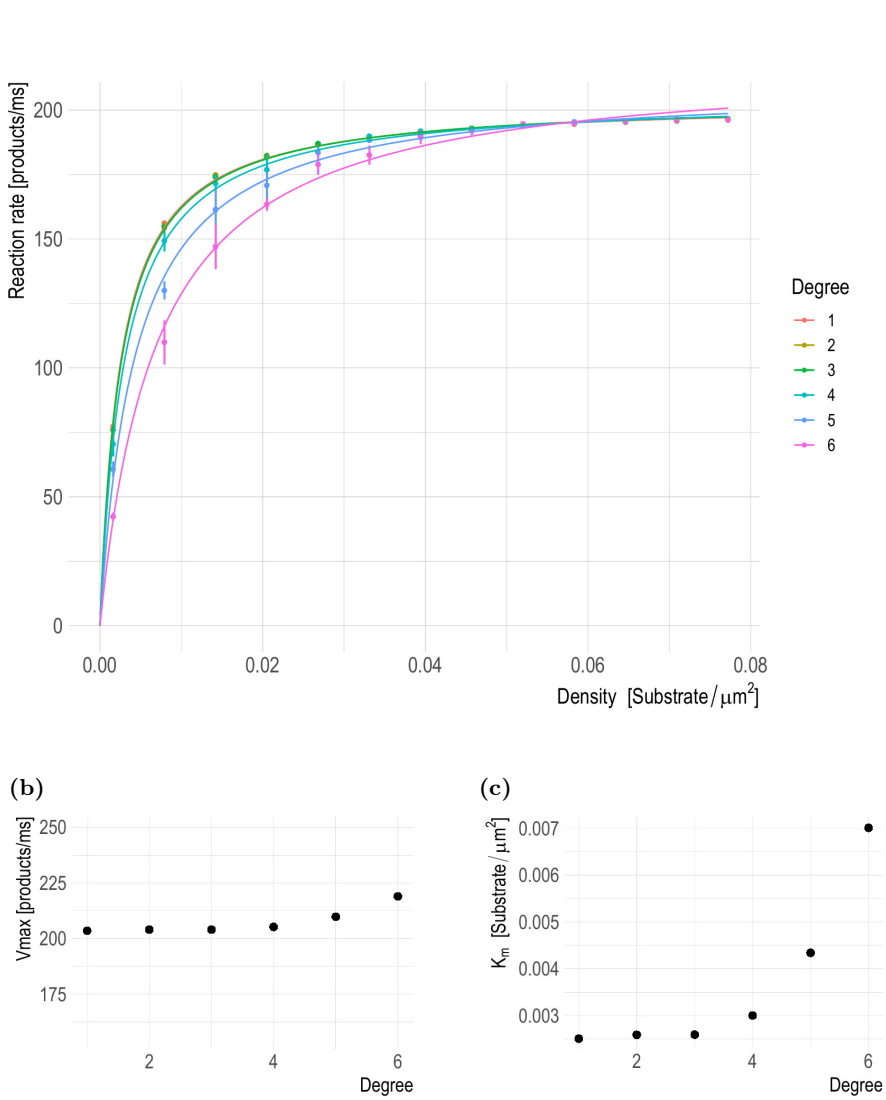


Figure 2.22: Reaction curves (a), the maximum rate of reaction $V_{max}$ (b) and the half-saturation constant $K_m$ (b) varying the degree parameter. Initial number of enzyme particles = 200. Micro-parameters: affinity = 50%, velocity = 175 $\mu m/ms$, complex turnover rate = 1 $ms^{-1}$, decay time = 2000.1 ms

### Enzyme decay time

The maze model degree six was explored varying the decay time micro-parameter (see Fig. 2.24). Curves with long decay times show a larger $K_m$. Therefore, the density at which the curve saturate is affected by decay time settings.

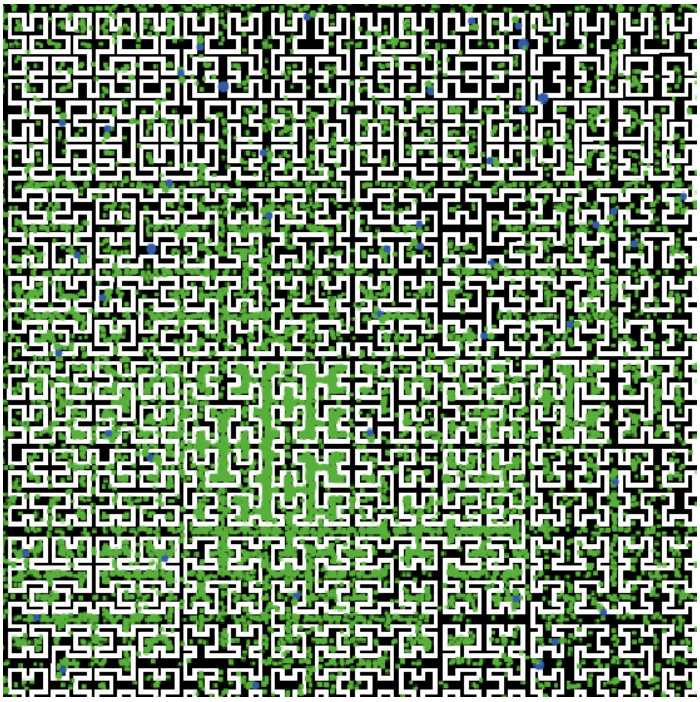

Figure 2.23: Substrate distribution of the maze scenario at 1500 ms, substrate (green), enzymes (blue), there is an enrichment of substrate in the lower-left quadrant, maze degree = 6, initial number of substrate = 10000, initial number of enzymes = 50, affinity = 100%, complex turnover rate = 1 $ms^{-1}$, velocity = 175 $\mu m/ms$, decay time = 2000.1 ms

The highest decay time (200 ms) effectively turns off the decay of enzymes, since the model was run only for a duration slightly below 200 ms. For the second highest decay time value (100 ms) the decay of all enzymes was triggered exactly once and for decay times of 50 ms, 25 ms, and 12.5 ms the decay event was triggered 3, 7 and 15 times, respectively. Every time a decay event is triggered, all enzymes cease to exist at the same time step and are randomly placed back into the grid. The separation through an unmixing process that emerges as enzyme and substrate particles move randomly inside the maze is alleviated by this enzyme decay process. When decay time is longer, $K_m$ and $V_{max}$ are elevated. The former can be explained by a reduction of collisions, the latter might by an artifact of the curve fitting process known as overshooting however telling us that the Michaelis-Menten model fits better when decay times are low, i.e., spatial heterogeneity is less. Elevated $K_m$ values at longer decay times are caused by spatial organization of the particles — depleting and enriching in certain areas — making the

grid patchy (see Fig. 2.23). This would mean that enzymes are less effective at higher decay times.

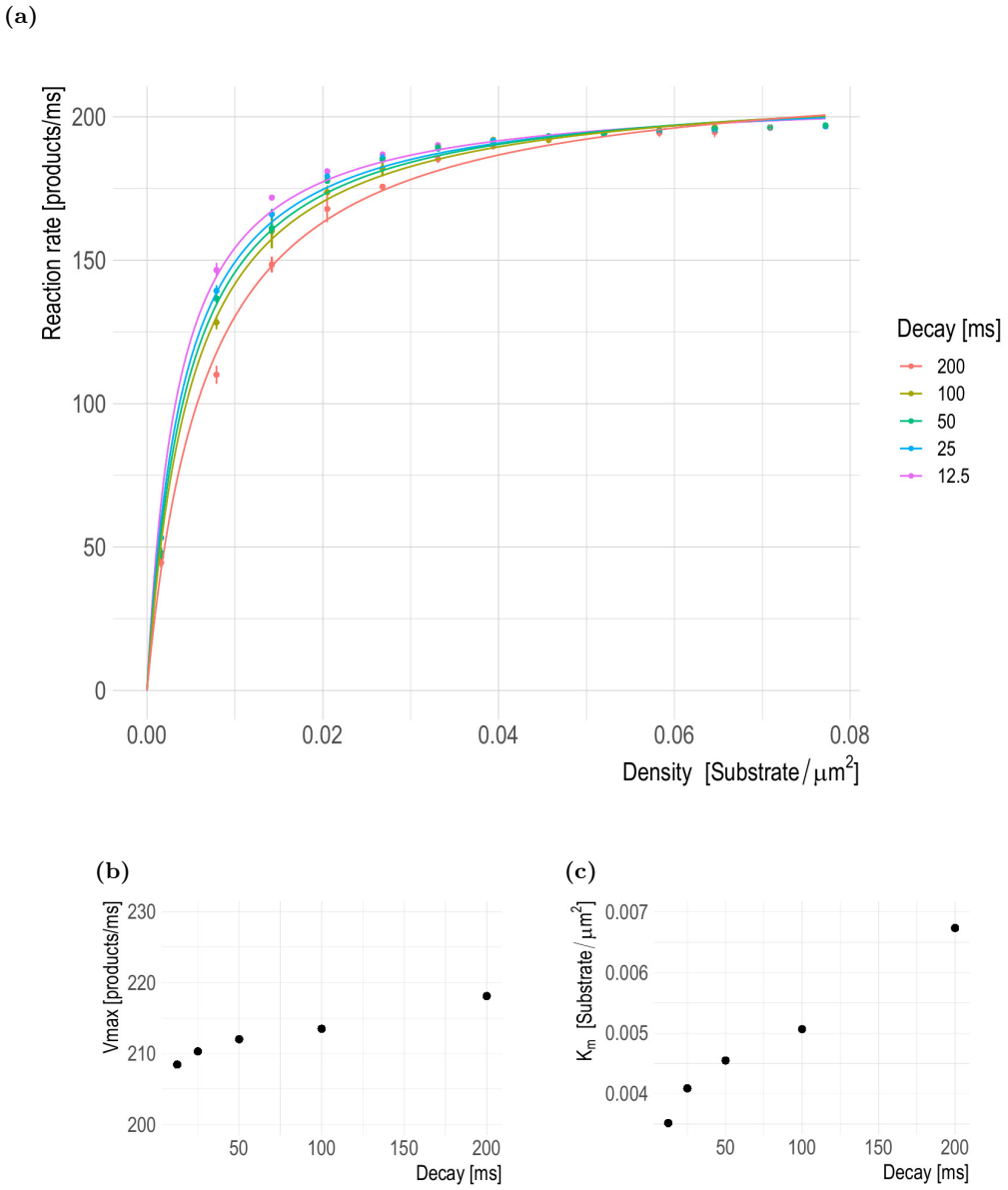


Figure 2.24: Reaction curves (a), the maximum rate of reaction $V_{max}$ (b) and the half-saturation constant $K_m$ (b) varying the decay time parameter. Maze degree = 6. Initial number of enzyme particles = 200. Micro-parameters: affinity = 50%, velocity = 175 $\mu m/ms$, complex turnover rate = 1 $ms^{-1}$

However, extracellular enzymes that are produced by soil microbes are not randomly distributed in the soil pore space, but are located in their vicinity.

### Heterogeneity of the maze models affect the local diffusion coefficient

The diffusion coefficient for every cell was calculated and visualized for the well-mixed as well as for the maze model variants. Subsequently, the mean and the standard deviation of the diffusion coefficients were calculated.

In addition, to contrast clustering from complexity, Moran's I was calculated (see figure 2.25). Moran's I gives us a sense of the amount of spatial clustering of the local diffusion coefficient. We calculated it to understand the reason for the spatial separation of enzyme and substrate particles due to the barriers. The spatial distribution of the local diffusion coefficient is determined by the shape of the Hilbert curve and in turn influences the movement of the particles.

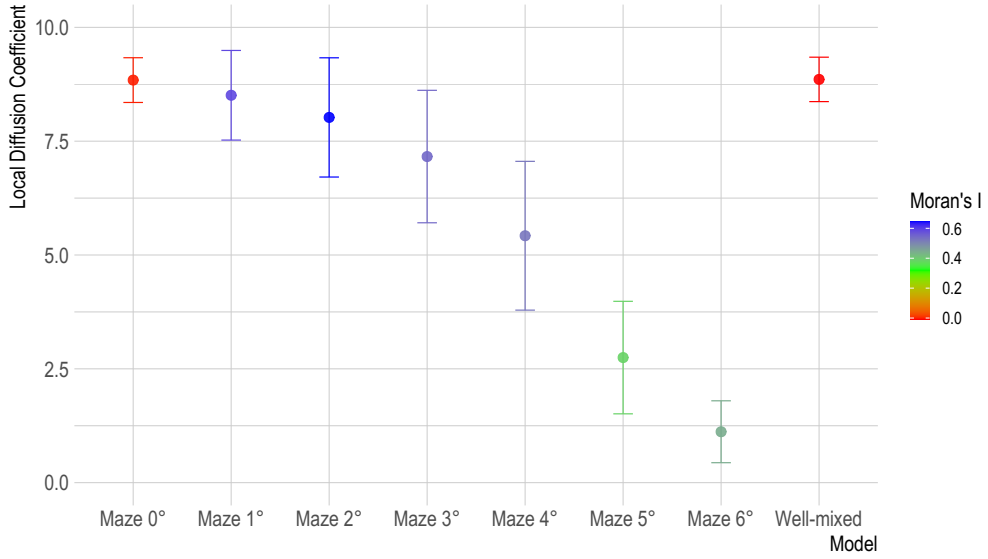


Figure 2.25: Diffusion coefficients and Moran's I of the well-mixed model and the maze models degree 0 to 6

We see that while the mean diffusion coefficient decreases with degree, the amount of spatial clustering (positive Moran's I) is higher for models with degrees 1 to 4, whereas models with degrees 5 and 6 show intermediate Moran's I. The maze model degree zero (no barriers) and the well-mixed model are almost identical in mean local diffusion

coefficient and Moran's I. The fact that the pattern of Moran's I values across the maze model variants differs from that of $K_m$ (see Fig. 2.22c) points towards the difference between clustering and complexity. The clustering of maze variant degree 2 for example is higher than variant degree 6, however the complexity and $K_m$ are higher at degree 6 settings. Therefore, $K_m$ change seems not to be an artifact of clustering of local diffusion coefficients, rather a response to the separation of enzymes from substrate (see Fig. 2.21) due to increased spatial complexity.

## 2.4 Discussion

With SOC being the majority of actively cycling carbon on land, its dynamics depend on the activity of soil microbes that digest long-chained carbohydrates in an extracellular process using enzymes. Most soil C turnover models that include extracellular enzyme activity approximate it with the MM equation. However, the central underlying assumption — namely that space is homogeneous and therefore particles move with random motion and are always in a well-mixed state — is violated in soil, where pore space is highly heterogeneous at multiple scales.

We used individual-based modelling to evaluate extracellular enzyme kinetics under conditions in which the spatial homogeneity assumption is no longer valid. We also investigated the effects of soil temperature and moisture (with the velocity micro-parameter), as well as physiological properties of the enzyme itself (with the affinity, decay time, and complex turnover rate micro-parameters) on enzyme activity. We fitted the classical MM model to our simulation results to gain insight into the applicability of the MM model for soil extracellular enzyme activity measurement.

The ability to simulate the behaviour of individual particles at the micro-scale gives us the opportunity to manipulate micro-parameters that control the fundamental processes of enzyme kinetics that would be impossible to recreate in a wet lab experiment. Nonetheless, the three scenarios presented in this study aim to represent real-live situations that, at an aggregate level, can be measured in the lab.

Our well-mixed scenario represents the classical view of enzyme kinetics. The pore and maze scenarios, in turn, are completely different from the view of enzyme kinetics Leonor Michaelis and Maud Menten put into equations. However, they are much more likely to occur in soil than the well-mixed scenario.

**The well-mixed scenario.** The well-mixed scenario can be considered as the null model we used to evaluate how our microscale parameters translate into the parameters of the MM kinetics that can be measured from the system experimentally ($V_{max}$ and $K_m$). Its assumptions that the substrate, enzyme and substrate-enzyme complex concentrations are on average time-invariant once the system has reached dynamic equilibrium hold. This is unsurprising because every time a substrate is turned into a product by the complex it is hard-coded that a new substrate will appear in a random location on the grid. Therefore, when the complex concentration is stable, the enzyme and substrate concentrations will follow. Complex particle numbers were approximately constant because the rate of collisions was stable per run. This held true even for the velocity settings where velocity was under the threshold at which holes would appear.

Table 2.2: Effects of the parameters on $V_{max}$ and $K_m$

| Parameter | $V_{max}$ | $K_m$ |
|---|---|---|
| velocity | = | unclear |
| complex turnover rate | + | + |
| affinity | = | — |
| pore size | + | + |
| decay time (well-mixed model) | = | = |
| decay time (pore model) | + | — |
| decay time (maze model) | unclear | + |
| degree of complexity | unclear | + |

Results of the effect of parameter settings on $V_{max}$ and $K_m$ are summarized in Table 2.2. When we varied the complex turnover rate micro-parameter we saw a perfect fit for all settings. Complex turnover rate is the reciprocal of the time a complex exists between its creation at the time of collision of the substrate with the enzyme and the time of the release of the product and the enzyme. We ran the simulation for 100 ms, meaning the complex turnover rate settings were 0.5% to 2% of the total time. This means if the next collision happened always right after the release of the enzyme, one enzyme would be involved in ca. 50 to 200 subsequent complexes until the simulation ended. In the regression models, the complex turnover rate was a strong predictor of $V_{max}$ and also part of the regression model ($\frac{\text{affinity + complex turnover}}{\text{velocity}}$) that explained 41% of the variation of $K_m$ in the group of curves where the velocity parameter setting was high enough so that the system was well-mixed (homogeneous group). Because $V_{max} = k_{cat} \cdot E_T$ (where $E_T$ is the total enzyme concentration, i.e. the concentration of free enzymes and enzymes involved in complexes) holds in the equilibrium approximation and the quasi-steady-state approximation and also $K_m = \frac{k_{-1}+k_{cat}}{k_1}$ holds only in the quasi-steady-state approximation, the result from the regression analysis points towards a strong association with the phenomenological rate constant $k_{cat}$ which is the rate of the last step in the two-step process of the most basic enzyme kinetics model. Furthermore, the quasi-steady-state approximation, as opposed to the equilibrium approximation, is supported by this result. We could therefore successfully relate our micro-parameters, which are properties of the particles, to rate constants in the chemical equation. The specific enzyme-substrate interaction and the efficiency of the catalytic reaction of the enzyme determine the duration of the complex (i.e., $k_{cat}$) in the real soil system, which is very difficult to measure (Marangoni, 2003).

Next, the velocity micro-parameter was investigated. The velocity in our model is the displacement of the particles in one direction per time step and therefore related to the

mean squared deviation in the Stokes-Einstein equation (Miller and Walker, 1924). It is determined by the frictional resistance of the molecule (which depends on the viscosity of the liquid medium at the microsite and the geometry of the particle) and temperature. The viscosity, in turn, depends in part on the soil moisture. As we varied the velocity settings, a certain threshold emerged at sufficiently low velocity where below it the assumption of the MM model — that the spatial distribution of substrate is homogeneous — was no longer valid. At those settings, substrate holes around enzymes and complexes started to appear at relatively low substrate concentrations, in particular when substrate concentration was below enzyme saturation (i.e., when the overall reaction rate was well below $V_{max}$). Results above this velocity threshold show no change in macro-parameters. Conditions in this fast regime seem to be as well-mixed as possible. Increasing velocity has therefore no effect on the homogeneity of the system once we are over the threshold. What is surprising is that higher velocity does not seem to increase the collision rate and therefore substrate turnover. This might be explained by an interaction between velocity and substrate concentration. When substrate concentration is so high that enzymes become saturated (i.e., when reaction rates reach $V_{max}$), substrate and enzyme particles are at the same time very densely packed. Thus, under these conditions velocity does not play a role anymore, because when one enzyme dissociates from the complex again, there is always free substrate in the immediate vicinity. Below the threshold, $K_m$ decreases with velocity, whereas $V_{max}$ is unaffected (see Table 2.2). When the model was run with velocity settings below the threshold, velocity was the main predictor for $K_m$, because heterogeneity reduced reaction rates in non-enzyme-saturated conditions (when the reaction rate was well below $V_{max}$). This can be explained by the increase in hole diameter with decreasing velocity when substrate densities where small to intermediate. At such substrate densities, the larger the hole, the longer the enzyme takes to reach the next substrate, thus lowering collision rate. On the other hand, when substrate densities were at enzyme saturation (thus $V_{max}$ was reached), velocity had no effect on the collision rate because there were no substrate holes.

As noted before, lower velocity is caused by frictional resistance, in part due to the viscosity of the liquid surrounding the enzyme. This could be achieved by soil bacteria by producing extracellular polymeric substances (EPS) (Or et al., 2007; Nunan et al., 2020). One reason why a microbe would produce EPS is to keep particles close to the cell, preventing diffusional losses of products and extracellular enzymes (Romaní et al., 2008; Costa et al., 2018). Another reason for EPS production is to even out fluctuations in environmental conditions (Roberson and Firestone, 1992), such as moisture and temperature.

Since velocity also depends on soil temperature, measuring extracellular enzyme activity from thawing permafrost soils in the lab at room temperature, could be inaccurate, because in the soil at low temperatures, the $K_m$ parameter might be different, as was shown in this study.

Moving on to the affinity in the well-mixed model, we found that affinity is proportional to $K_m$, with high affinity leading to low $K_m$ just as in real systems. On a molecular level, the affinity of an enzyme for a specific substrate depends on the precise positioning of the substrate relative to the catalytic groups at the active site (Yabukarski et al., 2020). Moreover, affinity is not solely a property of the enzyme. Additionally, the micro-environment (e.g., pH or the presence of co-factors) around the active site can enhance affinity (Lancaster et al., 2018). Affinity had no effect on $V_{max}$ since at high enough substrate density the probability of the collision resulting in a complex does not matter because the next enzyme-substrate collision will occur very soon after. When the model was in a homogeneous state due to high enough velocity settings, affinity was the denominator in the model ($\frac{\text{complex turnover}}{\text{affinity}}$) that was the strongest predictor for $K_m$. Affinity plays a role in the first step of the two step process in the chemical term representing the basic enzyme kinetics model. Affinity in our models is the probability of the successful irreversible binding event which is different from the view of traditional enzyme kinetics that the binding process is reversible. It is thus not directly comparable (such as complex turnover rate and $k_{cat}$ are) to the rate constants $k_1$ and $k_{-1}$. Furthermore, affinity, in addition to velocity, determines the threshold at which inhomogeneities start to appear in the well-mixed scenario. Since affinity determines the probability of a collision leading to complex formation, high affinity means that holes will form sooner because the enzyme needs less encounters with substrate to remove it from its neighbourhood. Also, at very high affinity ($> 40\%$), the fit of the MM curve worsened. This might be an artefact of the curve-fitting technique we used.

According to (Schurr, 1970), diffusion limitation can occur when the diffusion of substrate molecules to the enzyme active sites is a rate-limiting step. This might happen under oligotrophic conditions, when substrate concentrations are in the nanomolar range, which is typical for most of the soil volume (Leitner et al., 2017). Under these conditions, when the concentrations of both substrate and enzymes (a sufficient enzyme pool could not build up) are very low, the probability of enzyme-substrate encounters decreases, and diffusion becomes the rate-limiting factor (Kim and Shin, 2007). Also spatial constraints — in environments where the movement of molecules is restricted, such as within cellular compartments or in highly crowded biochemical environments — diffusion limitations can become prominent (Schnell and Turner, 2004). This might also apply to soil pore

space, which we will explore further in the final part of the study.

In summary, MM kinetics were representative of the underlying dynamics in most of the well-mixed scenarios with the exception of scenarios with very high affinity rates. Additionally, inhomogeneities in substrate and enzyme concentrations were forming at a certain threshold of affinity and velocity settings, affecting the half-saturation constant.

**The pore scenario.** Explicitly violating the assumptions of MM kinetics, in the pore scenario, space is heterogeneous with the pore separating enzymes from substrate and ultimately the product from the microbe. In nature, this situation where a pore physically separates substrate from microbe, and the microbe can only secrete enzymes that diffuse to the substrate may occur quite often. Passive resource acquisition strategies, where resources diffuse towards an immobile or only slowly moving soil microbe, might be much more common than active foraging for resources (Nunan et al., 2020).

However, the other assumptions of MM kinetics, namely that the substrate, enzyme, and complex concentrations are time-invariant, were met by the pore scenario, and the most crucial precondition that the product concentration rises linearly with time in order to calculate the reaction rate from it, was upheld. This is in part because a steady enzyme concentration formed within the pore, which depends on the enzyme production, its diffusion through the pore, and the decay rate.

The first parameter we investigated in the pore scenario was the decay time of the enzyme which is the time an enzyme has to move around in random motion before it is again placed in a random position on the right side of the grid — outside the pore, where the microbe (not modeled) produces the enzymes. In nature, the enzyme's decay time can be determined by temperature and the presence of proteases (Wallenstein et al., 2011). Decay time was varied between 0.5% and 6% of the total runtime of the experiment, which was estimated to be around 100 ms. With increasing decay time $V_{max}$ increased and $K_m$ decreased, meaning that when extracellular enzymes lasted longer both the overall production at optimal substrate densities as well as the efficiency of the enzyme went up. The first effect is easily explained: As enzymes had more time to diffuse into the pore, the number of equilibrium complexes went up. On the contrary, the second effect is difficult to understand but is possibly explainable with enzymes being able to have multiple subsequent binding events in one lifetime making the enzyme more efficient because it does not have to diffuse through the pore opening to reach the subsequent binding locations. Interestingly, decay time had only an effect on $V_{max}$ and $K_m$ in the spatially heterogeneous scenarios (see Table 2.2). It may thus play a larger role in enzyme kinetics in soils than is usually assumed. Furthermore, its interaction with pore size indicates that the importance of the lifetime of soil enzymes may vary with soil architecture.

Next, we varied the pore size as a percentage of the total length of the square grid. For both $V_{max}$ and $K_m$, the increase with pore size diminishes progressively, approaching a plateau. As the pore opening became larger, more enzymes could diffuse inside the pore, react with the substrate and form complexes. As a result, complex concentrations were larger, and a higher $V_{max}$ could be achieved. In real soil, pore sizes range from macro-pores (75 to 100 $\mu m$ in diameter) that can be easily entered by small- to medium-sized soil bacteria to crypto-pores (0.007–0.1 $\mu m$ in diameter) that can only be entered by smaller proteins (Cameron and Buchan, 2006). As the average diameter of most extracellular enzymes is 0.003-0.005 $\mu m$, they can enter most crypto-pores (Burns and Dick, 2002).

The combined effects of decay time and pore size showed similar trend for $V_{max}$, in which the maximum reaction rate increases smoothly with pore size and decay time. This is because there is no negative interaction between the parameters. We expected that decay time would play a stronger role at smaller pore openings since the chance of the enzyme going through the pore is lower making the time enzymes have once they made it through the pore more valuable. However, the opposite was found: at 4% opening the decay time had almost no effect and at larger openings the difference in decay time mattered more. This can be explained by pore sizes being far more limiting than decay times. Within a small pore (4%) decay time may still play a certain role, but only within the limits set by the pore opening. Even the longest decay time could not compensate for the limitation imposed by the pore. The wider the pore, the fewer its limitations are, and so decay time can play a bigger role.

We also investigated the combined effects of complex turnover rate and pore size. Whereas $K_m$ showed no pattern, which was probably due to the relatively high decay time we had chosen, $V_{max}$ increased gradually with pore size and complex turnover rate. Subsequently, we performed an analysis of variance, which showed that the pore size explained more than twice the variation in $V_{max}$ compared to that explained by complex turnover rate. Thus, soil architecture might be more important for enzyme kinetics in soil than the physiological properties of the enzyme system.

**The maze scenario.** Finally, we discuss our last scenario, the maze, where progressively more complex barriers are placed into the grid. It required a much greater number of time steps to reach a steady state than the other models, which was computationally more demanding. We simulated two seconds and used only the last second for further analysis. Especially the more complex mazes (degree 4 to 6) needed much more time to reach equilibrium. Also the maze model grid is about ten times larger than the grid in the well–mixed and pore scenarios, because, in the simulation software we used (NetLogo), the barriers had to be the size of whole grid cells. We accounted for this by using substrate

densities rather than particle counts.

Similarly to the velocity micro-parameter in the well-mixed scenario, inhomogeneities did form in the six-degree maze model. This lowered the fit to the MM model and is likely the reason for the slight increase in $V_{max}$ for degrees 5 and 6. These inhomogeneities are the result of an unmixing process in which substrate accumulated in certain areas as can be seen in a snapshot at 1.5 s. $K_m$ increased with maze degree, this was expected because the more complex the barriers, the more was the random movement of particles inhibited and paths to binding events became on average longer, decreasing the efficiency of the enzyme.

The fractal-like structure of pore space (Dathe and Thullner, 2005) is represented by the Hilbert curve fractal that we used. The convenient thing about the Hilbert curve is that areas are connected and so particles can move along the channels similarly to how they would move in pore space. We saw with the radial distribution function the appearance of holes at six-degree settings. This behaviour was observed because substrate could move between areas and ultimately accumulate or deplete in certain areas of the maze leading to substrate patchiness as observed in nature. These results are similar to the low-velocity limit in the well-mixed scenario and the process by which those inhomogeneities were formed might also be similar in the two situations. In the low velocity regime, enzymes depleted the substrate around them and substrate was moving too slowly to replace it. In the six-degree maze model, it is apparent that the maze complexity reduces the velocity of particles due to lowering the local diffusion coefficients. Enzyme activities deplete the substrate at the microsite around them, but substrate located elsewhere is only very slowly filling up the voids, because of their delayed movement due to many barriers.

Next, decay time in the six-degree maze scenario was investigated. With decay time $K_m$ increased and there was an increase in $V_{max}$ for the longest decay time (10% of the total runtime). We also observed that the fit became worse with decay time just as it did with the maze degree settings. This can be explained by understanding how the decay time micro-parameter works. When the decay time expires, enzymes are taken off the grid and placed back into the grid in a random position. Recall that over time, substrate forms holes around enzymes in the six-degree maze scenario. When the positions of enzymes are randomly reset, enzyme particles are no longer at the centre of those holes. Thus, when decay time is short enough that this unmixing process could not have taken place yet, the fit to the MM model is better and $K_m$ is smaller.

Imagine a flat layer of soil where extracellular enzymes diffuse onto its surface from all sides. Inside this layer, these enzymes continue to move but gradually decay due to denaturation and the degradative activity of extracellular proteases. Our model suggests

that as the flux of extracellular enzymes from the outside and the rate of enzyme turnover change, the efficiency of these enzymes ($K_m$) will also change. For soil microbes, this implies that it might be more advantageous to produce a larger quantity of extracellular enzymes, even if they are of lower quality and decay more rapidly, as there is a well-known trade-off between enzyme quantity and quality in soil microbes (Allison and Vitousek, 2005). However, in reality, enzymes are produced by microbes, and are thus bound to their location. Instead of having many random places where new enzymes appear, there would likely be a few hotspots where microbes or microbial colonies are producing them. Still we could imagine a situation at the boundaries of an area of soil that has a common enzyme pool where the microbes that produced those enzymes might be further away and enzymes, that diffused in all directions away from the microbial hotspot, might be more homogeneously distributed.

**Conclusion.** In conclusion, we set up models that investigated the effects of soil temperature, moisture and architecture on SOC decomposition dynamics. We simulated temperature and moisture with the velocity, physiological properties of the enzyme with the affinity and complex turnover rate parameters, and soil architecture by placing barriers into the models (see Table 2.2). In all three scenarios, we could fit the MM equation to our observed enzyme kinetics, even in models that explicitly violated the spatial homogeneity assumption. Nonetheless, when affinity exceeded 40% in the well-mixed scenarioor or the maze degree surpassed 3, the fit of the MM model became progressively worse. In the low-velocity regime in the well-mixed scenario, $K_m$ decreased with velocity, probably due to emergent spatial heterogeneity, whereas the maximum reaction rate did not respond. We could observe the same pattern in the maze scenario where we forced an increase in spatial complexity. In both scenarios, holes in substrate density around enzymes emerged at certain thresholds. The effect of decay time on $V_{max}$ and $K_m$ differed across all three scenarios. Decay time did not matter in the well-mixed scenario as expected, whereas the effect on $K_m$ was negative in the pore scenario and positive in the maze scenario making it difficult to understand it in a spatial context. Also, the effect of decay time on $V_{max}$ was positive in the pore scenario but unclear in the maze scenario. SOC turnover models that include enzyme dynamics are often parameterized by taking $V_{max}$ and $K_m$ from experimental measurements of soil enzymes (German et al., 2012). However, these experiments disrupt soil structure, creating a well-mixed environment. Our findings demonstrate that enzyme kinetics in soil are governed by the soil architecture and that soil structural properties, such as pore size diameter and complexity may have a greater impact on enzyme rates and efficiencies than the enzyme properties themselves. Therefore, future soil model parameterization should take our findings into account.

## 2.5 Supplementary Material

Table 2.3: Micro-parameter models for $V_{max}$ (all velocity classes)

| Model | Adjusted $R^2$ | p-value |
|---|---|---|
| velocity | 0 | $3.958 \cdot 10^{-4}$ |
| complex turnover rate | 0.7237 | $< 2.2 \cdot 10^{-16}$ |
| affinity | 0 | 0.7159 |

Table 2.4: Micro-parameter models for $V_{max}$ (velocity $\leq 3.5$ $\mu m/ms$)

| Model | Adjusted $R^2$ | p-value |
|---|---|---|
| velocity | 0 | 0.002017 |
| complex turnover rate | 0.8321 | $< 2.2 \cdot 10^{-16}$ |
| affinity | 0 | 0.5517 |

Table 2.5: Micro-parameter models for $V_{max}$ (velocity $> 3.5$ $\mu m/ms$)

| Model | Adjusted $R^2$ | p-value |
|---|---|---|
| velocity | 0 | 0.8483 |
| complex turnover rate | 0.9879 | $< 2.2 \cdot 10^{-16}$ |
| affinity | 0 | 0.8422 |

Table 2.6: Micro-parameter models for $K_m$ (all velocity classes)

| Model | Adjusted $R^2$ | p-value |
|---|---|---|
| velocity / affinity | 0.005611 | 0.1769 |
| complex turnover rate / affinity | 0.09651 | $6.458 \cdot 10^{-5}$ |
| (affinity + complex turnover rate) / velocity | 0.4108 | $2.2 \cdot 10^{-16}$ |
| (affinity + velocity) / complex turnover rate | 0.07199 | $5.282 \cdot 10^{-4}$ |
| (velocity + complex turnover rate) / affinity | 0.004617 | 0.1955 |
| affinity | 0.0461 | 0.004796 |
| velocity | 0.2222 | $6.88 \cdot 10^{-10}$ |
| complex turnover rate | 0.02626 | 0.02658 |

Table 2.7: Micro-parameter models for $K_m$ (velocity $\leq 3.5$ $\mu m/ms$)

| Model | Adjusted $R^2$ | p-value |
|---|---|---|
| velocity / affinity | 0 | 0.425 |
| complex turnover rate / affinity | 0.09868 | 0.003514 |
| (affinity + complex turnover rate) / velocity | 0.2639 | $1.453 \cdot 10^{-6}$ |
| (affinity + velocity) / complex turnover rate | 0.07133 | 0.01172 |
| (velocity + complex turnover rate) / affinity | 0.001114 | 0.3016 |
| affinity | 0.03899 | 0.04916 |
| velocity | 0.6559 | $2.2 \cdot 10^{-16}$ |
| complex turnover rate | 0.08962 | 0.005241 |

Table 2.8: Micro-parameter models for $K_m$ (velocity $> 3.5$ $\mu m/ms$)

| Model | Adjusted $R^2$ | p-value |
|---|---|---|
| velocity / affinity | 0.4958 | $1.104 \cdot 10^{-11}$ |
| complex turnover rate / affinity | 0.9928 | $2.2 \cdot 10^{-16}$ |
| (affinity + complex turnover rate) / velocity | 0.107 | 0.00243 |
| (affinity + velocity) / complex turnover rate | 0.5041 | $5.963 \cdot 10^{-13}$ |
| (velocity + complex turnover rate) / affinity | 0.5021 | $6.905 \cdot 10^{-13}$ |
| affinity | 0.5534 | $1.254 \cdot 10^{-14}$ |
| velocity | 0 | 0.6886 |
| complex turnover rate | 0 | 0.328 |

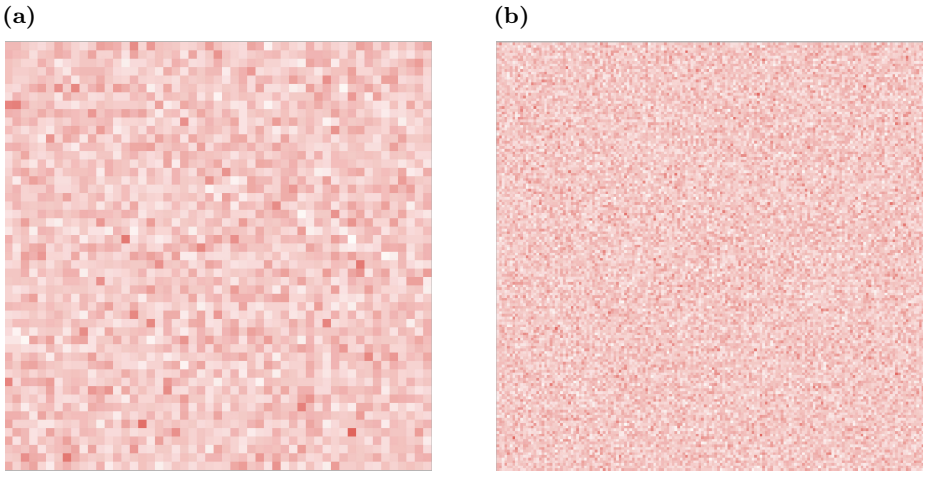


Figure 2.26: Local diffusion coefficients of all cells for the well-mixed model (a) and the maze model degree 0 (b), we see that the maze model is larger than the well-mixed model and that both have similar mean local diffusion coefficients which are higher compared to the other model variants.

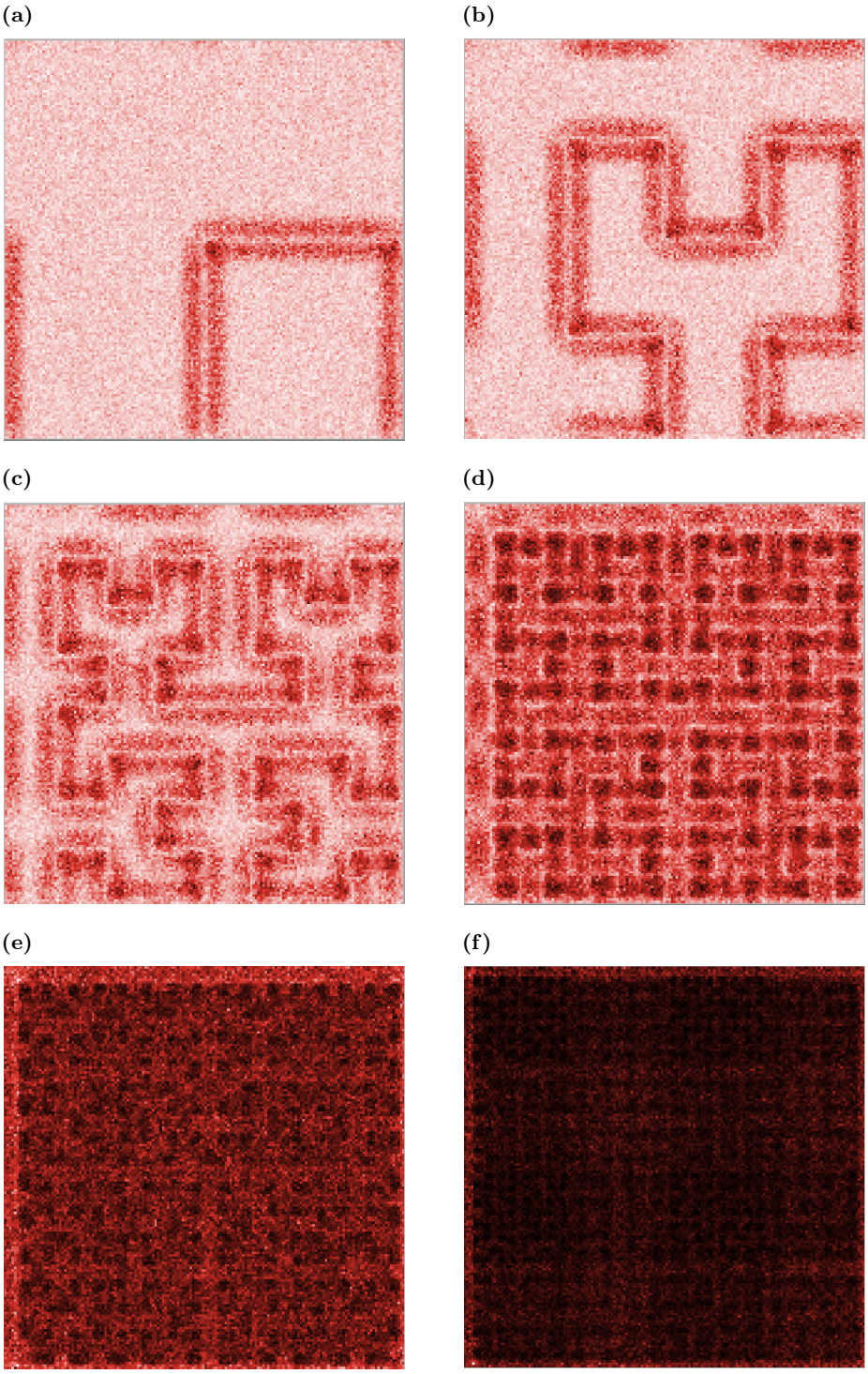


Figure 2.27: Diffusion coefficients of all cells for the maze model degree 1 to 6 (a-f)

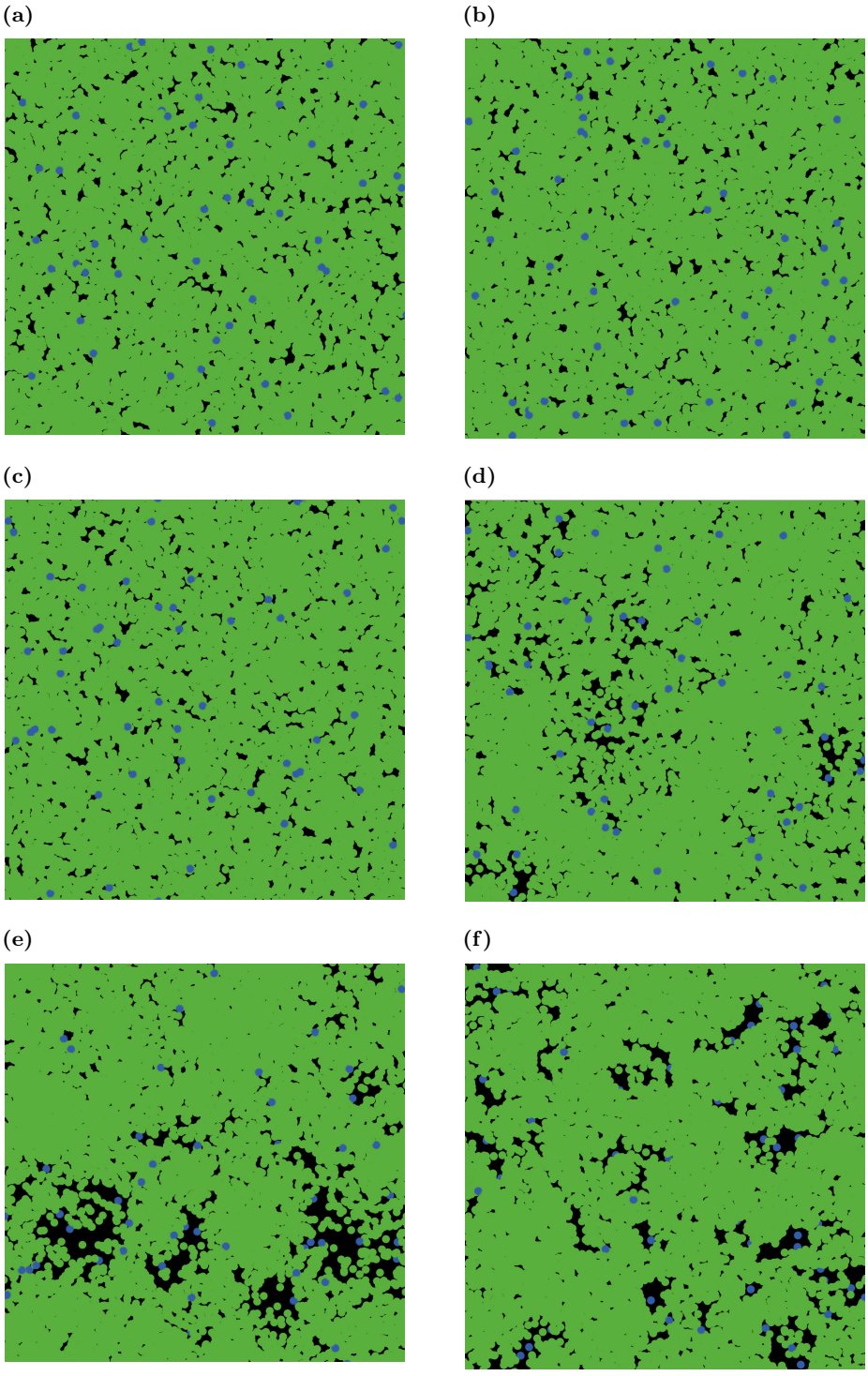


Figure 2.28: Substrate (green) and enzyme (blue) distributions at varying velocity settings (a: velocity = 350 $\mu m/ms$, b: 175 $\mu m/ms$, c: 35 $\mu m/ms$, d: 3.5 $\mu m/ms$, e: 1.75 $\mu m/ms$, f: 0.35 $\mu m/ms$); we can see holes appearing at velocity micro-parameter settings of $\leq 3.5$ $\mu m/ms$

# 3 Summary/Zusammenfassung

## 3.1 Summary

Microbial decomposition of soil organic carbon (SOC) is the major source of land carbon dioxide emissions and therefore a key component of the terrestrial carbon cycle. The initial phase of soil organic matter degradation is facilitated by extracellular enzymes, which are secreted by soil microbes into the soil solution. Most biogeochemical models represent this process through 'Michaelis-Menten' enzyme kinetics, which assume that the reactants, namely enzymes and complex organic matter molecules interact within a well-mixed environment. However, soil is characterized by a complex network of physical pores and a heterogenous distribution of organic matter at the micrometre to millimetre scale, creating a highly spatially structured environment where enzyme reactions occur. It remains uncertain whether enzyme kinetics, which are usually observed in well-mixed soil slurries, accurately reflect those in spatially structured soil environments.

The aim of this thesis was to examine the influence of a spatially structured environment on the kinetics of extracellular enzymes degrading complex organic matter. Towards this goal, I developed an individual-based model to simulate the interactions between enzyme and substrate particles at the micrometre-scale. This allowed me to recreate the dynamics that form the foundations of enzyme kinetics based on molecular-scale (i.e., first principle) interactions: individual enzyme and substrate particles in my model diffuse within the soil solution and, upon collision, form an enzyme-substrate complex, which subsequently produces enzymatic breakdown products available for microbial uptake. I first tested the feasibility of the model by fitting a Michaelis-Menten curve to the aggregated simulation results in a well-mixed environment. After that, I generated two scenarios where the spatial environment explicitly violated the homogeneity assumption of Michaelis-Menten kinetics. In the first scenario, organic matter was situated within a soil pore inaccessible to microbes, necessitating the diffusion of microbially-produced enzymes into the pore and the diffusion of enzymatic products out of it before they become available for microbial uptake. The last scenario involved increasing levels of spatial complexity in the soil. To simulate the fractal-like maze structure of soil pore space, I added progressively more

complex Hilbert curves as spatial barriers to the model, thereby investigating whether and how soil structual complexity governs enzyme kinetics.

My results show that the Michaelis-Menten curve could be fitted to reaction rate data from all three scenarios. However, its kinetic parameters (i.e., the maximum rate of enzyme activity, $V_{max}$ and the half-saturation constant, which is also a proxy for the efficiency of an enzyme system, $K_m$) differed between and were influenced by different factors in the well-mixed and spatial settings. As expected from the theory on enzyme kinetics, microscale parameters related to the enzyme reaction physiology, such as the turnover time of the enzyme-substrate complex, particle movement velocity and enzyme-substrate complex formation probability, were the main drivers of $V_{max}$ and $K_m$ in the well-mixed setting. In spatial settings, however, other microscale parameters related to the spatial structure partly played a greater role, overruling the influence of physiological parameters. Pore size exerted a bigger influence on the maximum rate of enzyme activity (defined as breakdown products becoming available to the microbes) compared to physiological micro-parameters. Enzyme lifetime, which did not play a role in well-mixed settings, had a positive effect on maximum enzyme rates in the pore scenario, and was positively associated with $K_m$ in the maze scenarios. Increasing fractal complexities led to an exponential increase of $K_m$ (i.e., decreasing enzyme efficiency at non-saturation substrate concentrations), as substrate and enzyme spatial distributions became increasingly separated with higher maze complexities. In addition to the influence of spatial structure on the regulation of kinetic parameters, I also observed that, certain conditions diminished the overall fit of a Michaelis-Menten curve to the model output. Specifically, when maze complexity exceeded degree 3, substrate depletion occurred around enzymes, forming holes in substrate density, increasing heterogeneity of substrate distribution. This, in turn, affected the saturation profile of the enzyme kinetics. Such a feedback from microscale interactions on the spatial homogeneity of substrate distribution was also observed in the well-mixed scenario when particle velocity was below 35 $\mu m/ms$.

By recreatinge enzyme kinetics based on first principles using an individual-based model, I demonstrated that micro-scale spatial structure significantly influences the parameters of enzyme kinetics ($V_{max}$ and $K_m$), which is usually not accounted for in the parametrisation of larger models that include SOC decomposition dynamics. This suggests that kinetic parameters obtained from measurements in well-mixed soil slurries have limited utility for model parameterization and should be used with caution. It also indicates that evolutionary pressures on microbial enzyme systems in soils likely target not only physiological parameters, but also the enzymes' capacity to operate under certain soil physical conditions. The latter aspect may enhance the relative importance of enzyme

life-times, and diminish the significance of physiological affinities, as low-substrate enzyme efficiency is significantly controlled by soil structural complexity rather than physiological affinities alone.

## 3.2 Zusammenfassung

Mikrobielle Zersetzung von organischem Bodenkohlenstoff (SOC) ist die Hauptquelle der landbasierten Kohlendioxidemissionen und daher ein zentraler Bestandteil des terrestrischen Kohlenstoffkreislaufs. Die initiale Phase des Abbaus von organischer Bodensubstanz wird von extrazellulären Enzymen durchgeführt, die von Bodenmikroben in die Bodenlösung abgegeben werden. Die meisten biogeochemischen Modelle stellen diesen Prozess durch die „Michaelis-Menten"-Enzymkinetik dar, die davon ausgeht, dass die Reaktanten, nämlich Enzyme und komplexe organische Moleküle, in einer gut durchmischten Umgebung interagieren. Allerdings ist der Boden durch ein komplexes Netzwerk physikalischer Poren und eine heterogene Verteilung organischer Substanz im Mikro- bis Millimeterbereich gekennzeichnet. Dies schafft eine hochgradig räumlich strukturierte Umgebung, in der enzymatische Reaktionen ablaufen. Es bleibt ungewiss, ob die Enzymkinetik, die üblicherweise in gut durchmischten Bodensuspensionen beobachtet wird, tatsächlich die Verhältnisse in räumlich strukturierten Bodenumgebungen widerspiegelt.

Das Ziel dieser Arbeit war es, den Einfluss einer räumlich strukturierten Umgebung auf die Kinetik extrazellulärer Enzyme, die komplexe organische Substanz abbauen, zu untersuchen. Zu diesem Zweck habe ich ein individualbasiertes Modell entwickelt, um die Wechselwirkungen zwischen Enzym- und Substratteilchen auf der Mikrometerebene zu simulieren. Dadurch konnte ich die Dynamiken nachbilden, die die Grundlage der Enzymkinetik auf molekularer Ebene (d. h. aus erster Prinzipien) bilden: In meinem Modell diffundieren einzelne Enzym- und Substratteilchen in der Bodenlösung und bilden bei einer Kollision einen Enzym-Substrat-Komplex, der anschließend enzymatische Abbauprodukte erzeugt, die für die mikrobielle Aufnahme verfügbar sind. Zunächst testete ich die Anwendbarkeit des Modells, indem ich eine Michaelis-Menten-Kurve an die aggregierten Simulationsergebnisse in einer gut durchmischten Umgebung anpasste. Danach erzeugte ich zwei Szenarien, in denen die räumliche Umgebung explizit gegen die Homogenitätsannahme der Michaelis-Menten-Kinetik verstieß. Im ersten Szenario befand sich organische Substanz in einer Bodenpore, die für Mikroben unzugänglich war, sodass mikrobiell produzierte Enzyme in die Pore diffundieren mussten und enzymatische Abbauprodukte aus der Pore herausdiffundieren mussten, bevor sie für die mikrobielle Aufnahme verfügbar wurden. Das letzte Szenario umfasste zunehmende Stufen räumlicher Komplexität im Boden. Um die fraktalartige Labyrinthstruktur des Bodenporenraums zu simulieren, fügte ich dem Modell schrittweise komplexere Hilbert-Kurven als räumliche Barrieren hinzu und untersuchte so, ob und wie die strukturelle Komplexität des Bodens die Enzymkinetik beeinflusst.

Meine Ergebnisse zeigen, dass die Michaelis-Menten-Kurve an die Reaktionsraten-Daten aus allen drei Szenarien angepasst werden konnte. Allerdings unterschieden sich die kinetischen Parameter (d. h. die maximale Enzymaktivität $V_{max}$ und die Halb-Sättigungskonstante, die auch als Proxy für die Effizienz eines Enzymsystems dient, $K_m$) zwischen den gut durchmischten und räumlichen Szenarien und wurden von unterschiedlichen Faktoren beeinflusst. Wie aus der Theorie der Enzymkinetik zu erwarten war, waren mikroskalige Parameter, die mit der physiologischen Enzymreaktion zusammenhängen, wie die Umsatzzeit des Enzym-Substrat-Komplexes, die Geschwindigkeit der Teilchen und die Wahrscheinlichkeit der Enzym-Substrat-Komplex-Bildung, die Haupttreiber von $V_{max}$ und $K_m$ in der gut durchmischten Umgebung. In räumlichen Umgebungen spielten jedoch andere mikroskalige Parameter, die mit der räumlichen Struktur zusammenhingen, teilweise eine größere Rolle und überlagerten den Einfluss physiologischer Parameter. Die Porengröße hatte einen größeren Einfluss auf die maximale Enzymaktivität (definiert als die Menge an Abbauprodukten, die Mikroben zur Verfügung steht) als physiologische Mikroparameter. Die Lebenszeit eines Enzyms, die in gut durchmischten Umgebungen keine Rolle spielte, hatte im Pore-Szenario einen positiven Effekt auf die maximale Enzymaktivität und war in den Labyrinth-Szenarien positiv mit $K_m$ assoziiert. Eine zunehmende fraktale Komplexität führte zu einem exponentiellen Anstieg von $K_m$ (d. h. einer abnehmenden Enzymeffizienz bei nicht-saturierenden Substratkonzentrationen), da sich die räumlichen Verteilungen von Substrat und Enzym mit zunehmender Labyrinthkomplexität immer stärker trennten. Neben dem Einfluss der räumlichen Struktur auf die Regulation kinetischer Parameter beobachtete ich außerdem, dass unter bestimmten Bedingungen die Anpassung einer Michaelis-Menten-Kurve an die Modellausgabe insgesamt schlechter wurde. Insbesondere wenn die Labyrinthkomplexität den Grad 3 überschritt, führte die Substratverarmung in der Nähe von Enzymen zur Bildung von „Löchern“ in der Substratdichte, was die Heterogenität der Substratverteilung erhöhte. Dies wiederum beeinflusste das Sättigungsprofil der Enzymkinetik. Eine solche Rückkopplung mikroskaliger Wechselwirkungen auf die räumliche Homogenität der Substratverteilung wurde auch im gut durchmischten Szenario beobachtet, wenn die Geschwindigkeit der Teilchen unter 35 $\mu m/ms$ lag.

Durch die Nachbildung der Enzymkinetik aus erster Prinzipien mithilfe eines individualbasierten Modells konnte ich zeigen, dass die mikroskalige räumliche Struktur die Parameter der Enzymkinetik ($V_{max}$ und $K_m$) erheblich beeinflusst – ein Faktor, der in größeren Modellen zur SOC-Zersetzungsdynamik meist nicht berücksichtigt wird. Dies legt nahe, dass kinetische Parameter, die aus Messungen in gut durchmischten Bodensuspensionen gewonnen wurden, nur eingeschränkt für die Modellparametrisierung geeignet

sind und mit Vorsicht verwendet werden sollten. Zudem deutet es darauf hin, dass evolutionäre Selektionsdrücke auf mikrobielle Enzymsysteme im Boden nicht nur auf physiologische Parameter abzielen, sondern auch auf die Fähigkeit der Enzyme, unter bestimmten physikalischen Bodenbedingungen zu funktionieren. Dieser Aspekt könnte die relative Bedeutung der Enzym-Lebenszeit verstärken und die Relevanz physiologischer Affinitäten verringern, da die Enzymeffizienz bei niedrigen Substratkonzentrationen erheblich durch die strukturelle Komplexität des Bodens und nicht allein durch physiologische Affinitäten gesteuert wird.

# Bibliography

Rose Z Abramoff, Bertrand Guenet, Haicheng Zhang, Katerina Georgiou, Xiaofeng Xu, Raphael A Viscarra Rossel, Wenping Yuan, and Philippe Ciais. Improved global-scale predictions of soil carbon stocks with millennial version 2. *Soil Biology and Biochemistry*, 164:108466, 2022.

M Acín-Carrera, M José Marques, P Carral, AM Álvarez, C López, B Martín-López, and JA González. Impacts of land-use intensity on soil organic carbon content, soil structure and water-holding capacity. *Soil Use and Management*, 29(4):547–556, 2013.

Kristin Aleklett, E Toby Kiers, Pelle Ohlsson, Thomas S Shimizu, Victor EA Caldas, and Edith C Hammer. Build your own soil: exploring microfluidics to create microbial habitat structures. *The ISME journal*, 12(2):312–319, 2018.

Steven D Allison and Peter M Vitousek. Responses of extracellular enzymes to simple and complex nutrient inputs. *Soil Biology and Biochemistry*, 37(5):937–944, 2005.

Steven D Allison, Matthew D Wallenstein, and Mark A Bradford. Soil-carbon response to warming dependent on microbial physiology. *Nature Geoscience*, 3(5):336–340, 2010.

Steven D Allison, Michael N Weintraub, Tracy B Gartner, and Mark P Waldrop. Evolutionary-economic principles as regulators of soil enzyme production and ecosystem function. *Soil enzymology*, pages 229–243, 2011.

Carlos Arellano-Caicedo, Pelle Ohlsson, Martin Bengtsson, Jason P Beech, and Edith C Hammer. Habitat complexity affects microbial growth in fractal maze. *Current Biology*, 33(8):1448–1458, 2023.

Vivek K Arora, Anna Katavouta, Richard G Williams, Chris D Jones, Victor Brovkin, Pierre Friedlingstein, Jörg Schwinger, Laurent Bopp, Olivier Boucher, Patricia Cadule, et al. Carbon–concentration and carbon–climate feedbacks in cmip6 models and their comparison to cmip5 models. *Biogeosciences*, 17(16):4173–4222, 2020.

Ali Asaadi, Jörg Schwinger, Hanna Lee, Jerry Tjiputra, Vivek Arora, Roland Séférian, Spencer Liddicoat, Tomohiro Hajima, Yeray Santana-Falcón, and Chris D Jones. Carbon cycle feedbacks in an idealized simulation and a scenario simulation of negative emissions in cmip6 earth system models. *Biogeosciences*, 21(2):411–435, 2024.

Christian Azar and Daniel JA Johansson. Ipcc and the effectiveness of carbon sinks. *Environmental Research Letters*, 17(4):041004, 2022.

Richard D Bardgett, Chris Freeman, and Nicholas J Ostle. Microbial contributions to climate change through carbon cycle feedbacks. *The ISME journal*, 2(8):805–814, 2008.

Peggy Baudouin-Cornu, Yolande Surdin-Kerjan, Philippe Marliere, and Dominique Thomas. Molecular evolution of protein atomic composition. *Science*, 293(5528): 297–300, 2001.

Nyle C. Brady and Ray R. Weil. The nature and properties of soil. *Mac. Pub. Com. New York*, pages 625–640, 1999.

George Edward Briggs and John Burdon Sanderson Haldane. A note on the kinetics of enzyme action. *Biochemical journal*, 19(2):338, 1925.

Richard G Burns and Richard P Dick. *Enzymes in the environment: activity, ecology, and applications*. CRC press, 2002.

Richard G Burns, Jared L DeForest, Jürgen Marxsen, Robert L Sinsabaugh, Mary E Stromberger, Matthew D Wallenstein, Michael N Weintraub, and Annamaria Zoppini. Soil enzymes in a changing environment: current knowledge and future directions. *Soil Biology and Biochemistry*, 58:216–234, 2013a.

Richard G. Burns, Jared L. DeForest, Jürgen Marxsen, Robert L. Sinsabaugh, Mary E. Stromberger, Matthew D. Wallenstein, Michael N. Weintraub, and Annamaria Zoppini. Soil enzymes in a changing environment: Current knowledge and future directions. *Soil Biology and Biochemistry*, 58:216–234, 3 2013b. ISSN 00380717. doi: 10.1016/j.soilbio.2012.11.009.

Keith C Cameron and Graeme D Buchan. Porosity and pore size distribution. *Encyclopedia of soil science*, 2:1350–1353, 2006.

Florian Centler, Ingo Fetzer, and Martin Thullner. Modeling population patterns of chemotactic bacteria in homogeneous porous media. *Journal of Theoretical Biology*, 287:82–91, 2011.

Arjun Chakrawal, Anke M Herrmann, John Koestel, Jerker Jarsjö, Naoise Nunan, Thomas Kätterer, and Stefano Manzoni. Dynamic upscaling of decomposition kinetics for carbon cycling models. *Geoscientific Model Development*, 13(3):1399–1429, 2020.

Yi Chen, Yue Wen, Jing Cheng, ChongHua Xue, Dianhai Yang, and Qi Zhou. Effects of dissolved oxygen on extracellular enzymes activities and transformation of carbon sources from plant biomass: implications for denitrification in constructed wetlands. *Bioresource technology*, 102(3):2433–2440, 2011.

Edward A Codling, Michael J Plank, and Simon Benhamou. Random walk models in biology. *Journal of the Royal society interface*, 5(25):813–834, 2008.

Ohana YA Costa, Jos M Raaijmakers, and Eiko E Kuramae. Microbial extracellular polymeric substances: ecological function and impact on soil aggregation. *Frontiers in microbiology*, 9:1636, 2018.

Annette Dathe and Martin Thullner. The relationship between fractal properties of solid matrix and pore space in porous media. *Geoderma*, 129(3-4):279–290, 2005.

Vidal-Diez de Ulzurrun, JM Baetens, Jan Van den Bulcke, and Bernard De Baets. Modelling three-dimensional fungal growth in response to environmental stimuli. *Journal of Theoretical Biology*, 414:35–49, 2017.

Erez Dekel and Uri Alon. Optimality and evolutionary tuning of the expression level of a protein. *Nature*, 436(7050):588–592, 2005.

Richard P Dick. *Methods of soil enzymology*, volume 26. John Wiley & Sons, 2020.

WA Dick and MA Tabatabai. Kinetics and activities of phosphatase-clay complexes1. *Soil Science*, 143(1):5–15, 1987.

Albert Einstein. Über die von der molekularkinetischen theorie der wärme geforderte bewegung von in ruhenden flüssigkeiten suspendierten teilchen. *Annalen der physik*, 4, 1905.

Warren John Ewens. *Mathematical population genetics: theoretical introduction*, volume 27. Springer, 2004.

Ruth E Falconer, James L Bown, Nia A White, and John W Crawford. Modelling interactions in fungi. *Journal of the Royal Society Interface*, 5(23):603–615, 2008.

Simone Fatichi, Dani Or, Robert Walko, Harry Vereecken, Michael H Young, Teamrat A Ghezzehei, Tomislav Hengl, Stefan Kollet, Nurit Agam, and Roni Avissar. Soil structure is an important omission in earth system models. *Nature communications*, 11(1):522, 2020.

Jens Feder. *Fractals*. Springer Science & Business Media, 2013.

Sébastien Fontaine, Gérard Bardoux, Luc Abbadie, and André Mariotti. Carbon input to soil may decrease soil carbon content. *Ecology letters*, 7(4):314–320, 2004.

Pierre Friedlingstein, Malte Meinshausen, Vivek K Arora, Chris D Jones, Alessandro Anav, Spencer K Liddicoat, and Reto Knutti. Uncertainties in cmip5 climate projections due to carbon cycle feedbacks. *Journal of Climate*, 27(2):511–526, 2014.

Pierre Friedlingstein, Michael O'sullivan, Matthew W Jones, Robbie M Andrew, Dorothee CE Bakker, Judith Hauck, Peter Landschützer, Corinne Le Quéré, Ingrid T Luijkx, Glen P Peters, et al. Global carbon budget 2023. *Earth System Science Data*, 15(12):5301–5369, 2023.

F Gabbiani and SJ Cox. Mathematics for neuroscientists. *San Diego*, 2010.

Pablo García-Palacios, Thomas W Crowther, Marina Dacal, Iain P Hartley, Sabine Reinsch, Riikka Rinnan, Johannes Rousk, Johan van den Hoogen, Jian-Sheng Ye, and Mark A Bradford. Evidence for large microbial-mediated losses of soil carbon under anthropogenic warming. *Nature Reviews Earth & Environment*, 2(7):507–517, 2021.

Katerina Georgiou, Avni Malhotra, William R Wieder, Jacqueline H Ennis, Melannie D Hartman, Benjamin N Sulman, Asmeret Asefaw Berhe, A Stuart Grandy, Emily Kyker-Snowman, Kate Lajtha, et al. Divergent controls of soil organic carbon between observations and process-based models. *Biogeochemistry*, 156(1):5–17, 2021.

Donovan P German, Kathleen RB Marcelo, Madeleine M Stone, and Steven D Allison. The m ichaelis–m enten kinetics of soil extracellular enzymes in response to temperature: a cross-latitudinal study. *Global Change Biology*, 18(4):1468–1479, 2012.

Domenic PJ Germano, Adriana Zanca, Stuart T Johnston, Jennifer A Flegg, and James M Osborne. Free and interfacial boundaries in individual-based models of multicellular biological systems. *Bulletin of Mathematical Biology*, 85(11):111, 2023.

Joshua I Gold and Michael N Shadlen. The neural basis of decision making. *Annu. Rev. Neurosci.*, 30:535–574, 2007.

John M Halley. Ecology, evolution and 1f-noise. *Trends in ecology & evolution*, 11(1): 33–37, 1996.

John M Halley and William E Kunin. Extinction risk and the 1/f family of noise models. *Theoretical Population Biology*, 56(3):215–230, 1999.

RA Houghton. Balancing the global carbon budget. *Annu. Rev. Earth Planet. Sci.*, 35: 313–347, 2007.

Nicolas E Humphries, Nuno Queiroz, Jennifer RM Dyer, Nicolas G Pade, Michael K Musyl, Kurt M Schaefer, Daniel W Fuller, Juerg M Brunnschweiler, Thomas K Doyle, Jonathan DR Houghton, et al. Environmental context explains lévy and brownian movement patterns of marine predators. *Nature*, 465(7301):1066–1069, 2010.

Hosagrahar V Jagadish. Analysis of the hilbert curve for representing two-dimensional space. *Information Processing Letters*, 62(1):17–22, 1997.

Kenneth A Johnson and Roger S Goody. The original michaelis constant: translation of the 1913 michaelis–menten paper. *Biochemistry*, 50(39):8264–8269, 2011.

Christina Kaiser, Oskar Franklin, Ulf Dieckmann, and Andreas Richter. Microbial community dynamics alleviate stoichiometric constraints during litter decay. *Ecology letters*, 17(6):680–690, 2014.

Christina Kaiser, Oskar Franklin, Andreas Richter, and Ulf Dieckmann. Social dynamics within decomposer communities lead to nitrogen retention and organic matter build-up in soils. *Nature communications*, 6(1):1–10, 2015.

Hyojoon Kim and Kook Joe Shin. Diffusion influence on michaelis–menten kinetics: Ii. the low substrate concentration limit. *Journal of Physics: Condensed Matter*, 19(6): 065137, 2007.

AN Kravchenko, AK Guber, BS Razavi, J Koestel, MY Quigley, GP Robertson, and Y Kuzyakov. Microbial spatial footprint as a driver of soil carbon stabilization. *Nature communications*, 10(1):3121, 2019.

Louis Lancaster, Walaa Abdallah, Scott Banta, and Ian Wheeldon. Engineering enzyme microenvironments for enhanced biocatalysis. *Chemical Society Reviews*, 47(14):5177–5186, 2018.

Sonja Leitner, Peter M Homyak, Joseph C Blankinship, Jennifer Eberwein, G Darrel Jenerette, Sophie Zechmeister-Boltenstern, and Joshua P Schimel. Linking no and n2o emission pulses with the mobilization of mineral and organic n upon rewetting dry soils. *Soil Biology and Biochemistry*, 115:461–466, 2017.

E Lugato, Francesco Morari, Serenella Nardi, Antonio Berti, and L Giardini. Relationship between aggregate pore size distribution and organic–humic carbon in contrasting soils. *Soil and Tillage Research*, 103(1):153–157, 2009.

Benoit B Mandelbrot. *The Fractal Geometry of Nature*. WH freeman New York, 1983.

Stefano Manzoni, SM Schaeffer, G Katul, A Porporato, and JP Schimel. A theoretical analysis of microbial eco-physiological and diffusion limitations to carbon cycling in drying soils. *Soil Biology and Biochemistry*, 73:69–83, 2014.

Alejandro G Marangoni. *Enzyme kinetics: a modern approach*. John Wiley & Sons, 2003.

Valérie Masson-Delmotte, Panmao Zhai, Anna Pirani, Sarah L Connors, Clotilde Péan, Sophie Berger, Nada Caud, Y Chen, L Goldfarb, MI Gomis, et al. Climate change 2021: the physical science basis. *Contribution of working group I to the sixth assessment report of the intergovernmental panel on climate change*, 2, 2021.

Filip JR Meysman, Jack J Middelburg, and Carlo HR Heip. Bioturbation: a fresh look at darwin's last idea. *Trends in Ecology & Evolution*, 21(12):688–695, 2006.

Christina Cruickshank Miller and James Walker. The stokes-einstein law for diffusion in solution. *Proceedings of the Royal Society of London. Series A, Containing Papers of a Mathematical and Physical Character*, 106(740):724–749, 1924. doi: 10.1098/rspa.1924.0100. URL `https://royalsocietypublishing.org/doi/abs/10.1098/rspa.1924.0100`.

Paolo Nannipieri, Ellen Kandeler, Pacifico Ruggiero, et al. Enzyme activities and microbiological and biochemical processes in soil. *Enzymes in the Environment*, pages 1–33, 2002.

Paolo Nannipieri, Judith Ascher, MariaTeresa Ceccherini, L Landi, G Pietramellara, and G Renella. Microbial diversity and soil functions. *European journal of soil science*, 54 (4):655–670, 2003.

Naoise Nunan. The microbial habitat in soil: scale, heterogeneity and functional consequences. *Journal of Plant Nutrition and Soil Science*, 180(4):425–429, 2017.

Naoise Nunan, Hannes Schmidt, and Xavier Raynaud. The ecology of heterogeneity: soil bacterial communities and c dynamics. *Philosophical Transactions of the Royal Society B*, 375(1798):20190249, 2020.

Akira Okubo, Simon A Levin, et al. *Diffusion and ecological problems: modern perspectives*, volume 14. Springer, 2001.

Magdalena Olkiewicz, Bartosz Tylkowski, Josep M Montornés, Ricard Garcia-Valls, and Iwona Gulaczyk. Modelling of enzyme kinetics: cellulose enzymatic hydrolysis case. *Physical Sciences Reviews*, 7(8):901–921, 2020.

Brian C O'neill, Michael Oppenheimer, Rachel Warren, Stephane Hallegatte, Robert E Kopp, Hans O Pörtner, Robert Scholes, Joern Birkmann, Wendy Foden, Rachel Licker, et al. Ipcc reasons for concern regarding climate change risks. *Nature Climate Change*, 7(1):28–37, 2017.

D Or, Barth F Smets, JM Wraith, Arnaud Dechesne, and SP Friedman. Physical constraints affecting bacterial habitats and activity in unsaturated porous media–a review. *Advances in Water Resources*, 30(6-7):1505–1527, 2007.

Francisco J Pérez-Reche, Sergei N Taraskin, Wilfred Otten, MP Viana, L da F Costa, and Christopher A Gilligan. Prominent effect of soil network heterogeneity on microbial invasion. *Physical Review Letters*, 109(9):098102, 2012.

Giacomo Pietramellara, Judith Ascher, MARIA TERESA Ceccherini, Giancarlo Renella, et al. Soil as a biological system. *Annals of microbiology*, 52(2):119–132, 2002.

Xavier Portell, Valérie Pot, Patricia Garnier, Wilfred Otten, and Philippe C Baveye. Microscale heterogeneity of the spatial distribution of organic matter can promote bacterial biodiversity in soils: insights from computer simulations. *Frontiers in microbiology*, 9: 368481, 2018.

Valérie Pot, Xavier Portell, Wilfred Otten, Patricia Garnier, Olivier Monga, and Philippe C Baveye. Accounting for soil architecture and microbial dynamics in microscale models: Current practices in soil science and the path ahead. *European Journal of Soil Science*, 73(1):e13142, 2022.

Haluk Resat, Vanessa Bailey, Lee Ann McCue, and Allan Konopka. Modeling microbial dynamics in heterogeneous environments: growth on soil carbon sources. *Microbial Ecology*, 63:883–897, 2012.

Emily B Roberson and Mary K Firestone. Relationship between desiccation and exopolysaccharide production in a soil pseudomonas sp. *Applied and environmental microbiology*, 58(4):1284–1291, 1992.

David Victor Roberts. Enzyme kinetics. Technical report, 1977.

Joeri Rogelj, Malte Meinshausen, and Reto Knutti. Global warming under old and new scenarios using ipcc climate sensitivity range estimates. *Nature climate change*, 2(4): 248–253, 2012.

Anna M Romaní, Katharina Fund, Joan Artigas, Thomas Schwartz, Sergi Sabater, and Ursula Obst. Relevance of polymeric matrix enzymes during biofilm formation. *Microbial ecology*, 56:427–436, 2008.

David S Schimel and Dustin Carroll. Carbon cycle–climate feedbacks in the post-paris world. *Annual Review of Earth and Planetary Sciences*, 52, 2024.

Joshua Schimel. Modeling ecosystem-scale carbon dynamics in soil: the microbial dimension. *Soil Biology and Biochemistry*, 178:108948, 2023.

JP Schimel and SM Schaeffer. Microbial control over carbon cycling in soil. front microbiol 3: 348, 2012.

S Schnell and TE Turner. Reaction kinetics in intracellular environments with macromolecular crowding: simulations and rate laws. *Progress in biophysics and molecular biology*, 85(2-3):235–260, 2004.

J Michael Schurr. The role of diffusion in enzyme kinetics. *Biophysical Journal*, 10(8): 717–727, 1970.

Erik Schwarz, Samia Ghersheen, Salim Belyazid, and Stefano Manzoni. When and why microbial-explicit soil organic carbon models can be unstable. *Biogeosciences*, 21(14): 3441–3461, 2024.

Andong Shi, Arjun Chakrawal, Stefano Manzoni, Benjamin MC Fischer, Naoise Nunan, and Anke M Herrmann. Substrate spatial heterogeneity reduces soil microbial activity. *Soil Biology and Biochemistry*, 152:108068, 2021.

Priyadarshi R Shukla, Jim Skea, E Calvo Buendia, Valérie Masson-Delmotte, Hans Otto Pörtner, DC Roberts, Panmao Zhai, Raphael Slade, Sarah Connors, Renée Van Diemen, et al. Ipcc, 2019: Climate change and land: an ipcc special report on climate change,

desertification, land degradation, sustainable land management, food security, and greenhouse gas fluxes in terrestrial ecosystems. 2019.

Daniel R Smith and Matthew R Chapman. Economical evolution: microbes reduce the synthetic cost of extracellular proteins. *MBio*, 1(3):10–1128, 2010.

Noah W Sokol, Eric Slessarev, Gianna L Marschmann, Alexa Nicolas, Steven J Blazewicz, Eoin L Brodie, Mary K Firestone, Megan M Foley, Rachel Hestrin, Bruce A Hungate, et al. Life and death in the soil microbiome: how ecological processes influence biogeochemistry. *Nature Reviews Microbiology*, 20(7):415–430, 2022.

Fengbin Song, Xiying Han, Xiancan Zhu, and Stephen J Herbert. Response to water stress of soil enzymes and root exudates from drought and non-drought tolerant corn hybrids at different growth stages. *Canadian Journal of Soil Science*, 92(3):501–507, 2012.

David J Spurgeon, Aidan M Keith, Olaf Schmidt, Dennis R Lammertsma, and Jack H Faber. Land-use and land-management change: relationships with earthworm and fungi communities and soil structural properties. *BMC ecology*, 13:1–13, 2013.

G Stotzky. Microbial respiration. *Methods of Soil Analysis: Part 2 Chemical and Microbiological Properties*, 9:1550–1572, 1965.

J. Y. Tang. On the relationships between the michaelis–menten kinetics, reverse michaelis–menten kinetics, equilibrium chemistry approximation kinetics, and quadratic kinetics. *Geoscientific Model Development*, 8(12):3823–3835, 2015. doi: 10.5194/gmd-8-3823-2015. URL `https://gmd.copernicus.org/articles/8/3823/2015/`.

J. Y. Tang and W. J. Riley. A total quasi-steady-state formulation of substrate uptake kinetics in complex networks and an example application to microbial litter decomposition. *Biogeosciences*, 10(12):8329–8351, 2013. doi: 10.5194/bg-10-8329-2013. URL `https://bg.copernicus.org/articles/10/8329/2013/`.

KEO Todd-Brown, JT Randerson, F Hopkins, V Arora, T Hajima, C Jones, E Shevliakova, J Tjiputra, E Volodin, T Wu, et al. Changes in soil organic carbon storage predicted by earth system models during the 21st century. *Biogeosciences*, 11(8):2341–2356, 2014.

Sachia J Traving, Uffe H Thygesen, Lasse Riemann, and Colin A Stedmon. A model of extracellular enzymes in free-living microbes: which strategy pays off? *Applied and environmental microbiology*, 81(21):7385–7393, 2015.

Henry Clavering Tuckwell. Nonlinear and stochastic theories. *Introduction to Theoretical Neurobiology.*, 2, 1988.

Marius Usher and James L McClelland. The time course of perceptual choice: the leaky, competing accumulator model. *Psychological review*, 108(3):550, 2001.

Gandimohan M Viswanathan, Sergey V Buldyrev, Shlomo Havlin, MGE Da Luz, EP Raposo, and H Eugene Stanley. Optimizing the success of random searches. *nature*, 401 (6756):911–914, 1999.

H-J Vogel, J Tölke, VP Schulz, M Krafczyk, and K Roth. Comparison of a lattice-boltzmann model, a full-morphology model, and a pore network model for determining capillary pressure–saturation relationships. *Vadose Zone Journal*, 4(2):380–388, 2005.

Laure E Vogel, David Makowski, Patricia Garnier, Laure Vieublé-Gonod, Yves Coquet, Xavier Raynaud, Naoise Nunan, Claire Chenu, Ruth Falconer, and Valérie Pot. Modeling the effect of soil meso-and macropores topology on the biodegradation of a soluble carbon substrate. *Advances in Water resources*, 83:123–136, 2015.

LE Vogel, Valerie Pot, David Makowski, Patricia Garnier, and PC Baveye. To what extent do uncertainty and sensitivity analyses help unravel the influence of microscale physical and biological drivers in soil carbon dynamics models? *Ecological modelling*, 383:10–22, 2018.

Matthew Wallenstein, Steven D Allison, Jessica Ernakovich, J Megan Steinweg, and Robert Sinsabaugh. Controls on the temperature sensitivity of soil enzymes: a key driver of in situ enzyme activity rates. *Soil enzymology*, pages 245–258, 2011.

Matthew D Wallenstein and Edward K Hall. A trait-based framework for predicting when and where microbial adaptation to climate change will affect ecosystem functioning. *Biogeochemistry*, 109:35–47, 2012.

Gang Wang and Dani Or. Aqueous films limit bacterial cell motility and colony expansion on partially saturated rough surfaces. *Environmental Microbiology*, 12(5):1363–1373, 2010.

Gang Wang and Dani Or. Trophic interactions induce spatial self-organization of microbial consortia on rough surfaces. *Scientific Reports*, 4(1):6757, 2014.

Gangsheng Wang and Wilfred M Post. A note on the reverse michaelis–menten kinetics. *Soil Biology and Biochemistry*, 57:946–949, 2013.

William R Wieder, Steven D Allison, Eric A Davidson, Katerina Georgiou, Oleksandra Hararuk, Yujie He, Francesca Hopkins, Yiqi Luo, Matthew J Smith, and Benjamin Sulman. Explicitly representing soil microbial processes in earth system models. *Global Biogeochemical Cycles*, 29(10):1782–1800, 2015.

William R Wieder, Melannie D Hartman, Benjamin N Sulman, Ying-Ping Wang, Charles D Koven, and Gordon B Bonan. Carbon cycle confidence and uncertainty: Exploring variation among soil biogeochemical models. *Global change biology*, 24(4):1563–1579, 2018.

Wen Xiao, Xiao Chen, Xin Jing, and Biao Zhu. A meta-analysis of soil extracellular enzyme activities in response to global change. *Soil Biology and Biochemistry*, 123: 21–32, 8 2018. ISSN 00380717. doi: 10.1016/j.soilbio.2018.05.001.

Qingrong Xiong, Todor G Baychev, and Andrey P Jivkov. Review of pore network modelling of porous media: Experimental characterisations, network constructions and applications to reactive transport. *Journal of contaminant hydrology*, 192:101–117, 2016.

Huacheng Xu and Laodong Guo. Intriguing changes in molecular size and composition of dissolved organic matter induced by microbial degradation and self-assembly. *Water research*, 135:187–194, 2018.

Filip Yabukarski, Justin T Biel, Margaux M Pinney, Tzanko Doukov, Alexander S Powers, James S Fraser, and Daniel Herschlag. Assessment of enzyme active site positioning and tests of catalytic mechanisms through x-ray–derived conformational ensembles. *Proceedings of the National Academy of Sciences*, 117(52):33204–33215, 2020.

Yifei Zhang and Henry Hess. Enhanced diffusion of catalytically active enzymes. *ACS central science*, 5(6):939–948, 2019.